Title
ADSORPTION OF DILUTE-AQUEOUS ZINC IONS IN THE ELECTRICAL DOUBLE LAYER OF A POROUS-CARBON ELECTRODE

Author
Sisler, G.

Publication Date
1987-12-01

Lawrence Berkeley Laboratory
UNIVERSITY OF CALIFORNIA

Materials & Chemical Sciences Division

Adsorption of Dilute-Aqueous Zinc Ions in the Electrical Double Layer of a Porous-Carbon Electrode

G. Sisler
(M.S. Thesis)

December 1987

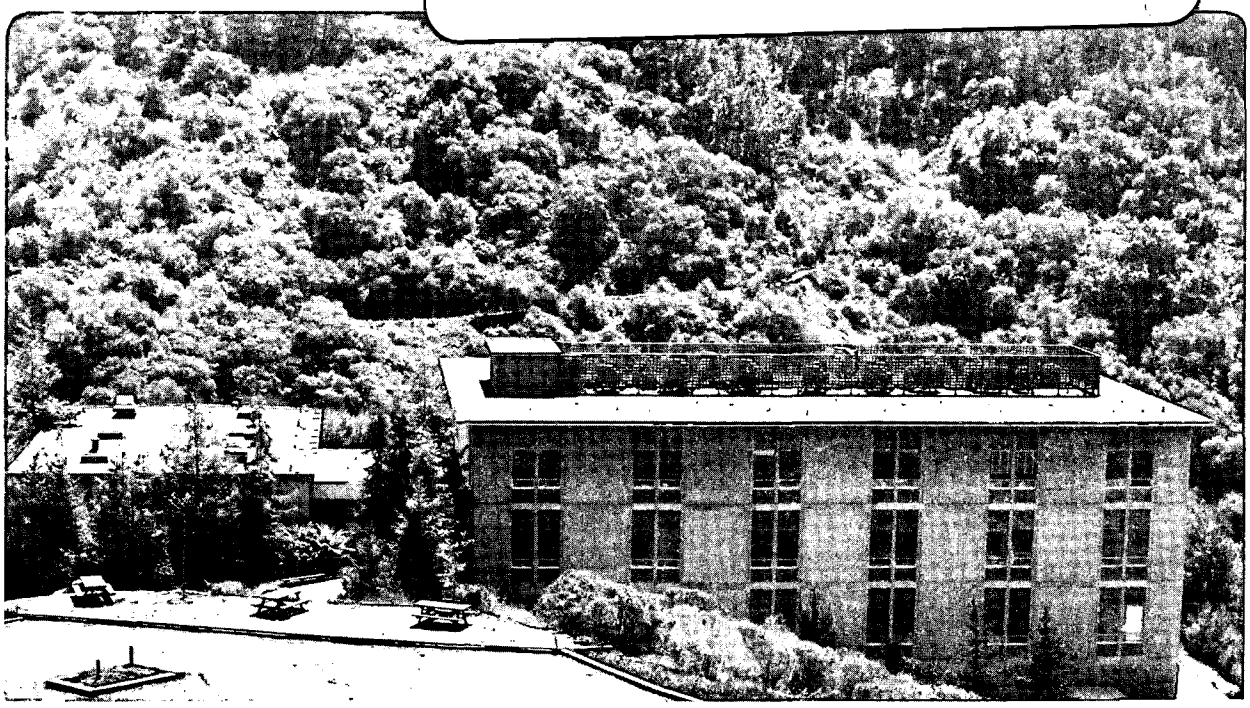

Prepared for the U.S. Department of Energy under Contract DE-AC03-76SF00098

DISCLAIMER

LBL-24406

Adsorption of Dilute-Aqueous Zinc Ions in the Electrical Double Layer of a Porous-Carbon Electrode

Gregg Sisler

M.S. Thesis

December 15, 1987

Lawrence Berkeley Laboratories
University of California
Berkeley, California 94720

Abstract

The removal of heavy-metal ions from dilute-aqueous waste streams by double-layer adsorption in a porous-carbon electrode was investigated. Most heavy metals are divalent ionic species and are thus preferentially adsorbed in the double layer by coulombic attraction over monovalent species. Metals which are difficult to remove from dilute streams by electroplating could potentially be removed by double-layer adsorption at potentials less negative than those which would cause hydrogen evolution.

Preliminary work was performed on a rotating-disk electrode. The effect of pH on the overall double-layer capacitance was studied and a region of potentials within which only double-layer charging should occur was determined. Later work was done on a porous-carbon electrode using zinc solutions. Effluent zinc concentration and cell current were monitored versus time. Results did not compare favorably with predictions from theory for charging an ideally-polarizable porous electrode, possibly due to the specific adsorption of zinc-chloride complexes.

Specific adsorption of zinc-chloride complexes was found to depend on the sodium chloride concentration. Zinc could be removed from the surface without passage of current by lowering the sodium chloride concentration. A new cell design and different electrolyte is proposed for future work.

This thesis is dedicated to Sandy and Michael, who have always stood by me.

I would like to thank Professor Newman for his help and guidance. He is an extremely thorough and methodical thinker. I have learned a great deal from his approach.

My wife Sandy and son Michael have been a great influence on me. Much of my time in graduate school has been stressful. My family helped me relax and was a constant reminder that work is only one part of life. For this I am thankful.

I would like to thank Tom Morrison of the analytical lab. He trained me on the atomic absorption spectrophotometer, which saved both time and money. He also had the time to answer questions about analytical techniques and inorganic chemistry.

This work was supported by the Assistant Secretary of Conservation and Renewable Energy, Office of Energy Systems Research, Energy Storage Division of the U.S. Department of Energy under contract number DE-AC03-76SF00098.

Table of Contents

CHAPTER 1

Introduction

1.1. Background

Heavy metal ions are found in many process effluents. Processes leading to such wastes include photographic fixing operations, general electroplating, as in nickel-chrome plating, galvanizing, printed circuit board manufacturing, and battery production. The metals commonly involved in these processes are, respectively, silver, nickel, chromium, zinc, copper, and lead. The concentration of heavy metals in the untreated rinse water of a typical process is usually less than 100 parts per million (ppm).[1] This figure is variable, depending on rinsing methods. The methods of conventional sewage treatment plants do not remove many of the metals, creating the need for treatment prior to discharge. Waters containing high levels of heavy metals entering a sewage treatment plant can incapacitate the bacteria used by the plant, potentially allowing sewage to pass through the plant untreated.[2] ,[3]

As is normally the case with pollution control, the government assumes responsibility for evaluating risks and setting standards. These governmental tasks come more directly under the jurisdiction of the Environmental Protection Agency (EPA), formed in 1970 under the direction of President Richard Nixon. The risks they must evaluate include the detrimental effects of heavy metals on the sewage treat-

ment biomass as well as on the ecosystems of natural waters. In natural waters, heavy metals complex with phosphates and are taken up as nutrients by the flora and fauna. High levels of heavy metals result in increasingly high concentrations in the larger animals, altering biological mechanisms in unknown but detrimental ways.

The EPA combats this potential situation by setting discharge limits on individual polluters, usually by effluent size. Discharge limits are also typically set independently by the local water quality control board, in tandem with the local treatment facility, for a given area. Table 1-1 lists effluent standards for any electroplating plant in Oakland, California. These values will vary slightly from city to city. The limits are set based on considerations of the best available technology (BAT) for metals removal, as well as end-

Table 1-1. Electroplating Effluent Limits[4]

pollutant	Federal Max (ppm) (one day max)		Local Max (ppm)
	<10,000 GPD	>10,000 GPD	
Cd	1.2	1.2	1.0
Pb	.6	.6	2.0
CN	5.0	1.9	
Ag		1.2	1.0
Cr		7.0	2.0
Cu		4.5	5.0
Ni		4.1	5.0
Zn		4.2	5.0
Fe			100.0
Total Metals (Cr,Cu,Ni,Zn)		10.5	

point water quality objectives.

1.2. Process Economics

Incentives for cleaning effluent waters come from the threat of local and Federal fines as well as the possibility of recovery and reuse of the metals. The disincentive is the relatively high cost of treatment, especially to smaller plants. Fines are becoming larger and more frequent. The environment can no longer tolerate unregulated pollution. In November of 1986, a mid-sized U.S. electroplating company was fined over one-million dollars for discharging 44,000 gallons of water containing roughly one-hundred times the maximum levels of copper, nickel, and zinc into the sewer over a one year time span. The fine was the first ever assessed in a criminal court for violations of the Federal Clean Water Act, passed in 1985.[5] It is interesting that the discharged metals The discharged metals To minimize the fine, the company will spend 900-thousand dollars to install a pretreatment system. As government fines escalate, pretreatment becomes more economical. When precious metals are involved, recovery and reuse become more desirable.

The difficulty of the separations involved lead to the high cost of pretreatment. A separation process must reduce 50 to 100 ppm to less than 1 to 5 ppm and perhaps treat upwards of 10,000 gallons per day.

1.3. In-Plant Changes

Metals appear in effluent streams as a result of liquid solutions from the plating bath clinging to parts being carried to the rinsing bath, called drag-out. Studies have shown that one important step to lowering effluent concentrations and volumes is altering rinsing techniques.[6] The concept of using two rinses, called drag-out rinse, has proven useful. The first rinse tank may be a nonflow rinse and equipped with metals removal equipment. By design, the dilution factor as parts are moved from this rinse to the flowing rinse is sufficient to meet effluent requirements.

Other techniques have proven useful as well. Extended drip times over the main tank prior to rinsing have been used. The addition of surfactants to the plating bath solution lowers the surface tension and therefore lessens the volume of solution which will cling to parts. The use of a spray-rinse over the main tank will conserve plating bath solution. The volume of spray rinse that can be used is limited, and must roughly equal the volume of evaporation losses to maintain a steady plating bath level.

The above conservation techniques, in various combinations, are being used by individual plants. They all have in common the concept of stopping the problem at the source. In any plant, however, some metals will enter the rinsing bath(s), where they must be treated and removed.

1.4. Pretreatment Techniques

Any metals removal process operating on a rinse-water bath or stream is called "pretreatment." Figure 1-1 shows the location of a typical pretreatment scheme in an electroplating plant. Often the only pretreatment necessary is heavy-metals removal and pH adjustment. State of the art technology appears to be chemical precipitation of the heavy metals with caustic soda and lime. The separation is governed by the solubility products of the metal hydroxides. Remaining metal-ion concentrations meet effluent standards without difficulty. The metal-hydroxide sludge is settled in a clarifier and must be disposed of, according to government regulations,[7] leading to handling and disposal costs. The inability to recover the metals and the problems with disposal are two major drawbacks with this technique. Even so, the method is readily available, can process large volumes easily, and remains very popular.

Recent interest has concentrated on foam flotation as a means of clarifying the precipitate solution.[8] ,[9] The method works by adding a surfactant to the solution, which causes the precipitate particles to flocculate. The floc is then attracted to the interface of a rising bubble because both the floc and the gas bubble are non-polar whereas the surrounding water is polar. At the surface the floc can be scraped off and disposed of. The method significantly shortens the settling times required in a gravitational clarifier. It also allows the solution to be processed in smaller equipment.

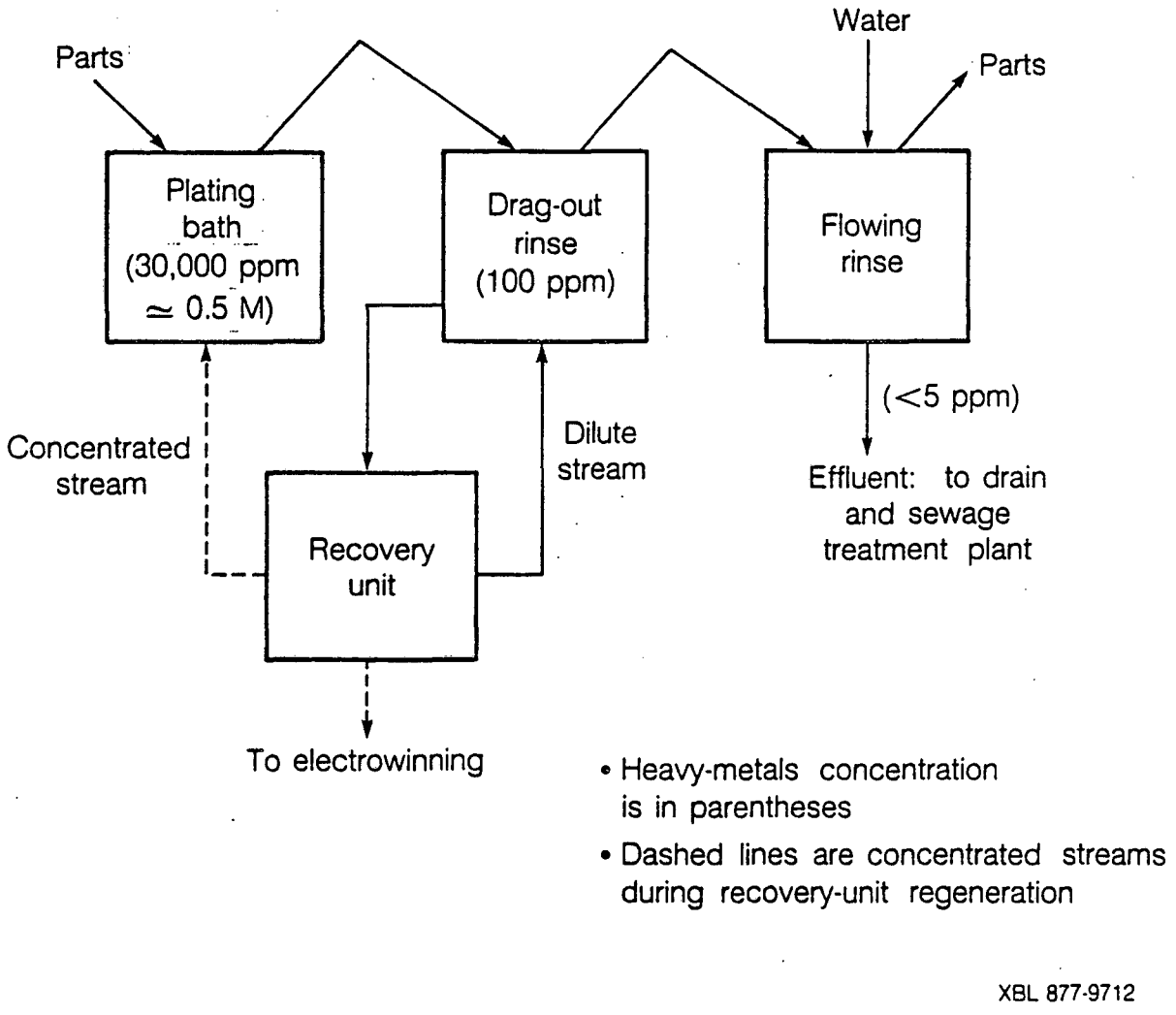

Figure 1-1. Electroplating plant with effluent pretreatment.

An alternative technique which is quite effective for metal-ion removal is ion exchange.[6],[10] Cation exchange columns are designed to exchange H^+-ions for the heavy-metal ions. Ion exchange is most useful when the metals concentration is low, on the order of 25 ppm, and for low rinse water flow rate processes. Ion exchange can also be coupled with chemical precipitation techniques to produce very pure water. Dilute streams of metal ions give rise to long times between regeneration steps. Saturated resin is typically regenerated with acid, yielding a concentrated solution of metal ions as a result. The metals in this stream are normally recovered by electrowinning.

Other methods have been examined mostly on a laboratory scale. These include adsorption on activated carbons,[11], [12], [13] adsorption on a zeolite,[14] biological treatment with algae,[15] biosorption by microbial cells,[16] reverse osmosis, electrodialysis, as well as electrochemical methods using porous electrodes (see section 1.6 below).

1.5. Electrochemical Methods

Electrochemical waste-water treatment schemes deserve attention as methods lending to environmental protection. Streams can be processed electrochemically without the addition of chemicals. The separating agent, electrical energy, is clean and non-polluting. Removal of many metals is essentially complete, and regeneration is achieved by varying the cell potential, allowing reuse of the electrode and recovery of the metal by electrowinning or by recycling to

the plating bath.

Electrochemical methods also have drawbacks. Treatment of dilute streams requires electrodes of extremely high surface area per unit volume. In practice, these can contribute large pressure drops to the flow. The electrode material must also exhibit good electrical conductivity and have surface properties receptive to metal adsorption or deposition. Few materials meet these criteria (porous carbons perhaps meet them best).[17], [18] Moreover, electrochemical cells are not always selective for the desired reaction. Often a side reaction, such as hydrogen evolution, competes with the desired reaction, resulting in wasted current and lower efficiencies. Because all metals have different redox potentials, treating a complex feed stream requires applying a potential negative enough to remove the most electronegative component (likely zinc or chromium). Such conditions also tend to enhance side reactions.

Other elements influencing the design of electrochemical systems are the conductivity of ions in solution and the counterelectrode placement,[19] for these affect the cell voltage and therefore the power required. In waste-water streams, conductivities may be low. Large voltages may be needed to drive the current. Acid can be added to increase conductivity and later be neutralized, but this undesirable chemical cost should be avoided. Instead, minimizing the distance between the electrodes conducting current will lower the cell voltage required more efficiently.

1.6. Past Electrochemical Work

Porous electrodes have been used in the past for removal of aqueous ions of copper,[20], [21] silver,[22], [23] lead,[24], [25] mercury,[26] antimony,[27] cadmium,[28] chromium,[28] and zinc.[28] The different reduction potentials of the various metals have led to varying degrees of success. Matlosz[26] achieved a 5000-fold reduction in mercury concentration using a reticulated-vitreous carbon electrode (RVC). RVC is a rigid porous carbon material. Trost[24] achieved minimal success with a high-pressure porous lead reactor for lead removal. Pressure was used in attempts to minimize the hydrogen evolution side reaction. He eventually achieved 98% removal using an RVC electrode at atmospheric pressure. Efforts to remove chromium and zinc (among other metals), two thermodynamically difficult metals to deposit, were made by Agarwal, *et al.*,[28] using RVC electrodes. These metals were not easily removed. The chromium required 10 passes through the electrode at a potential of -2.0 V versus the saturated calomel electrode (SCE) for 50% removal at a feed concentration of 50 μM (2.6 ppm). Zinc required 5 passes at -2.2 V versus SCE for 100% deposition at a feed concentration of 50 μM (3.2 ppm).

For metals that are thermodynamically or kinetically difficult to deposit from dilute solution (i.e., chromium and zinc), alternatives to electrodeposition should be investigated. An electrochemically-modulated adsorption process could provide the separation based on an electrostatic attraction between the metal ions and an oppositely charged electrode of high surface area. The

adsorption process could operate at lower applied potentials than a deposition process, thus minimizing potential dependent side reactions and creating higher current efficiencies for the separation. A disadvantage of an adsorption process is that all ions in solution can compete for sites at the surface. It is hoped that the divalent character of the heavy metals will yield preferential adsorption over monovalent ions (such as sodium), creating the needed selectivity.

1.7. Nonfaradaic Electrochemical Processes

A nonfaradaic process is one in which no charge transfer reactions occur. Rather, ions from solution migrate to the electrode surface of opposite charge, where they are electrostatically held, but do not react. For this to occur, the applied surface potential must be less than that required for a charge transfer reaction. In practice, extremely high surface areas are required because the bed becomes saturated in much the same manner as the beds of ordinary adsorption processes. This is in contrast to electrodeposition (faradaic) methods, where many layers can plate on the same surface area.

Electrochemically modulated adsorption was applied by the Marquardt Company in the mid-1960's to the problem of desalting water.[29], [30] They used a laboratory cell one inch in diameter and consisting of three anodes and three cathodes each 3/8-inch thick and made of granular activated carbon. Polarizing the electrodes should attract sodium ions to the negative electrode and chloride ions to the positive electrode, in the ideal case. Regeneration is achieved

by reversing the potential. The electrode-stack-treated sodium chloride yields a desalted stream on the removal step and a concentrated saline solution on regeneration. Results show that a feed stream of 1575 ppm NaCl produced a 1375 ppm stream on removal and roughly a 1800 ppm stream on regeneration. Experiments on complex feed waters demonstrated roughly a 2.3 selectivity factor of the process for divalent over monovalent ions. Use of unsymmetrical removal and regeneration times and potentials significantly improve the process. The method appears to affect the ionic concentration only mildly, but perhaps it could significantly influence the metal concentration in a dilute waste stream (i.e., 100 ppm metals). That possibility has been the focus of this research.

CHAPTER 2

Theory

2.1. The Electrical Double Layer

Electrical double layers arise due to charge separations near interfaces. When a conductor, such as carbon, is immersed in electrolyte, one of the ions in solution may have a preference for being near the interface. If the conductor is uncharged, the charges of the ions near the surface must be balanced by counterions in a diffuse region further out. The potential of the uncharged conductor, relative to a suitable reference potential, is known as the potential at the point of zero charge. At this potential, the solution double layer has a net neutral charge. The potential of zero charge is the open-circuit potential only when the electrode is uncharged. When dealing with ideally polarizable electrodes, the open-circuit potential will fluctuate depending on the surface charge. Carbon immersed in electrolyte will arrive, for example, at some open-circuit potential at which its surface is charged. Polarizing a conductor positively from the point of zero charge will force a net negative charge on the solution side to balance the positive conductor charge; and vice-versa.

The most widely accepted view of the electrical double layer was put forth by Gouy and Chapman and modified by Stern. Gouy and Chapman viewed the double layer as a balance between electrical attractive

forces and thermal dispersive forces. Thus concentrations follow a Boltzmann distribution decaying exponentially with distance from the surface. Stern modified this by setting an inner limit on the closeness with which molecules could approach the electrode. Solvated molecules can approach only to a plane, called the outer Helmholtz plane. Outside this plane the diffuse-double-layer theory of Gouy and Chapman holds. Inside the outer Helmholtz plane molecules can shed their solvation sheaths and move to an inner plane called the inner Helmholtz plane. These ions are said to be specifically adsorbed. Solvent molecules can also penetrate this region. The entire double layer region exists within 10 to 100 Ångstroms of the surface, depending on the ionic strength of solution. This distance is very short compared to a diffusion layer, which typically extends over 100 microns. Figure 2-1a shows a typical distribution of charges at a metal/solution interface. Here the metal is polarized negatively, leading to an excess of positive charges at the outer Helmholtz plane (OHP) and extending into the solution. Ions at the inner Helmholtz plane (IHP) exhibit adsorptive forces dependent on the conductor material, its potential, the ion chemistry, ionic concentration, and degree of hydration. These ions are said to be specifically adsorbed. On mercury, specific adsorption is normally limited to anions. On activated carbon, negatively charged surface groups will cause cations to specifically adsorb. Figure 2-1a shows specific adsorption forces for anions overcoming electrostatic repulsion forces from the metal. Thus, more cations are held in the diffuse region than would be predicted by considering only coulombic

forces and neglecting specific adsorption.

Figure 2-1b shows the potential profile corresponding to the charges from figure 2-1a. The charges relate to the potentials through Gauss's law. Gauss's law states that the integral of the normal electric field component times the permittivity of the medium over the surface of any closed volume equals the charge enclosed,

$$\oint \epsilon \mathbf{E} \cdot d\mathbf{S} = \int \rho_e dV = Q_{enclosed}. \tag{2-1}$$

Here ϵ is the permittivity, and ρ_e is the charge per unit volume enclosed. Drawing a rectangular box with end faces of unit area parallel to the electrode interface and using the definition of electric field,

$$\mathbf{E} = -\nabla\phi, \tag{2-2}$$

simplifies equation (2-1). Since the field strength is zero on the sides of this box, only the ends contribute. Thus Gauss's law becomes,

$$\epsilon\left(\frac{d\phi}{dy}A\right)_{\substack{outer \\ face}} - \epsilon\left(\frac{d\phi}{dy}A\right)_{\substack{inner \\ face}} = Q_{enclosed}, \tag{2-3}$$

where y is the distance from the surface and A is the cross-sectional area of a face parallel to the surface. Drawing the box from inside the metal, where $\frac{d\phi_M}{dy} = 0$, to just inside the IHP yields,

$$q_M = \frac{-\epsilon_i(\phi_{IHP}-\phi_M)}{d_o}, \tag{2-4}$$

where d_o is the distance from the interface to the inner Helmholtz plane and ϵ_i the permittivity in that region. Equation (2-4) is

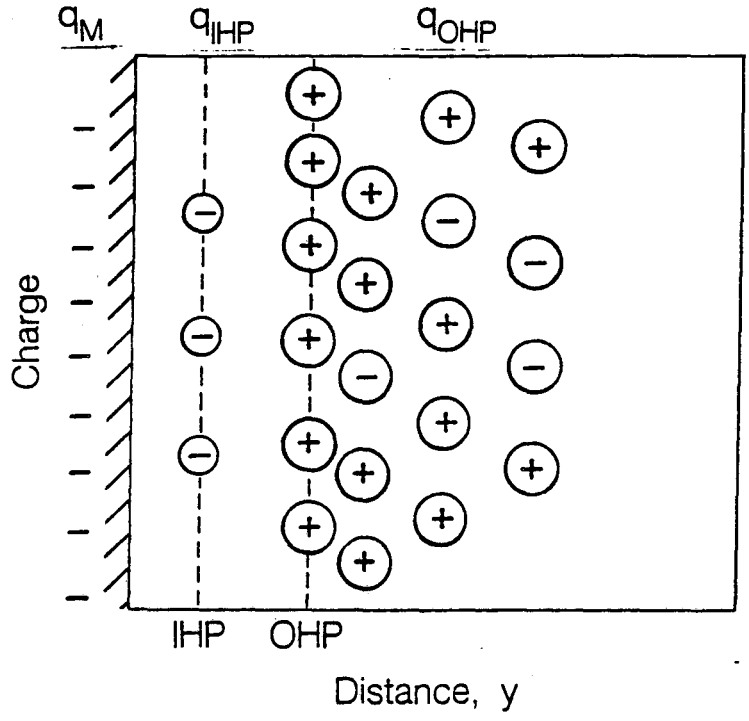

XBL 877-9714

Figure 2-1a. Typical distribution of charges in the electrical double layer.

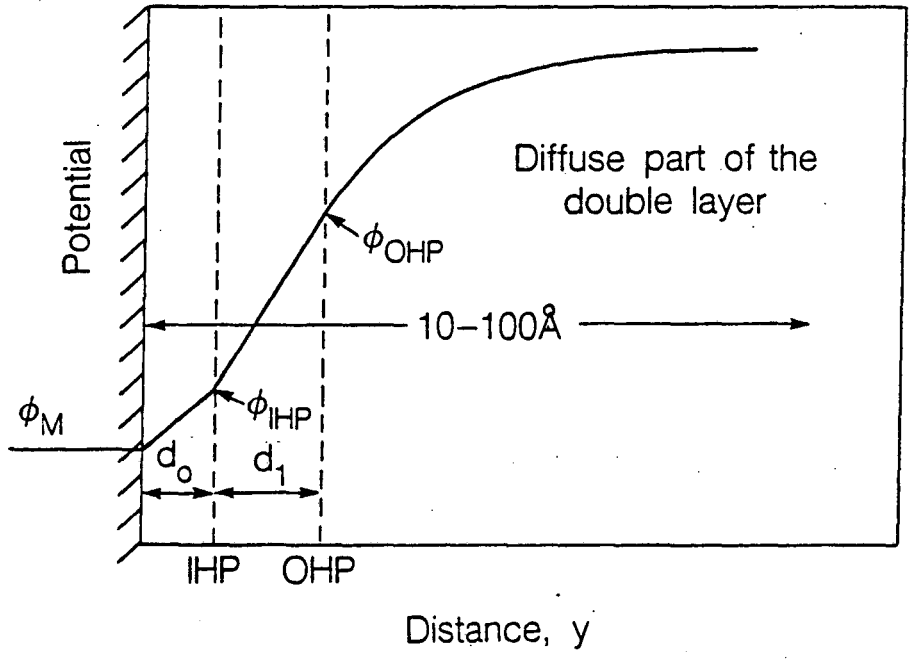

XBL 877-9715

Figure 2-1b. Potential profile for the charge distribution shown.

written as a difference because both the electrons in the metal and the ions at the inner Helmholtz plane (IHP) are assumed to exist as planes of charge separated by a medium of constant permittivity ϵ_i and by a distance d_o. Drawing the Gaussian box from just outside the inner Helmholtz plane to the end of the diffuse double layer (where $\frac{d\phi}{dy} = 0$ in the absence of current flow) shows

$$q_2 = \frac{-\epsilon_1(\phi_{IHP}-\phi_{OHP})}{d_1}, \tag{2-5}$$

where d_1 and ϵ_1 are the distance and the permittivity, respectively, between the inner and the outer Helmholtz planes. The charge q_2 is diffuse, therefore the slope of the potential profile is continuous at the outer Helmholtz plane. This follows from Gauss's law, where a box infinitely thin at the outer Helmholtz plane will show no charge enclosed. The variation of charge with distance throughout the diffuse double layer accounts for the smooth variation of potential in this region.

Electroneutrality of the overall double layer requires

$$q_M + q_1 + q_2 = 0. \tag{2-6}$$

This could also be found by drawing a Gaussian box around the entire double layer ($\frac{d\phi}{dy} = 0$ on both ends).

While equations (2-4) to (2-6) help to interpret a potential profile, the profile itself cannot be generated without knowledge of the adsorption process at the interface. Only certain quantities are measurable, such as the metal potential with respect to a reference electrode, the total current, and the overall double-layer capacity,

so that any modeling effort becomes an interesting challenge. A model would have to account for the dependence of adsorption on the electrode potential and bulk concentration. Adsorption will depend on the valency of each ion. Equations (2-4) to (2-6) above link the charges (which are determined by the ionic adsorption) to the potentials. To calculate the removal of ions in a flowing system, bulk transport equations must be solved where the generation term (i.e., adsorption) is calculated using the microscopic adsorption equations explained above. The bulk transport equations involve material balances on each species as applied in porous electrode theory. A model of double-layer adsorption in a porous electrode, as just described, requires experimental justification before developing.

For this study, the most straightforward way to proceed was to investigate the double-layer capacity. We will assume that the double-layer capacity is a constant and thus ignore any detailed analysis of the surface.

2.2. Double-Layer Capacitance

A double-layer capacity represents the quantity of charge held in the double layer at the interface, per unit voltage applied. For a study of metal ion removal by double-layer adsorption, the double-layer capacitance is a key parameter. The differential double-layer capacitance is defined as

$$C = \left(\frac{\partial q_M}{\partial U}\right)_{\mu,T} , \qquad (2\text{-}7)$$

where q_M is the charge density on the metal side of the double layer,

U is the potential of the working electrode relative to a reference electrode reversible to the anion in solution, and the subscript μ, the chemical potential, denotes constant composition. The charge q is also related to the surface tension, γ, by

$$q_M = -\left(\frac{\partial \gamma}{\partial U}\right)_{\mu,T} , \tag{2-8}$$

which comes from a thermodynamic analysis at an interface (i.e., the Lippmann equation [31]). Equations 2-7 and 2-8 combine to yield

$$C = -\left(\frac{\partial^2 \gamma}{\partial U^2}\right)_{\mu,T} , \tag{2-9}$$

which indicates that double-layer capacities can be calculated from data on surface tension versus potential. Liquid metal electrodes, such as the dropping mercury electrode (see Grahame [32]), are useful for measuring surface tension as a function of potential. Surface tension is a contractive force, but any charges present will weaken the attraction due to coulombic repulsion. Thus, surface tension is maximized at the point of zero charge.

At solid electrodes, surface-tension measurements are difficult to make. Thus, double-layer capacities must be measured directly. Equation (2-7) is useful if the charge-potential relationship of the solid is known. Capacities can be measured by applying a small oscillation of potential (or current) onto a steady-state potential at an ideally-polarizable electrode. If no faradaic reactions can occur, any resulting current must be due to double-layer charging. While this procedure yields double-layer capacities as a function of potential, the point of zero charge remains unknown. Integration of

equation (2-7) reveals that the point of zero charge is essentially an unknown integration constant. This presents some uncertainty about the optimum potential range in a situation where heavy-metal cations are to be removed.

2.3. Double-Layer Capacity by Potential Sweep

Sweeping the potential on an ideally-polarizable electrode will yield a current due solely to double-layer charging. The potential-sweep analysis, presented later in this section, was originally worked out by Bard.[33] He treats an ideal RC circuit with a potential difference which is sweeping in time. Potential sweep experiments were done by Evans[34] to determine double-layer capacities of carbon-paste electrodes. He found that, in the ideally-polarizable range, the double-layer capacity of carbon did not vary with potential.

An ideally-polarizable electrode is one in which no charge can transfer across the interface regardless of the potential applied. Real electrodes can behave as ideally polarizable only over certain potential ranges. Mercury electrodes have high hydrogen overpotentials and thus behave as ideally polarizable over wide potential ranges in appropriate electrolytes. A carbon electrode in salt water and zinc chloride solution, as in this study, should behave as ideally polarizable between the potentials of hydrogen and oxygen evolution. Figure 2-2 shows a Pourbaix diagram displaying the thermodynamic potentials for the various possible reactions in the system as a function of pH. Within a window of potential up to the oxygen

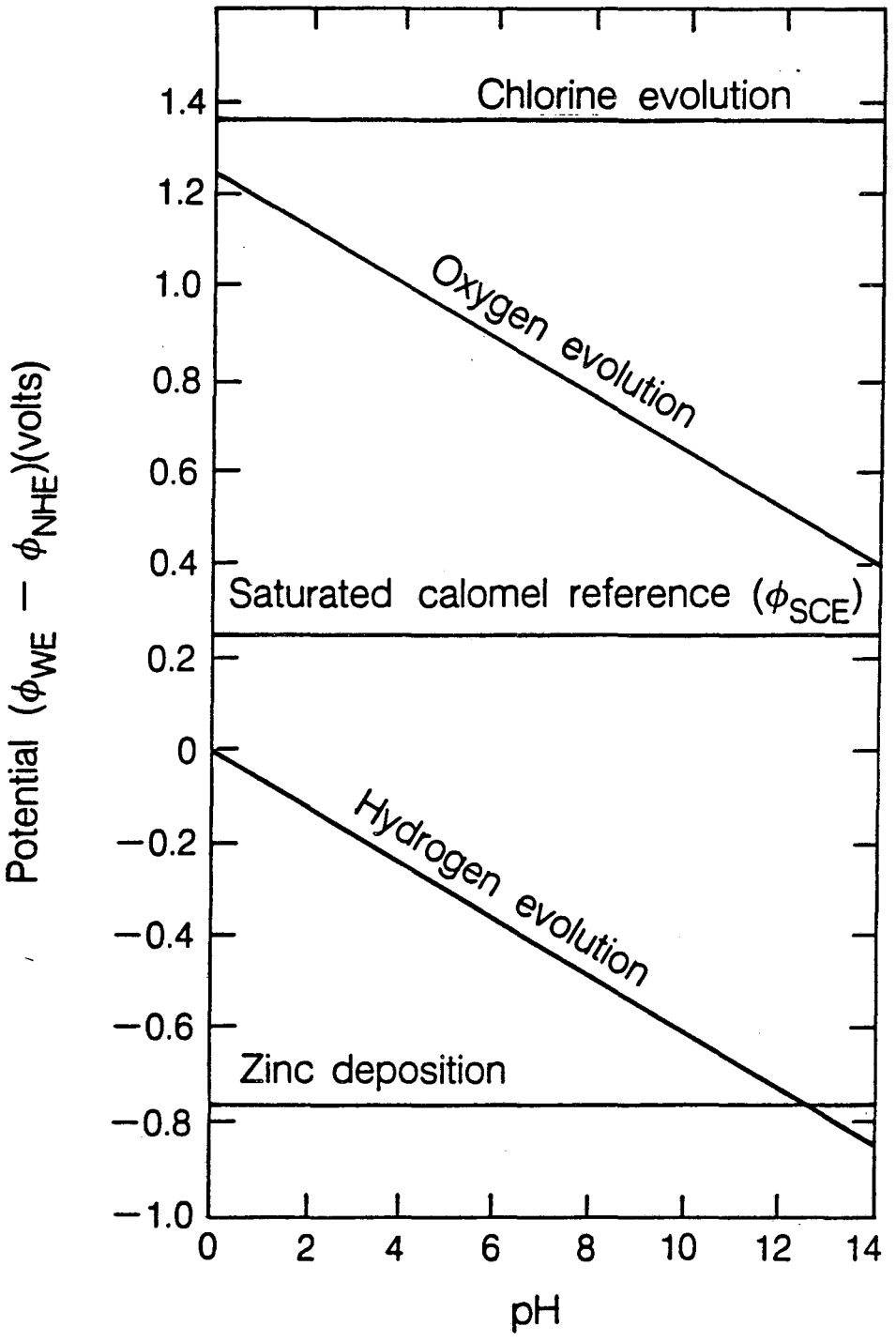

Figure 2-2. Pourbaix diagram showing thermodynamic potentials of charge-transfer reactions in the electrochemical system (WE - working electrode, NHE - normal hydrogen electrode, SCE - saturated calomel electrode).

line and down to the hydrogen line the solution will be thermodynamically stable (i.e., no charge transfer reactions can occur). This window may be larger if the kinetics for hydrogen or oxygen evolution require large overvoltages for reaction on carbon. Note that zinc is electroplated industrially because hydrogen has a huge overvoltage for reaction on pure zinc (i.e., poor kinetics).

In solution, an ideally polarizable electrode will behave electrically according to an RC circuit. Figure 2-3 shows the circuit. Here C_T is the total double-layer capacity of the working electrode, and R is the resistance in solution between the working

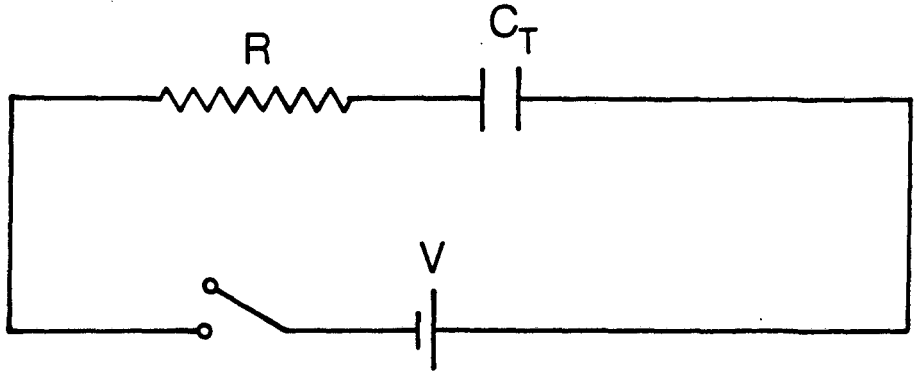

XBL 877-9713

Figure 2-3. Resistive-capacitive circuit for an ideally polarizable electrode.

and reference electrodes. The double-layer capacity at the reference electrode can be ignored because the reference electrode is not polarized. For a rotating-disk working electrode with a reference electrode infinitely far away, Newman[35] has shown the solution-phase resistance to be

$$R = \frac{1}{4\kappa r_o}, \tag{2-10}$$

where r_o is the disk radius and κ is the solution phase conductivity. The working electrode versus reference electrode potential ($\phi_{WE}-\phi_{RE}$) will vary with time according to

$$\phi_{WE}-\phi_{RE} = V = V_o' + \nu t, \tag{2-11}$$

where ν is the sweep rate, t is time, and V_o' is the initial system potential relative to the open-circuit potential. Distributing the potential over the RC_T circuit gives

$$V_o' + \nu t = IR + \frac{Q}{C_T}. \tag{2-12}$$

Recalling that $Q = \int I dt$ and with the initial condition

$$I = \frac{V_o'}{R} \qquad \text{at } t = 0, \tag{2-13}$$

we can solve equation (2-12) by taking Laplace transforms in time. After inversion, the result is

$$I = \nu C_T + \left[\frac{V_o'}{R} - \nu C_T\right] \exp\left[\frac{-t}{RC_T}\right]. \tag{2-14}$$

The term in brackets is a decaying transient with time constant RC_T. If the time constant RC_T is short enough, the steady term can be used

to measure C_T as a function of potential. For a 0.1 molar salt solution ($\kappa \approx 0.01$ mho/cm), a disk of radius 0.25 cm, and using a typical double-layer capacitance of 30 $\mu F/cm^2$, the time constant RC_T becomes about half a millisecond. Within a few milliseconds of beginning a sweep, the entire transient term will become negligible, and the steady term will relate the current flowing to the double-layer capacity at any potential.

2.4. Porous-Electrode Theory

Porous carbon materials normally possess huge surface areas of several hundred square meters per gram. Double-layer capacitances of porous carbons are also often high, roughly 30 $\mu F/cm^2$. With huge surface areas and large double-layer capacitances, significant amounts of ions can be stored in the electrical double-layer of porous carbon. However, a net deionization will occur only due to changes in the adsorbed-ion concentration. Consider the diagram of figure 2-4. The diagram was constructed from data at a mercury interface by Graham[36]. The CHARGE curve represents total solution-side charge, equal and opposite to the electrode charge (see equation 2-6). The sodium and chloride curves can be considered adsorbed-ion concentration curves. Any change in the overall CHARGE curve must accompany a passage of current. Also the slope of the CHARGE curve is the double-layer capacitance (see equation 2-7). The point of zero charge is at about -0.55 volts. At more negative potentials, the double layer is positively charged, and at more positive mercury potentials the double layer is negatively charged. If

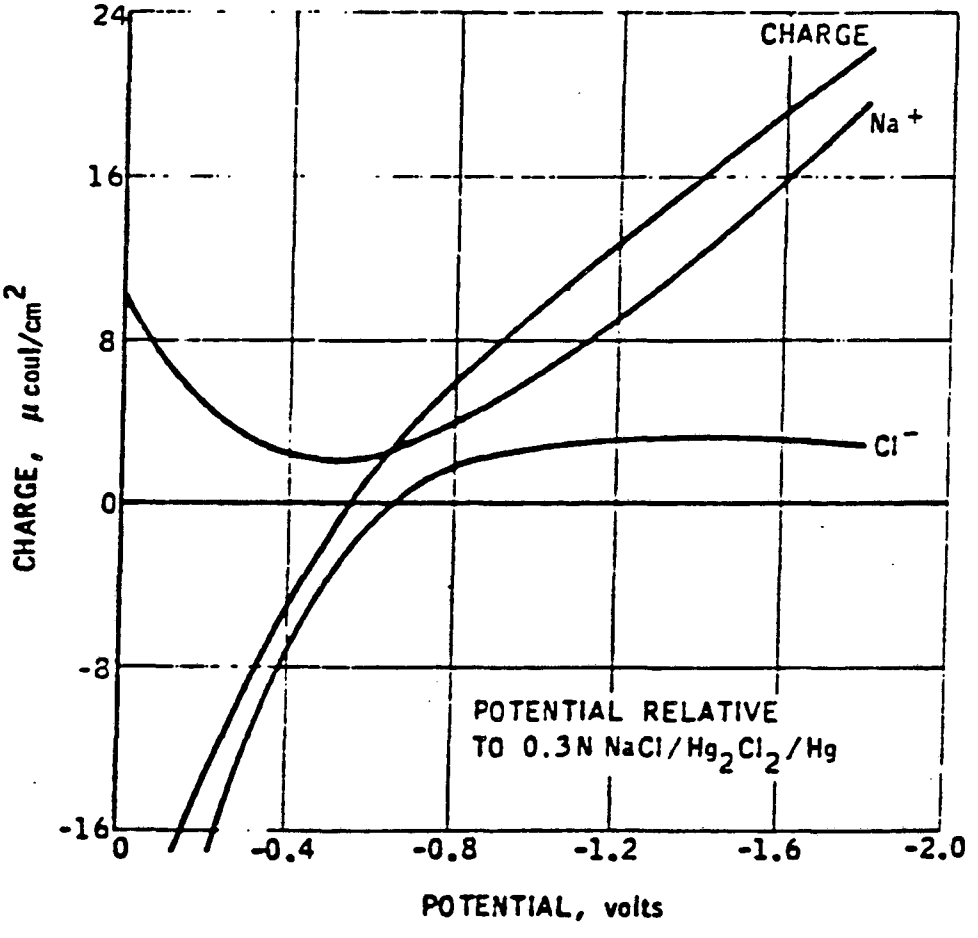

Figure 2-4. Adsorption of NaCl at a mercury electrode (from Graham[36]).

we want to remove sodium using a mercury interface, two useful ranges of potential are noticeable. First, the process could operate between -0.4 volts and either 0.0 volts or some positive potential not shown. Second, it could operate between about -0.8 volts and some more negative potential. The second choice leaves the chloride surface concentration relatively unchanged, and current is used exclusively on sodium. This is the region of highest current efficiency for adsorption of sodium, neglecting side reactions such as hydrogen evolution. Hydrogen evolution may become important at the large negative potentials of this region. At small negative potentials, the chloride-ion concentration changes rapidly, requiring current to do so. Here the chloride curve is more negative than the overall solution double-layer charge. This represents specific adsorption of chloride in addition to coulombic attraction. A corresponding uptake of sodium maintains the overall double-layer electroneutrality. Thus, more ions are held in the double layer than the mercury metal charge would predict (see figure 2-1a).

The problem of heavy-metal cation removal on porous carbon is analogous to the uptake of sodium on mercury. However, the inability to measure surface tensions and the subsequent uncertainty about the potential of zero charge make a plot like figure 2-4 difficult to construct on solid electrodes. Nonetheless, regions where the degree of adsorption of cations and/or anions varies with changes in the potential would still be expected to exist on carbon or any other solid electrode.

2.5. Porous-Electrode Model

The model detailed in the remaining sections of this chapter was originally developed by Johnson and Newman[30] for analyzing a water-desalting process based on double-layer adsorption. Here the model is developed for the case of an isolated porous electrode where the potential is controlled with respect to a reference electrode. The previous model applied to a cell with opposing porous electrodes where the potential is controlled between the two. In each case, as it turns out, the same model applies.

A porous electrode made of granular activated carbon or any other material contains a great amount of geometric detail. By necessity, this detail must be macroscopically averaged to allow mathematical analysis. The porous bed is seen as a superposition of two continua, a matrix (i.e., carbon) and a solution. Geometric detail, such as pore structure, is ignored. Quantities such as the specific surface area and solution phase potential or concentration are averaged over an electrode volume element. The effect is a cross-sectional smearing of all quantities resulting in a one-dimensional problem in axial distance. Figure 2-5 shows the current flow in a porous electrode (from Trost[24] p.32). The counterelectrode is assumed to be in the free solution to the right of the figure, and solution can flow through the electrode (i.e., see figure 3-3). In solution outside the porous electrode, all current is in the solution phase ($i_2 = I/A$). At the current collector (i.e., the porous metal backing plate) all current must be in the matrix phase

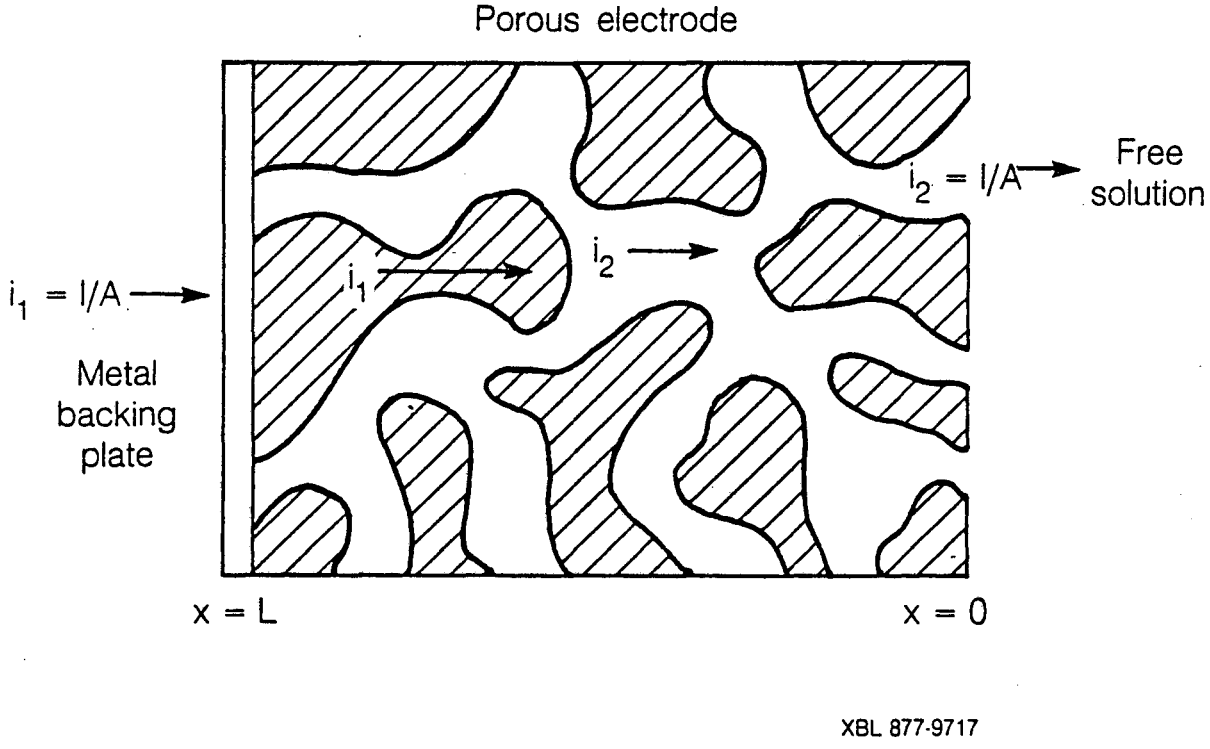

Figure 2-5. Flow of current in a porous electrode.

($i_1 = I/A$). The current collector is assumed to contact the matrix phase but not to engage in reactions directly with the solution. Within the electrode, all current must eventually transfer phases either by charge-transfer reactions or by double-layer charging. Solution can flow through the electrode, typically either parallel to the current (flow-through configuration) or perpendicular to the current (flow-by configuration). The current distribution will in general depend on the conductivities of each phase, on the flow configuration, and on any kinetic or mass-transfer effects on reaction or adsorption at the interface.

2.6. Governing Equations

The transfer of current between the solution and matrix phases is assumed, in our case, to be due solely to charging of the double layer

$$\nabla \cdot i_1 = -\nabla \cdot i_2 = -aC\frac{\partial(\phi_1-\phi_2)}{\partial t}. \qquad (2\text{-}15)$$

The subscripts 1 and 2 refer to the matrix and solution phases respectively and "a" is the specific surface area (surface area per total volume). In the porous electrode, any current leaving the matrix must enter the solution. This equation represents the major assumptions of the model. First, all charge-transfer reactions, which would involve Butler-Volmer type rate expressions, are neglected. Secondly, it assumes that ionic adsorption occurs by charging the electrical double layer. The double layer is assumed to be in local equilibrium at the potential difference $\phi_1-\phi_2$ (which will

vary with time). Throughout the porous electrode, the double layer will not charge instantaneously, but will charge according to the electrical resistances in the porous electrode circuit and the local time varying potentials. A third assumption is that the adsorption kinetics do not limit the rates.

In the pore phase, a material balance on species i shows

$$\epsilon\frac{\partial c_i}{\partial t} = -\nabla\cdot N_i + \frac{\partial a\Gamma_i}{\partial t}. \tag{2-16}$$

All terms here have units of moles per unit volume of matrix plus solution per time. The void fraction is ϵ (volume of solution per total volume). Γ_i is the surface concentration of species i (moles i per interfacial area). Thus ϵc_i is the superficial solution-phase concentration averaged over the matrix plus pores, and $a\Gamma_i$ the superficial surface concentration per total volume. The pore-phase flux of species i, N_i, is also averaged over the entire cross section of the bed. The last term of equation 2-16 represents the accumulation of ions in the double layer. This could be rewritten as

$$\frac{\partial a\Gamma_i}{\partial t} = \frac{dq_i}{dq}\frac{\nabla\cdot i_2}{z_i F}. \tag{2-17}$$

by realizing that $\nabla\cdot i_2 = d\,aq/dt$ and that $q_i = z_i\,F\,\Gamma_i$ where dq_i/dq is the charge fraction of species i adsorbed.

The flux of species i, N_i, is given by

$$N_i = -z_i u_i F\epsilon c_i\nabla\phi_2 - D_i\epsilon\nabla c_i + c_i v, \tag{2-18}$$

where the terms represent flux contributions from migration, diffusion, and convection, respectively. Any surface flux in the

electrical double layer has been ignored. The values of the mobility, u_i, and the diffusivity, D_i, in tortuous materials are equal to their free solution values except for tortuousity factors, assumed to be included.

The matrix-phase current density obeys Ohm's law,

$$i_1 = -\sigma \nabla \phi_1, \tag{2-19}$$

where σ is the effective conductivity of the matrix phase. In the solution phase, current is carried by ionic species

$$i_2 = F \sum_i z_i N_i. \tag{2-20}$$

Substitution of equation (2-18) into (2-20) gives

$$i_2 = -\kappa \nabla \phi_2 - F \sum_i z_i D_i \epsilon \nabla c_i, \tag{2-21}$$

where κ is the solution conductivity defined by

$$\kappa = F^2 \sum_i z_i^2 u_i \epsilon c_i. \tag{2-22}$$

The convective term of N_i cannot contribute to current flow if we assume electroneutrality holds outside the double layer, because bulk flow of neutral solution cannot carry current. It thus is zero in equation (2-21). The electroneutrality condition is given by

$$\sum_i z_i c_i = 0. \tag{2-23}$$

This equation may not hold extremely well within a small pore where double layers may cover most of the pore cross section. The activated carbon used in experiments contained approximately 60% of its surface area in micropores of less than 20 Å. For the solution

between carbon granules, however, where the most flow occurs, this assumption will be good.

The model as proposed contains several assumptions. First, the charge and potential are assumed to be the major factors determining ionic adsorption. The double-layer capacity has been assumed to be constant (see equation 2-15). In reality, it will vary with potential and concentration. The dependence of adsorption on bulk concentration is ignored. Also, the double layer is assumed to be in local equilibrium according to the potential difference $\phi_1-\phi_2$. The kinetics of adsorption are assumed to be very fast. As mentioned earlier, the solution-phase potential and concentration have been averaged and thus are uniform across any pore. This effectively neglects any mass-transfer resistance. Actually, species must diffuse from the bulk to the porous carbon, where it must diffuse in and adsorb. On regeneration, the reverse must occur. Any or all of these assumptions could be relaxed with varying degrees of difficulty. Experimental results should help in assessing the assumptions.

2.7. Model Solution

The way Johnson, *et al.*,[30] solve the above equations is to initially ignore concentration variations. This allows calculation of the current-time behavior. The current-time behavior can then be substituted back in to calculate the concentration variation it would imply. In the absence of concentration variations, equation (2-21) becomes

$$i_2 = -\kappa \nabla \phi_2, \tag{2-24}$$

which is Ohm's law for the solution phase. With no concentration variation, κ can be assumed constant, and equation 2-16 can be temporarily ignored. The system of equations reduces to Ohm's law in each phase (equations 2-19 and 2-24), a double-layer charging equation 2-15, and a conservation of current equation (see the divergence terms of equation 2-15). Thus we have four equations and four unknowns (i_1, i_2, ϕ_1, and ϕ_2). The matrix-phase conductivity σ will be assumed constant, along with the double-layer capacity per unit volume aC. With constant properties, the situation can be described using an equivalent circuit. Figure 2-6 shows the equivalent circuit through the porous electrode relative to a reference electrode placed in solution nearby. Charging the ideally-polarizable porous electrode is analogous to charging a series of capacitors. A variable transformation will reduce the remaining equations to a familiar form. Combining equations 2-19 and 2-24 with

$$Y = \frac{i_1}{\sigma} - \frac{i_2}{\kappa} \tag{2-25}$$

and

$$\theta = \phi_1 - \phi_2 \tag{2-26}$$

gives

$$Y = -\nabla \theta. \tag{2-27}$$

From equation 2-15, we see that

$$\nabla \cdot i_2 = aC \frac{\partial \theta}{\partial t}. \tag{2-28}$$

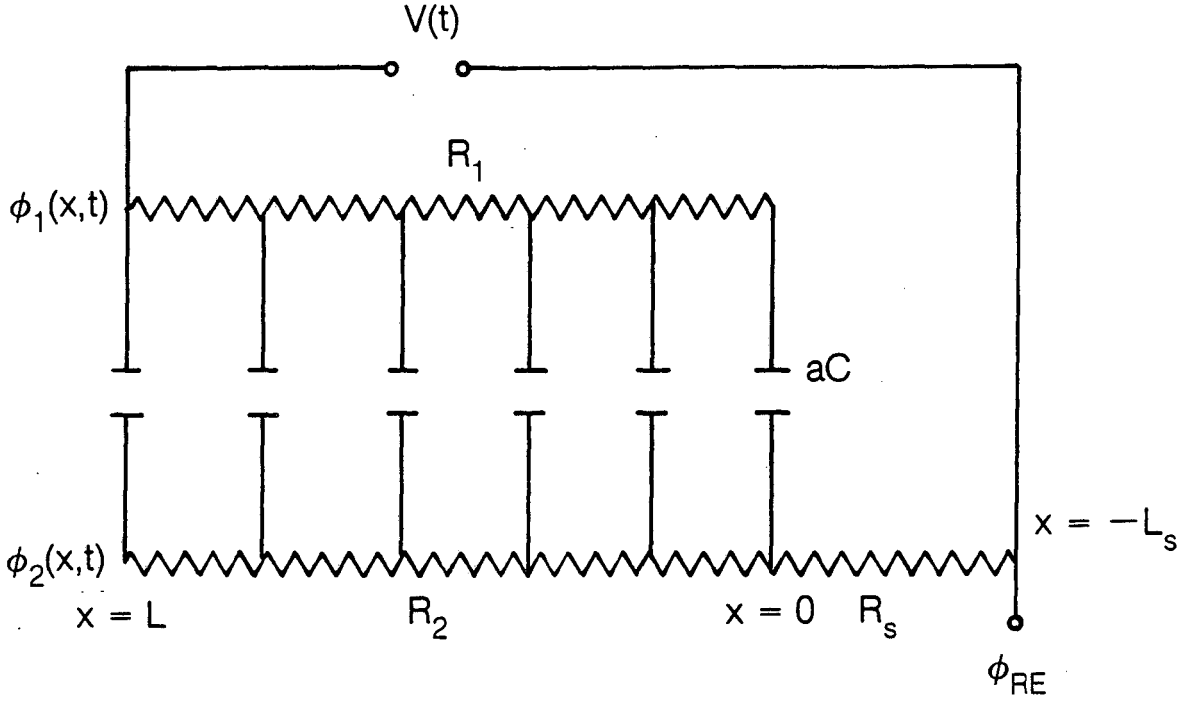

Figure 2-6. Equivalent electrical circuit for an ideally-polarizable porous electrode with a reference electrode in solution between the porous and counter electrodes.

The term $\nabla \cdot i_2$ can be eliminated by taking the divergence of equation 2-25 and noting that $\nabla \cdot i_2 = -\nabla \cdot i_1$ (see equation 2-15). The result is

$$\frac{\partial \theta}{\partial t} = \alpha \nabla^2 \theta \tag{2-29}$$

where

$$\alpha = \frac{\kappa \sigma}{aC(\kappa+\sigma)}. \tag{2-30}$$

Equation (2-29) is analogous to a transient diffusion or heat-conduction equation. Thus α could be considered an electrical diffusivity. A double-layer charging wave can be thought to penetrate the porous electrode from each end. The capacitors of figure 2-6 will charge from the ends towards the interior. The value of α is a relative measure of the rate at which the charging wave penetrates. In a case where α is large, as it is if the bed capacity aC is small, the wave moves rapidly, and the bed quickly saturates.

An expression equivalent to equation (2-29) is found by taking the gradient of equation (2-29) and substituting with equation (2-27) to yield

$$\frac{\partial \mathbf{Y}}{\partial t} = \alpha \nabla \nabla \cdot \mathbf{Y}. \tag{2-31}$$

Equation 2-31 is a vector equation. Since our problem is one dimensional in axial distance, the axial component becomes

$$\frac{\partial \mathbf{Y}}{\partial t} = \alpha \frac{\partial^2 \mathbf{Y}}{\partial x^2}. \tag{2-32}$$

It is perhaps easier conceptually to place boundary conditions on equation (2-32) than equation (2-29) because we know the individual phase currents at each end of the electrode and we know the current

at time zero. For a potential step between the porous electrode and the reference electrode at time t=0, boundary conditions can be assigned as follows:

$$t < 0, \quad Y = 0 \quad \text{or } (I=0 \text{ and } V = V_o), \tag{2-33}$$

where V_o is the open-circuit potential between the working and the reference electrode. No current is flowing at times prior to the potential step. At time zero, the potential step occurs. The capacitors in figure 2-6 are initially uncharged and provide no electrical resistance. Thus, the initial current is determined solely by the resistors of figure 2-6 and by the magnitude of the potential step. Because the matrix and solution phases are like resistors in parallel at time zero, each resistor sustains the same potential drop and Y remains zero,

$$t = 0, \quad Y = 0 \quad \text{or } (I_{t=0} = \frac{\Delta VA}{R_T} \text{ and } V = V_o + \Delta V). \tag{2-34}$$

The overall resistance R_T is given by equation (2-40).

At the electrode ends, the current is either all in the solution phase or all in the matrix phase (see figure 2-5). Thus boundary conditions are assigned as follows,

$$x = 0, \quad Y = \frac{-I(t)}{\kappa A} \quad \text{or } (i_2 = I(t)/A) \tag{2-35}$$

and

$$x = L, \quad Y = \frac{I(t)}{\sigma A} \quad \text{or } (i_1 = I(t)/A). \tag{2-36}$$

Solving equation (2-32) will yield Y as a function of position and time. This is accomplished by taking Laplace transforms with respect

to time and solving the resulting ordinary differential equation. The result is most useful when substituted into a voltage balance on the entire cell so that the overall current-versus-time behavior can be found. By Kirchhoff's Law, a voltage balance on the entire cell is given by (see figure 2-6)

$$V(t) + \phi_2(x=L) - \phi_1(x=L) + \int_0^L \frac{i_2}{\kappa}\, dx - \frac{I(t)L_s}{\kappa_s A} = 0. \qquad (2\text{-}37)$$

It is convenient to start at the reference electrode and consider it grounded. Then V(t) represents the working electrode minus the reference electrode potential. The terms of equation 2-37 represent (from the left) the overall working versus reference electrode potential as a function of time (i.e., this value will undergo a step change at time zero in the analysis), the solution and matrix-phase potentials at the current collector (x=L), the solution-phase ohmic potential drop in the electrode, and the potential drop between the reference electrode and the porous electrode. Taking the Laplace transform of equation 2-37 and solving for the Laplace transforms of the cell current $\bar{I}$ and cell potential $\bar{V}$ yields the cell behavior as a function of the transform of the time variable. Getting the result requires substitution with Y(x,s), equation (2-27), and use of a current balance

$$i_1 + i_2 = I(t)/A, \qquad (2\text{-}38)$$

to eliminate i_2, ϕ_1, and ϕ_2, replacing them with the total current as the dependent variable. Note that I(t) is the total current, which is independent of position but which will vary with time. The final

result is

$$\frac{\bar{V} - \frac{V_o}{s}}{\bar{I}} = \frac{R_T}{A}\left[1 + \frac{\frac{1}{\sqrt{s\tau_1}}}{e^{2\sqrt{s\tau_2}} - 1}\left(e^{2\sqrt{s\tau_2}} + 1 + \frac{4\kappa\sigma}{\kappa^2+\sigma^2}e^{\sqrt{s\tau_2}}\right)\right]. \quad (2\text{-}39)$$

Here

$$R_T = \frac{L}{\kappa+\sigma} + \frac{L_s}{\kappa_s}, \quad (2\text{-}40)$$

$$\tau_1 = \left[\frac{R_T(\kappa+\sigma)\kappa\sigma}{2\sqrt{\alpha}(\kappa^2+\sigma^2)}\right]^2, \quad (2\text{-}41)$$

and

$$\tau_2 = \frac{L^2}{\alpha}. \quad (2\text{-}42)$$

The resistance R_T accounts for the matrix and solution resistances in parallel within the electrode and some ohmic resistance between the porous electrode and the reference electrode. The system has two characteristic times, τ_1 and τ_2, which govern behavior at short and long times respectively. The values of τ_1 and τ_2 can often be quite different. In the case where τ_2 is large, $e^{\sqrt{s\tau_2}}$ is large and equation (2-39) reduces to

$$\frac{\bar{V} - \frac{V_o}{s}}{\bar{I}} = \frac{R_T}{A}\left[1 + \frac{1}{\sqrt{s\tau_1}}\right]. \quad (2\text{-}43)$$

For a step change in cell potential at t=0 from V_o to $V_o+\Delta V$, equation 2-43 becomes

$$I(t) = \frac{\Delta V A}{R_T} e^{\frac{t}{\tau_1}} \operatorname{erfc}\left(\sqrt{t/\tau_1}\right). \tag{2-44}$$

This equation is governed by the start-up time constant τ_1. The current has a finite limit at t=0 and decays like $1/\sqrt{t}$ for longer times. At short times (relative to τ_1), the electrode is utilized only near the ends. The electrode length and capillary tip separation play a role in this start-up time. At t=0, this equation yields a current governed solely by ohmic resistance,

$$I_{t=0} = \frac{\Delta V A}{R_T}, \tag{2-45}$$

as predicted from the initial condition since an uncharged capacitor has zero resistance.

For large values of t with respect to τ_1, equation (2-44) becomes

$$I\sqrt{t} \longrightarrow \frac{\Delta V A}{R_T} \sqrt{\tau_1/\pi} = \frac{\Delta V A}{2\sqrt{\pi}} \frac{\kappa+\sigma}{\kappa^2+\sigma^2} \sqrt{aC(\kappa+\sigma)\kappa\sigma}. \tag{2-46}$$

This equation shows that current will drop off with the square root of time roughly during the time between τ_1 and τ_2. Notice that the electrode length, L, and capillary tip separation, L_s, play no role at moderate times. When time becomes on the order of τ_2, the electrode is becoming saturated, and the current decays more rapidly than $1/\sqrt{t}$. Electrode length is important at long times because the electrode capacity depends on the length. The plot in figure 2-7 shows the various regions of current-versus-time during double-layer charging in a porous electrode. The plot displays $I\sqrt{t}$ on the ordinate to show clearly the charging region where $I\sqrt{t}$ is constant. At very

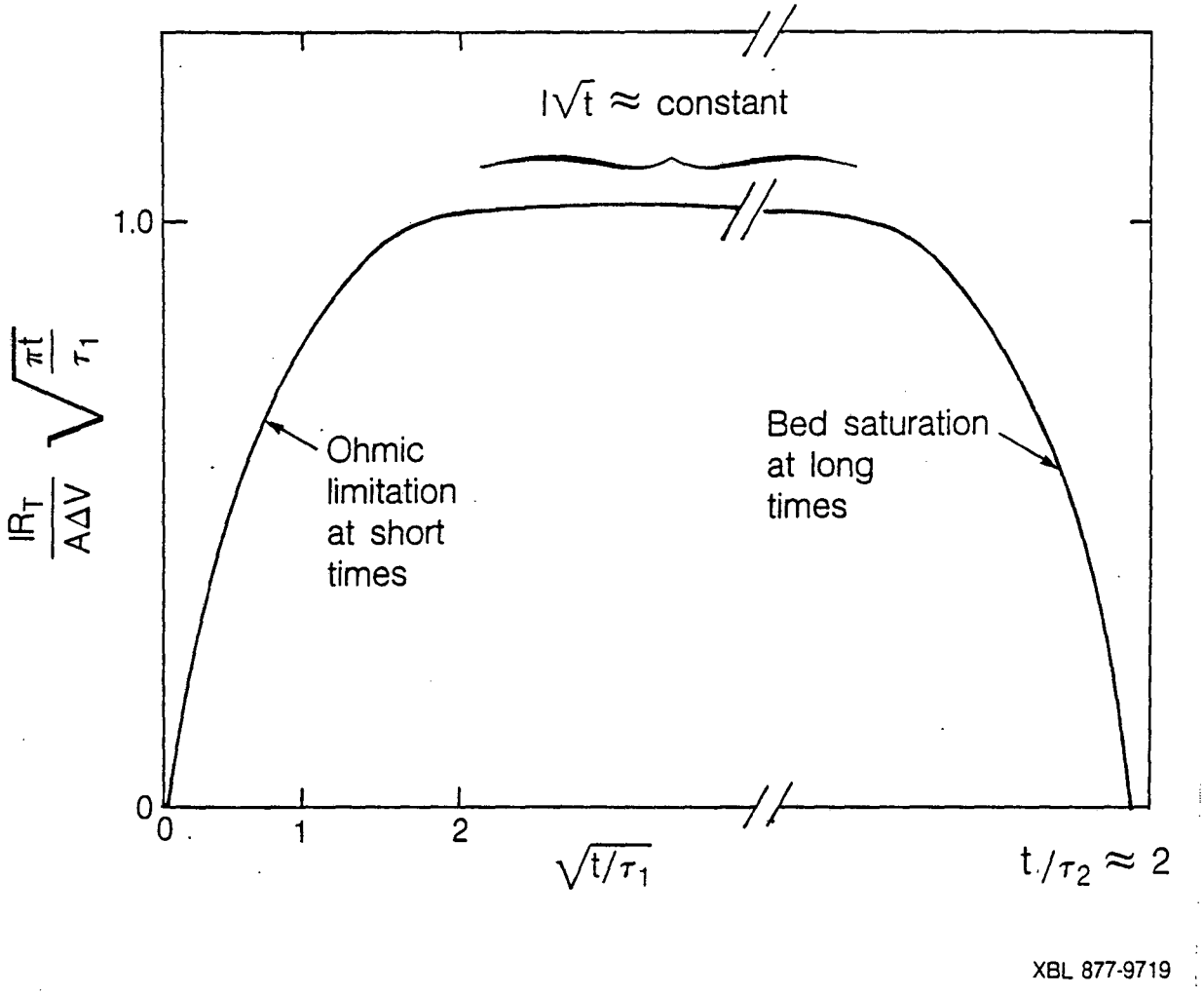

Figure 2-7. Current-versus-time behavior at short, medium, and long times for double-layer charging in a porous electrode.

short times on the figure, a finite rise time with time constant τ_1 is seen. At times roughly between τ_1 and τ_2 the current is decaying with the square root of time so a plateau region occurs. At long times, on the order of τ_2, the electrode is becoming saturated, and the current drops rapidly to zero (see Tiedemann [53] for additional information on the shape of the curve). The plateau region is analogous to the heating of or the diffusion into a semi-infinite slab. In our case the electrical boundary layer is growing in proportion to the square root of time

$$\text{penetration depth} \approx \sqrt{\alpha t}. \tag{2-47}$$

As time passes, only the capacitors deep within the electrode remain uncharged, so the cell current decreases faster than with the square root of time.

2.7.1. Concentration Profiles

Johnson, *et al.*,[30] have solved for the effluent concentration from a stack of porous electrodes with constant half-cycle times and symmetrical desalting and regeneration voltages. They used the method of characteristics to solve the resulting differential equation, a method described by Acrivos[37]. Here we follow the Johnson, *et al.*, paper but apply the analysis to zinc rather than sodium chloride. To generate a concentration profile for zinc ions, we combine equations 2-16 through 2-18 to get

$$\epsilon \frac{\partial c_{Zn}}{\partial t} + \mathbf{v}\cdot\nabla c_{Zn} = \frac{dq_{Zn}}{dq} \frac{I(t)}{A\ L\ z_{Zn}\ F}, \tag{2-48}$$

where the last term in equation 2-48 has been averaged over the length of the bed. Here we have neglected diffusion and migration in the flux expression relative to convection through the bed. The migration term can be neglected due to an excess of supporting electrolyte. The value of $\frac{dq_{Zn}}{dq}$ in reality depends on the relative concentrations of adsorbing species. Determining $\frac{dq_{Zn}}{dq}$ would involve solving the mass balance equations for the other species such as sodium and chloride. The equations would be coupled in concentration through the adsorption term. If we assume $dq_{Zn}/dq = 1$, however, we can progress toward a result of qualitative interest. If we also assume that the plateau region of figure 2-7 occupies a large fraction of a removal or regeneration half cycle, then $I\sqrt{t}$ will be constant. Thus I(t) can be replaced by a constant over $\sqrt{t}$ (see equation 2-46), and equation 2-48 can be solved.

The effluent zinc concentration is shown in figure 2-8, where Δc_{Zn} is the effluent minus the feed zinc concentration and I_{ave} is the average cell current during a half cycle of duration T. The bed void fraction is ϵ. The figure shows the zinc concentration cycling about some feed concentration, assumed constant. When t = T, the potential versus the reference electrode is reversed, and zinc is repelled from the surface. The magnitude of the concentration swings should be proportional to the applied potential and to $\frac{dq_i}{dq}$. The case solved had $dq_i/dq = 1$ and so is a best-case scenario. The presence of other adsorbing species such as sodium will compete with the zinc and hurt the separation. The relative lengths of the residence and

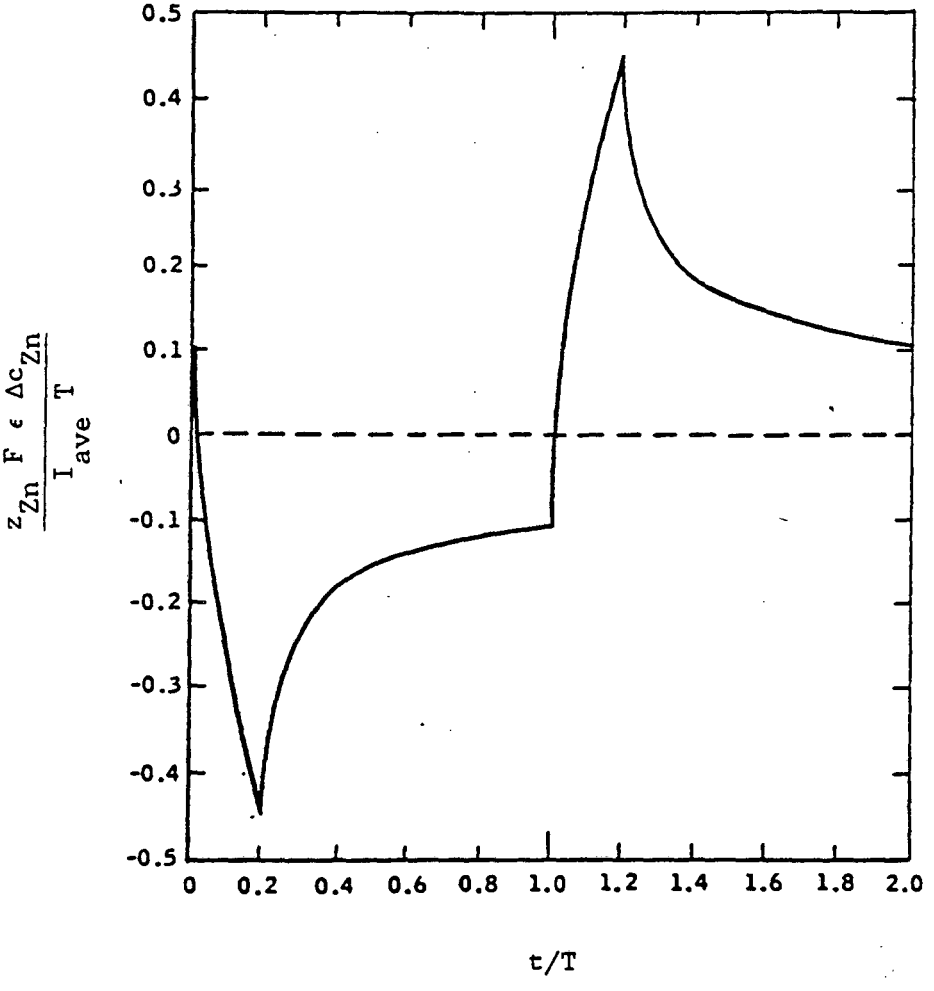

Figure 2-8. Effluent zinc concentration from porous electrosorption electrode.

half-cycle times are also important. Any half-cycle time must be greater than the residence time or product water will not have exited the reactor. The figure shows the case where $\frac{t_{res}}{T} = 0.2$. Fluid entering the electrode at the time of switching the potential (i.e., $t = 0$ or $t = T$) is in the bed when the current is highest and thus is the most desalted or concentrated at the exit. Fluid entering the bed later is subjected to lower currents and thus the effluent concentration varies less from the feed level. The sharp corners on the curve are a result of neglecting axial dispersion. Experimental results on desalination of brackish waters have shown effluent concentrations to follow roughly this form (see Johnson, *et al.*[29]).

CHAPTER 3

Experimental Procedures

3.1. Rotating-Disk Electrode Experiments

Preliminary experiments were performed on a rotating-disk electrode to characterize the electrochemical system. The objective was to use the double-layer capacity calculated from potential-sweep experiments as a design parameter for the column experiments. Various concentrations of NaCl and $ZnCl_2$ and various pH values were tried.

Another objective was to define a range of potentials within which charge-transfer reactions are negligible. This range was compared with the range found for the porous electrode.

3.1.1. Equipment

The equipment used for the RDE experiments consisted of a Pine Instruments RDE 3 Potentiostat, a Hewlett Packard 7047A X-Y chart recorder, and a Pine Instruments PIR working electrode rotator. The instrumentation is as shown in figure 3-1. Keithley 173A multimeters were inserted between the potentiostat and the recorder to check the current and potential outputs to the recorder. Upon verification that the recorder values matched the Keithley 173A readings, the multimeters were removed from the circuit.

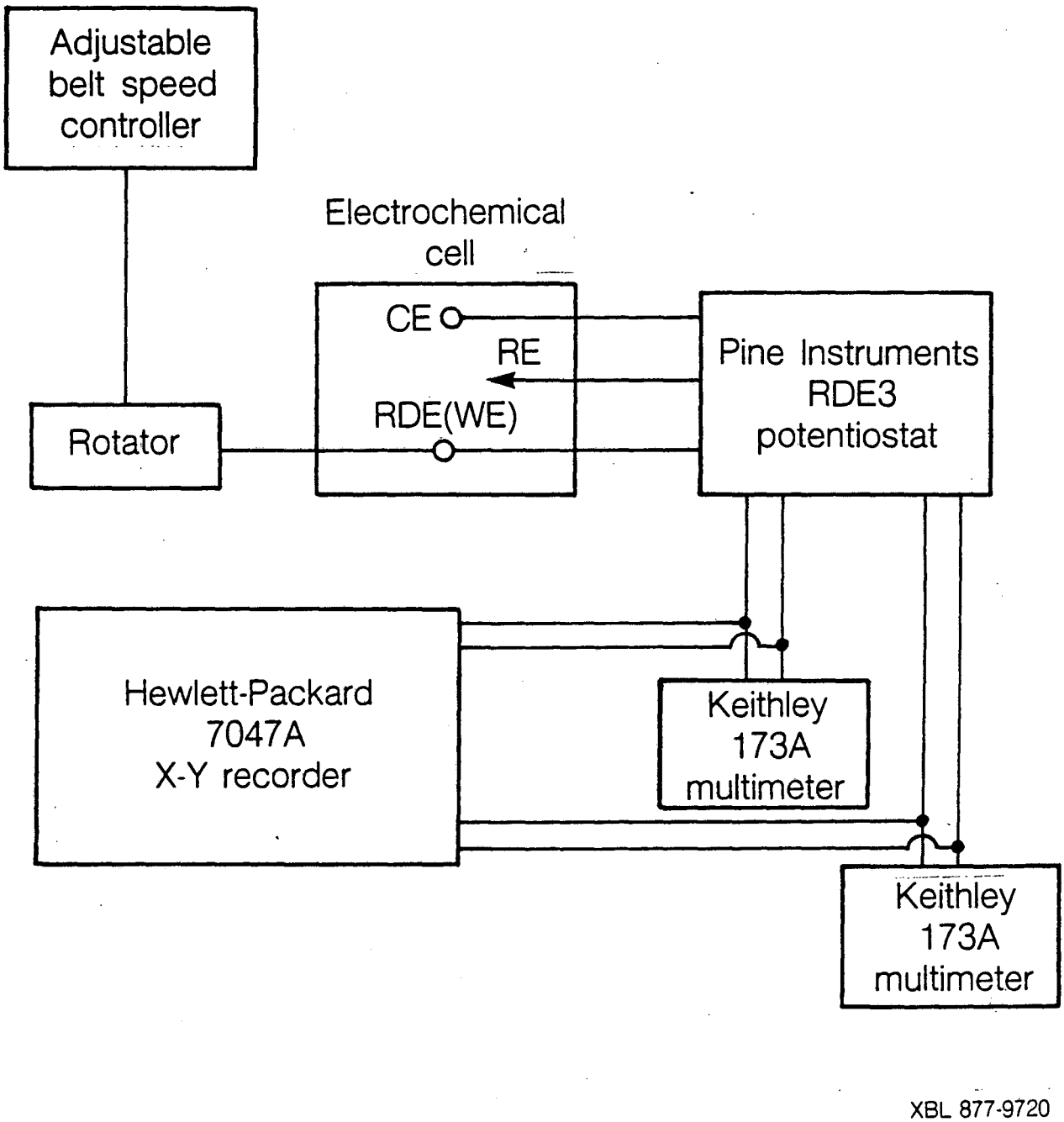

Figure 3-1. Schematic of equipment used in RDE experiments.

The multimeters were removed to simplify the circuitry and minimize the possibility of ground loops. The Keithley meters were the wall-plug-in type and, though the AC outlet is electrically isolated, presented the chance that current could leak to ground. Removing the meters did not change the system performance, so ground loops were not a problem.

3.1.2. Cell Apparatus

A diagram of the electrochemical cell is shown in figure 3-2. The cell held solutions of about one liter. The reference and counter electrodes were in side chambers, separated from the main chamber by glass frits. The frits inhibit convective mixing between the main and side chambers. The counterelectrode was a platinum-rhodium screen, as was used in the column experiments, and represents a noncorrosive surface for gas evolution reactions. The reference electrode was saturated calomel, chosen because it is reversible to chloride ion and chloride solutions were being studied. The working electrode (RDE) was glassy carbon. This was chosen to simulate the surface on granular activated carbon, although the surfaces are different. Electrosorption on granular activated carbon was under study in the column experiments.

The rotation rate of the RDE was set by manually gearing the belt drive. Rotation rates from 900 to 3600 rpm were investigated. Rates were checked with a Shimpo Digitacho DT-103B hand-held tachometer.

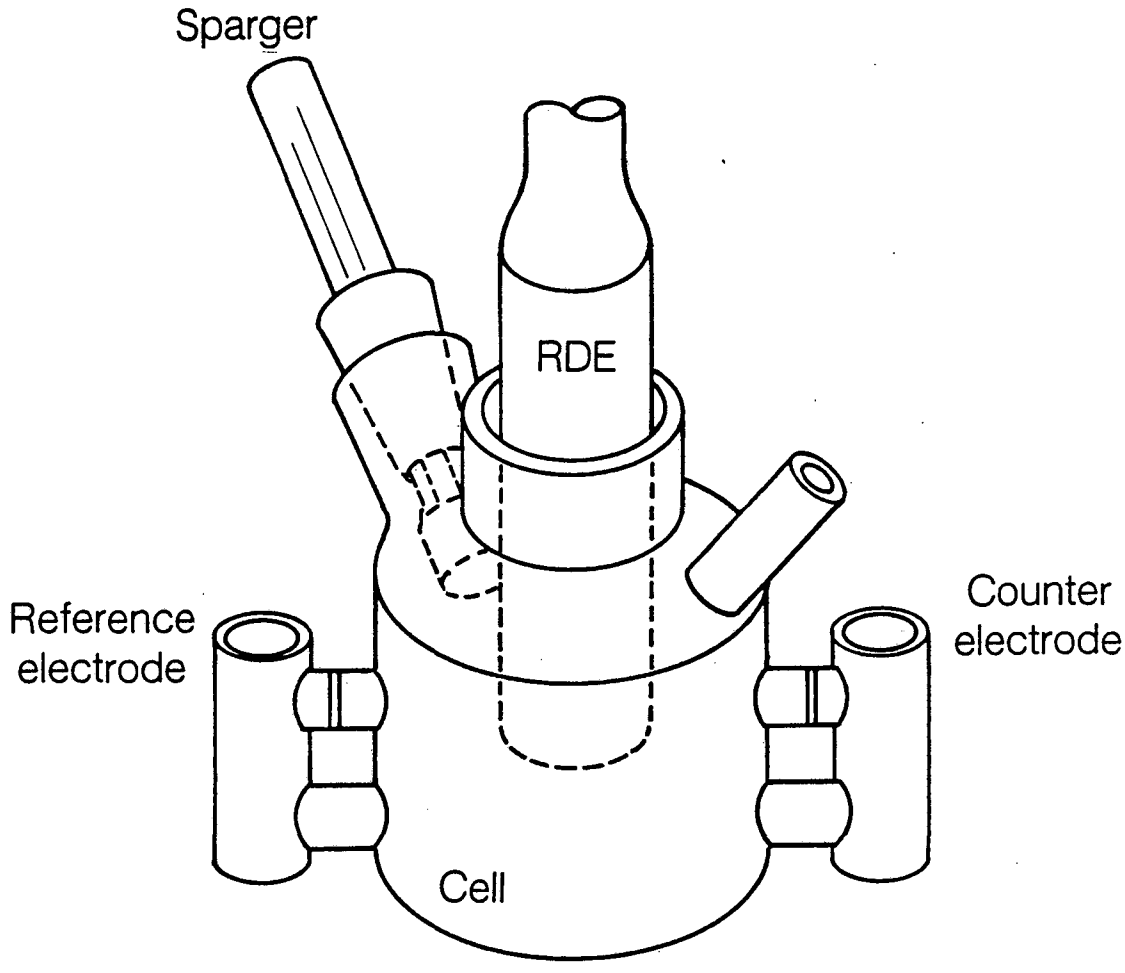

Figure 3-2. Sketch of the rotating disk electrode cell.

The RDE was cleaned using a Buehler Ecomet III polishing wheel, one-micron diamond paste, the microcloth reserved for one micron paste, and water as lubricant. Disks used in plating or corrosion studies typically require a coarser paste (i.e., 9 micron) for an initial polish. No plating was done here so only one micron paste was used. The disk was polished once or twice per day, rinsed, and blotted dry. Current/potential curves before and after polishing showed slight but irreproducible differences.

3.2. Cell Solutions

Cell solutions were made in a one liter Erlenmeyer flask. Water of resistivity over 16 MΩ-cm was used. Sodium chloride (99.5% pure, Baker Analyzed lot# 121376) in granular form was weighed on the two-arm balance (accuracy ± 0.1 gram). Granular zinc chloride (Mallinckrodt 8780 lot# KTTA, 99.18% pure) was weighed on the analytical balance. Roughly 300 mg $ZnCl_2$ in a liter yields 145 ppm Zn^{++}, whereas about 59 g NaCl makes one liter of 1 M NaCl. Obtaining similar accuracies required using the analytical balance for the $ZnCl_2$.

Zinc chloride crystals are hygroscopic. Atmospheric water vapor condenses measurably on the crystals in the time of a weighing. Thus, weighing was done by taring roughly 5 ml water, dissolving the crystals in this solution, and weighing again.

Solutions were sparged for 40 minutes with nitrogen gas prior to experimenting. This is because any dissolved oxygen in solution would be easily reduced at the RDE. Solution pH was adjusted using 1

M HCl solution, made from concentrated (37 wt% = 12 N) HCl solution. The pH was measured with a Leeds and Northrup nonrefillable tear-drop glass pH electrode. The reference electrode for pH measurements was SCE. The pH electrode was calibrated linearly between either standard buffers at pH 1.0 and 4.01 or at pH 4.01 and 7.00, as needed. Solution pH measured before and after a run showed little difference.

3.3. Procedures

Cyclic voltametry was used. The internal voltage generator of the potentiostat was set to sweep the working versus reference electrode at a specified rate between desired limits. The range was typically ±1 volt versus SCE at 2 or 10 volts per minute. In addition to varying the sweep rate, the disk rotation rate, zinc and sodium chloride concentrations, and solution pH all were varied. The X-Y recorder plotted current versus potential. Results were analyzed to determine the overall double-layer capacitance and the potentials at which the disk behaved as an ideally-polarizable electrode.

3.4. Porous-Electrode Experiments

The porous electrode apparatus was designed to isolate the adsorption electrochemistry to a single electrode. Previous studies on desalting water using double-layer adsorption had utilized an alternating stack of porous anodes and cathodes (see Johnson, *et al.*[29]). The cathodes were basically cation-responders, and the anodes attracted or repelled anions, depending on whether the cell was removing salt or whether it was being regenerated. Potentials of the cathode stack relative to the anode stack were controlled and measured against reference electrode potentials. Such a stack of electrodes cannot elucidate the role of the cation or anion responders.

3.4.1. Apparatus

To study the role of a cation responder, the cell contains a single porous electrode (see figure 3-3). Electroneutrality is maintained because the counterelectrode operates a faradaic reaction to balance the double-layer adsorption reaction. The charge transferred in this reaction must equal the charge equivalent of ions adsorbed on the porous electrode, neglecting side reactions. The reactions of figure 3-3 depict the situation where the porous electrode is poised negatively to adsorb cations. During bed regeneration, the desorption reactions occur at the porous electrode, and hydrogen evolution or reduction of dissolved oxygen or chlorine occurs at the counterelectrode. This cell was first used by Matlosz[26] to study mercury removal from contaminated brine on reticulated vitreous carbon

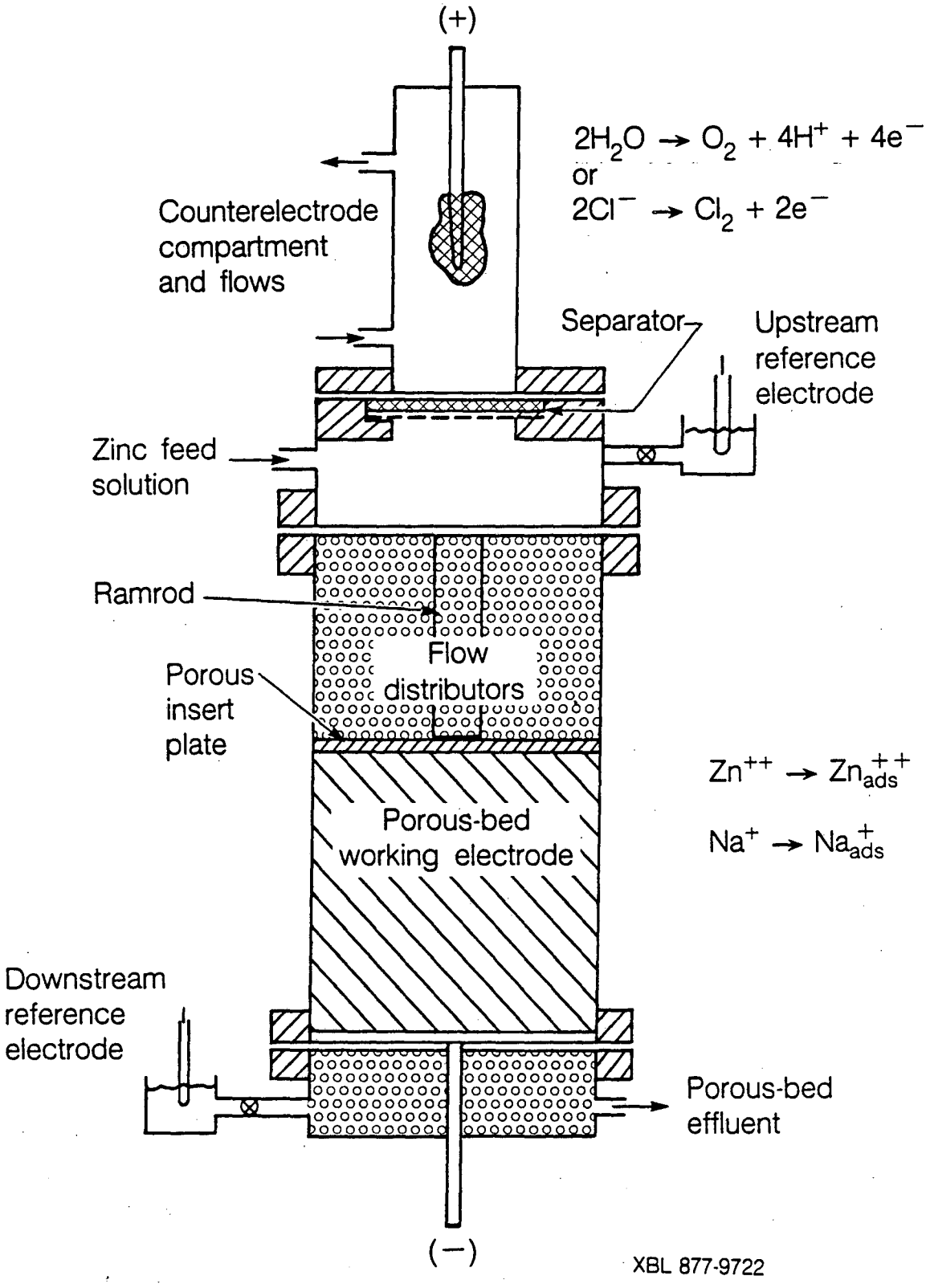

Figure 3-3. Features of the electrochemical cell.

(RVC). Later, Trost[24] used the same cell for examining lead removal on RVC. The cell is modified here to accommodate a granular porous electrode.

3.4.2. Equipment

Figure 3-4 shows the system. Not shown in the photograph are the sampling ports inserted near the bed entrance and exit to sample the feed and effluent solution. Potential was controlled by an AIS (Division of Floyd Bell Associates, Incorporated) model V-2LR-D potentiostat. The potentiostat grounds the working electrode. It drives the counterelectrode potential until the working electrode versus reference electrode potential becomes the operator-set value. Displays on the potentiostat show total current, cell voltage, and working versus reference-electrode potential. These values were checked using a Keithley 173A multimeter and then accepted (see "Measurements," section 3.4.6 for methods). Fluid Metering brand pumps controlled the flows through the porous and counter electrode compartments separately. Oscillations in the working-electrode flow were minimized by a flow-damper placed after the pump. The working electrode flow rate was measured by a rotameter (Gilmont B-6480; 0 to 35 ml/min). All tubing was Bev-A-Line® and tube-to-tube fittings (Cole-Parmer polypropylene) were wrapped on the threads with teflon tape to insure against leakage.

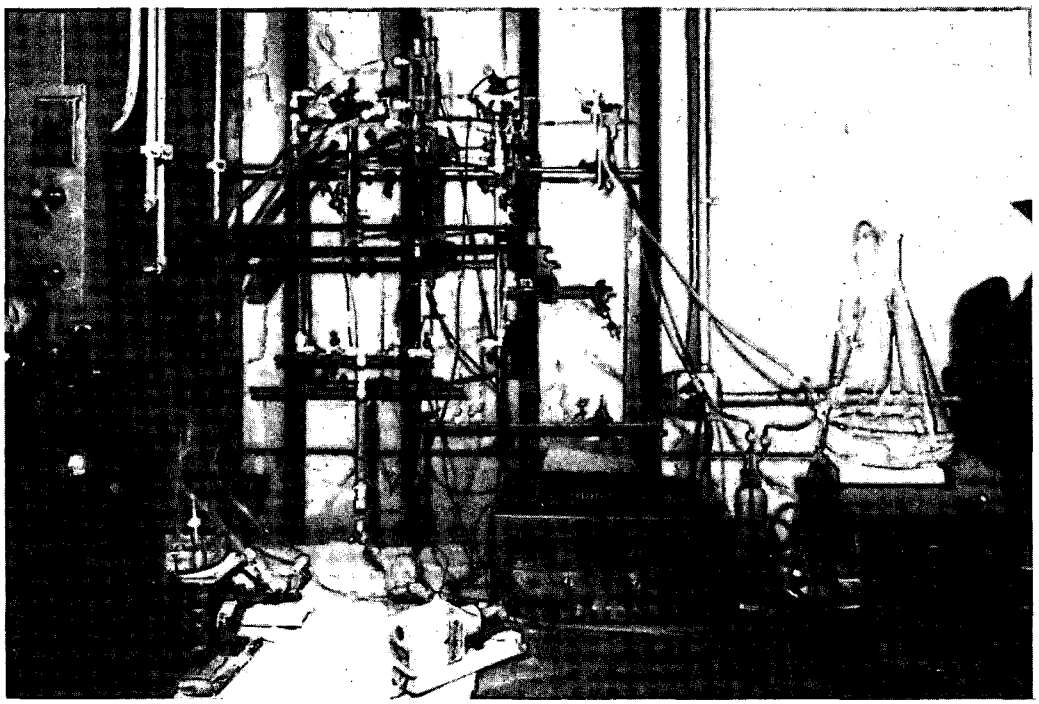

XBB 841-30

Figure 3-4. Photograph of the entire porous-electrode experimental system.

3.4.3. Cell Materials

All cell materials used were corrosion resistant. The entire porous electrode compartment was encased in 1/4" wall, 2" inner diameter Plexiglas® tubing. The porous electrode was made of pretreated granular activated carbon (see "Carbon Pretreatment," section 3.4.7 for details). Porous carbon was pressed against the current collector by means of a ramrod/insert plate assembly. This enhanced the electrical conductivity of the carbon by lowering particle-to-particle contact resistance.

The insert plate was machined from 1/8" Plexiglas® sheet to fit the column diameter within 0.003". A square matrix of 0.041" diameter holes spaced 0.063" on a side provided porosity. To enhance rigidity, a perimeter boundary 1/8" wide was left undrilled. The tight matrix of holes caused the piece to warp slightly and to become somewhat flexible. Though it transmitted ramrod pressure as designed, a thicker piece with larger holes, perhaps unevenly sized, would provide more rigidity and more evenly transmit ramrod pressure. The ramrod was 3/8" Plexiglas® rod. It was seated into a crossbar on an open-disk piece inserted beneath the zinc feed port (see figure 3-3). Two set screws on the insert tightened the ramrod into place prior to final cell assembly.

Glass beads (1/4" diameter) above and below the porous electrode served to smooth any velocity profiles. The beads beneath the bed also shortened the time for solution exiting the bed to reach the sampling port (roughly seven minutes at normal flow rates).

The current collector plate and both the working and counter electrode current collector rods were made of tantalum. Tantalum is extremely resistive to chemical attack at moderate temperatures. Each rod led out of the reactor through sealed polypropylene compression fittings, allowing attachment of potentiostat leads. The back of the current collector plate and the rod of the porous electrode compartment were each coated with Kyner® (Pennwalt Corporation, Philadelphia, PA) to prevent electrochemical reactions below the bed. A platinum-rhodium screen made up the counterelectrode and represents a corrosion resistant surface for gas evolution reactions.

Separating the working and counter electrode compartments was a Nafion® (Dupont Company) perfluorosulfonic acid ion exchange membrane. The membrane is negatively charged, with pores of molecular dimension. It is impervious to water and will transmit only cations. The membrane allows independent control of the working electrode flow rate and composition.

Reference-electrode compartments were separated from the main cell by lines containing glass stopcocks. Wetting the stopcocks and setting them closed prevented fluid from leaking out the lines while maintaining electrical continuity. Greasing the stopcocks tended to sever the electrical circuit and should be avoided.

3.4.3.1. Carbon Properties

The carbon used for the electrode material was a Darco® 20-40 mesh activated carbon (lot number 1209BJ). Activated carbon was

selected over reticulated vitreous carbon (RVC) because the specific surface area of activated carbon is roughly a million times greater. Measurements of the conductivity, the void fraction, and the density were made in the laboratory. The BET surface area was measured by N_2 desorption by the analytical laboratory. The density was calculated by weighing carbon of a volume as measured in a graduated cylinder. The void fraction was obtained by adding carbon to a known volume of liquid and measuring the liquid rise. The wetted carbon was stirred to remove trapped air and the cylinder was sealed and left overnight to aid in wetting the carbon pores. No check was made for testing whether the micropores were filled. We assume that an overall porosity, including macro and micro pores, was calculated. Perhaps alternating between applying vacuum and pressure to the wetted carbon could be used to achieve maximum filling. Porosities could be compared with those calculated at short times (i.e., macroporosity) to distinguish between micro and macro porosity.

Matrix conductivity was measured by packing the experimental cell with pretreated, dried carbon and using an ohmmeter. Leads were connected between the cell current collector and a piece of aluminum foil sandwiched between the ramrod-insert plate and the carbon. The length and cross sectional area of carbon allowed calculation of the conductivity. The conductivity was found to be very sensitive to applied pressure, indicating particle-to-particle contact resistance was important. Applying heavy hand pressure (versus light hand pressure) on the ramrod increased the conductivity by an order of magni-

tude. Screwing down the ramrod, as in actual cell operation, gave a conductivity roughly equal to that with maximum hand pressure. This is the value reported. Table 3-1 gives the carbon data measured.

3.4.4. Solutions

For most runs, both the working and counter electrode streams contained 1 M NaCl. The working electrode stream also contained roughly 145 ppm zinc ions. Solutions were made and housed in 3 to 5 liter Erlenmeyer flasks. Brands of chemicals, balances used, lot numbers, etc., are the same as those listed in the section headed Rotating Disk Experimental Procedure.

The counterelectrode solution was recycled continuously. Its pH would fluctuate depending on whether oxygen, chlorine, or hydrogen evolution was occurring. Thus, a pH change in the stream provided a quick way of determining the counterelectrode reaction. The counterelectrode solution flowed upwards, away from the Nafion®, sweeping evolved gases up and out.

Table 3-1. Data measured for Darco® 20-40 activated carbon.

parameter	value	units
σ	0.092	mho/cm
ρ	0.43	g/cm^3
ϵ	0.75	void frac
a	6.8×10^6	cm^2/cm^3*

* (This BET surface area is equivalent to 1580 m^2/g.)

Working electrode solution flowed downward, away from the counterelectrode, so fresh solution would meet the bed at the point nearest the counterelectrode. If a reaction is concentrated at the bed inlet, as many deposition reactions are, this flow configuration minimizes ohmic potential drop in the solution phase.[19] In an adsorption reaction, the reaction is probably more spread out, and it is unclear what the "best" arrangement might be.

Prior to filling or running, the working-electrode solution was sparged with nitrogen and stirred for at least 45 minutes. Light sparging continued throughout the run. Sparging removed dissolved oxygen, which would be readily reduced at the porous electrode. Sparging also drives off carbon dioxide, thus tending to raise the pH from just over 5 to over six. Upon passing through the bed, the pH tended to drop to roughly four units, apparently due to incomplete HCl removal after the carbon pretreatment. Untreated carbon was neutral in pH tests. A typical working electrode solution flow rate was 5.6 ml/min, giving a residence time of roughly 24 minutes in the bed. The effluent, working-electrode solution was collected in a waste flask and dumped.

3.4.5. Start-up/Shut-down

After sparging, initial column filling proceeded from the bottom to the top of the bed, and was completed from above, bypassing the bed. This procedure minimized the volume of solution contacting the bed prior to a run. Some difficulty was generally encountered in removing air bubbles from under the Nafion® membrane. To start a

run, the pumps and potentiostat were turned on, and a lab-timer (Kwik-set, 1000 minute) was started. The working electrode solution flow was set to 5.6 ml/min by reading the rotameter and controlling the pump setting. The rate was periodically checked with a stopwatch and a graduated cylinder. Shut-down involved turning off the pumps, potentiostat, and sparge-gas and stopping the timer. The column was not drained. Start-up at a later time is as listed above. New feed solution was made as necessary, taking care to match zinc-ion concentrations with the old feed.

3.4.6. Measurements

Data recorded during a run included the time, working electrode solution flow rate, cell current, cell potential, working electrode versus each reference electrode potential, effluent samples, feed samples, pH readings, and general comments. Before and after running, open-circuit potentials (typically the working electrode versus the upstream reference electrode potential) were recorded to determine if its value would reflect the "state" of the bed. Ideally polarizable electrodes have an open-circuit potential which can reflect the state of surface charge.[38] In general, the value of the working versus reference electrode potential was cycled approximately about the open-circuit potential in attempts to drive a removal or regenerative adsorption reaction.

The reason two reference electrodes were used deserves explaining. Reference electrodes sense the solution-phase potential at a point in the column. Assuming the chloride ion concentration

(typically 1 M) does not change upon passing through the bed, the two electrodes might be expected to detect the same potential. However, if current flows, the upstream and downstream points in solution are in different electrical states, and therefore the electrodes will detect different potentials. The magnitude of this potential difference is the solution-phase ohmic drop through the bed (i.e., $\phi_{SCE}^{upstream} - \phi_{SCE}^{downstream}$). The upstream reference electrode reads a value of potential containing one centimeter of uncompensated ohmic drop, due to placement of the capillary tip above the insert plate. This additional resistance raises the value of the start-up time constant τ_1 and therefore should be minimized.

Some care was required to measure the ohmic drop. Touching the lead of the reference electrode connected to the potentiostat with a multimeter lead or with fingers perturbed the cell voltage and current badly. Recovery sometimes took 10 minutes. To supply additional impedence relative to that through the reference electrodes, an electrometer (Keithley Model 601, input impedance 10^{14} Ω) was used. The Keithley 173A Multimeter had an input impedance of 10^9 Ω. With rubber gloves, the electrometer leads could be connected directly between the two reference electrodes with no system perturbation. A more stable way to measure the potential of the upstream versus the downstream reference electrode was to measure each with respect to the working electrode and difference the measurements (the working electrode versus the upstream reference was controlled by the potentiostat). The calculated difference is the solution-phase ohmic

drop.

3.4.7. Carbon Pretreatment

The granular activated carbon (GAC) was pretreated by refluxing in a Soxhlet apparatus with HCl/H_2O at azeotropic composition. Roughly 65 g GAC was treated to yield enough carbon to pack the bed. The reboiler was loaded with 253 ml 37 wt% HCl and 247 ml H_2O, which is nearly azeotropic. Figure 3-5 shows the process. Treatment continued for 1 hour of full reflux. The GAC was then rinsed, heated (over a hot plate), stirred, and the water decanted off. The rinsing procedure was repeated three times. Baking 15 hours at 110°C gave drying to approximately the original weight.

Refluxing in HCl was intended to remove acid-soluble impurities, such as metals, from the carbon. It will also neutralize any basic surface sites, which probably has an effect on specific adsorption, but ideally will not affect adsorption in the diffuse double layer. The reboiler solution always turned light-golden yellow during refluxing, a color that exactly matched test ferric chloride solutions. This indicates iron was stripped. Other compounds may have been removed as well. Tests on the pH of post-treated GAC solutions indicate very acidic conditions. When 2.5 grams of acid treated GAC were added to 50 ml water initially at pH 6, the pH dropped to just under 2. Perhaps the rinsing procedure used was not getting all the HCl out. Adding 2.5 grams of untreated GAC to 50 ml of water at pH 5.5 left the pH unchanged.

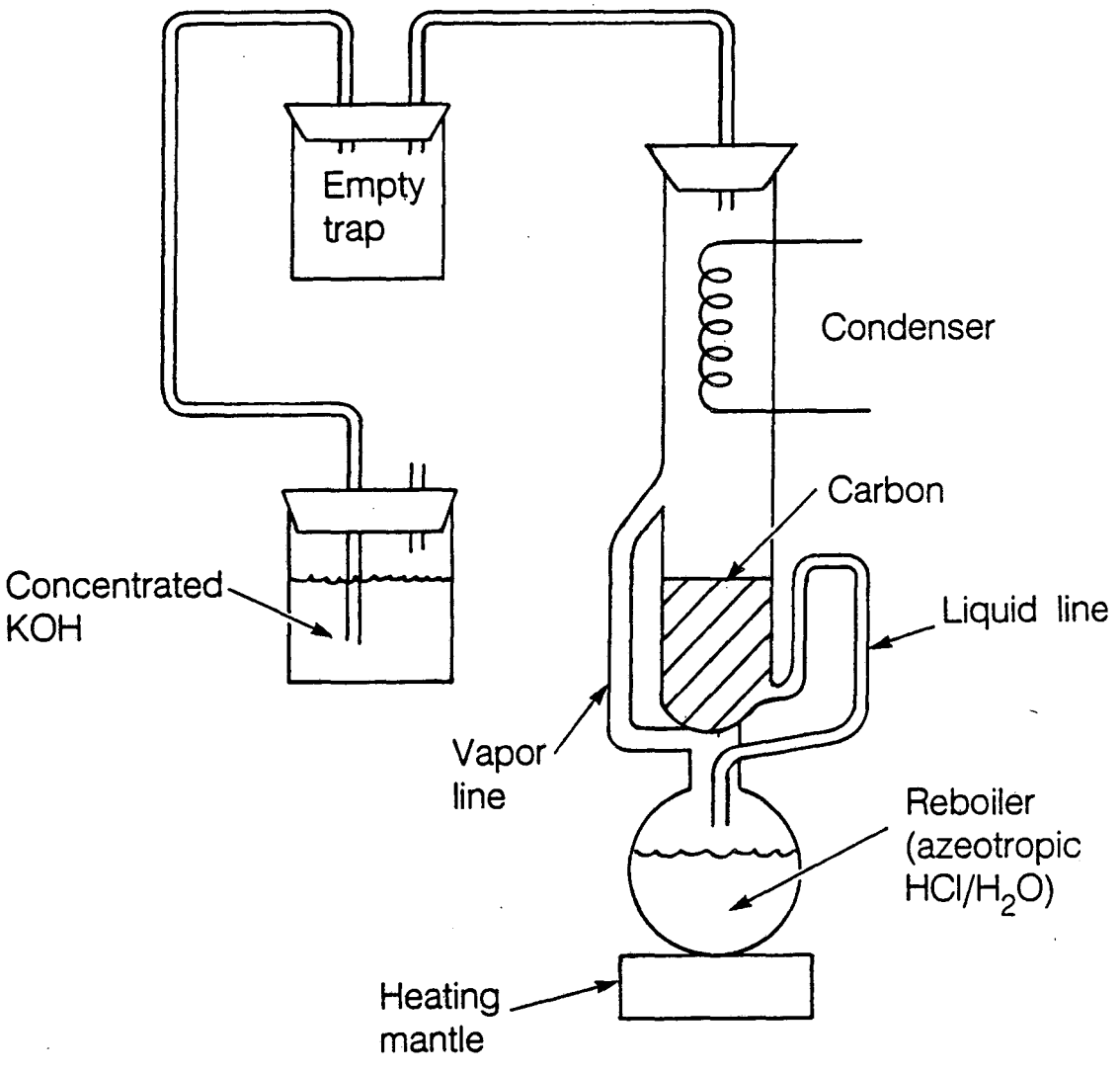

Figure 3-5. Carbon pretreatment refluxing apparatus.

Procedures from the Marquardt studies on desalting water by electrosorption describe a "mixed acid" treatment for the cation-responder. Two volumes of concentrated sulfuric and one volume of concentrated nitric acid were stirred with GAC for an hour or more. This oxidizes the surface. Therefore, they reason, it should be more polar and more receptive to ionic species. Mixed acid pretreatment was not undertaken here. It would be interesting, however, to study the effects of various pretreatment schemes in a well characterized experimental system.

3.4.8. Analytical Technique

Column samples were analyzed for zinc using a Perkin-Elmer 2380 Atomic Absorption Spectrophotometer Students can run samples at a considerable cost savings.

Atomic absorption spectrophotometry uses a hot flame to gasify and atomize a sample. For zinc, a zinc cathode lamp emitted radiation which the zinc in a sample could absorb. At 213.9 nm, the fraction of radiation passing to the detector is reduced significantly by the presence of zinc atoms in the flame. This sensitivity is thus calibrated to standards for determination of unknown concentrations.

Atomic absorption spectrophotometry was chosen for its accuracy, quickness, freedom from interferences, and applicability to compounds other than zinc. Analysis for sodium and many other heavy metals is standard, lending the method nicely to analysis in a study of competitive adsorption, which is a possible continuation of this work.

Zinc concentrations from 0.002 to 1 ppm can be analyzed directly. Samples in this range give a linear signal response versus concentration at 213.9 nanometers. More concentrated solutions can be diluted into this range.

A 500 ppm zinc standard was made by dissolving 0.5 grams of zinc metal, weighed on an analytical balance, into a stoichiometric amount of 37 wt% hydrochloric acid. This was diluted to the mark of a 1 liter volumetric flask with 1 %v/v (i.e., 1 % by volume 37 wt% solution and 99 % water). A 500 ppm standard in an acid-presoaked flask will keep for years.

All dilutions were made using a micropipette (Volac 100 to 1000 μl variable volume), 16 MΩ water, and 25, 50, or 100 ml volumetric flasks. All volumetric flasks were initially soaked overnight in 16 N nitric acid. Later, they were simply triple rinsed and reused. Untreated glassware can ion-exchange appreciably with metal ions at a concentration of 1 ppm in a few hours, seriously affecting detected concentrations. For analysis, standard solutions of 0.2, 0.6, and 1 ppm, as well as a water blank, were used to calibrate the spectrophotometer. The overall accuracy for zinc unknown concentration determinations is roughly ±5 %.

The general literature describes many other methods for zinc ion detection.[39], [40] Among these are a colorimetric method whereby zinc ions form a blue solution with a complexing agent, zincon[41]. The color can be calibrated to zinc concentration with an overall accuracy of ±3 %. This method was discarded because the complex

gradually deteriorates, meaning standards had to be prepared weekly.

Various electrochemical methods exist for metal-ion determination including polarography, coulometric titrations, anodic stripping voltametry,[42], [43] and ion specific electrodes.[44] Anodic stripping voltametry and ion-specific electrodes offer the most promise for on-line detection. An ion-specific electrode for zinc is presently not available on the market. Zinc can be measured by indirect titration using other ion-specific electrodes.

CHAPTER 4

Results and Discussion

The results and discussion will be presented in two parts. First the rotating disk electrode experiments will be discussed, and second the column experiments will be analyzed.

4.1. Rotating-Disk Electrode Results

The results of the rotating disk electrode experiments showed a region of potential for glassy carbon where faradaic reactions will not occur. In figure 4-1, the horizontal portion of the plot represents this capacitive region, where only double-layer charging is important. This region extends from about -0.4 volts to almost 1.0 volts versus SCE. The distance between the positive and negative sweep lines, B, is proportional to the double-layer capacitance. Applying equation 2-14 to the forward and backward sweeps and assuming the transient part dies quickly shows that the magnitude of B should be twice the value of νC_T. From the figure, a capacitance of 69 $\mu F/cm^2$ was calculated. This is quite high. The capacitance appears to be somewhat constant from about -0.2 volts to 0.8 volts versus SCE, however, lending support to the constant capacity assumption of the porous-electrode, double-layer-charging model. The time constant RC_T is roughly half a millisecond for a disk of radius 0.25 cm and capacitance 30 $\mu F/cm^2$ and a solution of conductivity 0.0126 mho/cm. Thus even at sweep rates of 10 volts/min, the transient part

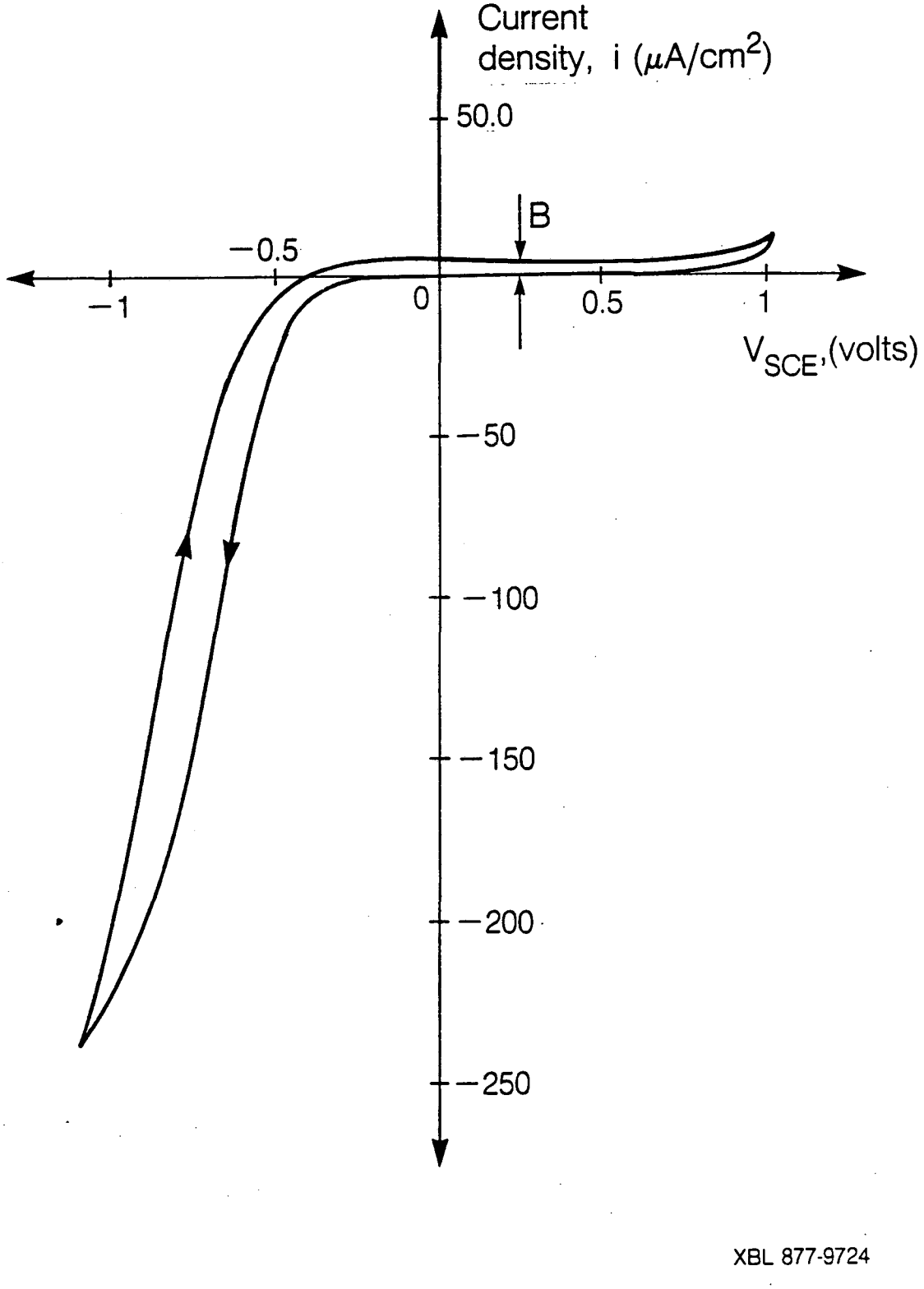

Figure 4-1. Cyclic voltammogram for glassy carbon in a solution of 0.1 M NaCl and 144 ppm Zn^{++} at pH 6 and a sweep rate of 0.033 volts/sec.

of equation 2-14 dies before the potential moves a millivolt into the sweep.

Voltage sweeps done with a resistor and capacitor in series showed current transients which died quickly, approximately according to equation 2-14. The curves traced were horizontal and were also symmetrical about the current axis. A 5 μF ±10% capacitor was tested and a capacity of 4.7 μF was calculated.

The curve of figure 4-1 does not establish uniform charging (i.e., on the negative sweep at 1.0 volt) quite as quickly as equation 2-14 would predict. Also the capacitive region is not symmetrical about the current axis. It appears that the glassy-carbon disk only approximately follows the ideal RC circuit assumed even in the capacitive region.

On a rotating-disk electrode, the mass-transfer boundary layer thickness is determined by the rotation rate. If a reaction is mass-transfer limited on a rotating-disk electrode, the current will increase with $\Omega^{1/2}$, where Ω is the disk rotation rate (see Levich[45]). The capacitive current did not vary with rotation rate, indicating that the adsorption reaction occurred without mass-transfer limitations. Double-layer adsorption generally occurs so close to the electrode that bulk convection has no effect, thus substantiating this result. The current at negative potentials in figure 4-1 appears to result from a charge-transfer reduction reaction at the potential for hydrogen evolution. The magnitude of the current at -1.0 volts versus SCE varied with the disk rotation rate.

This indicated a mass-transfer process from the bulk to the interface was occurring, as is characteristic of charge-transfer reactions such as hydrogen evolution.

The values of double-layer capacitance calculated should be independent of sweep rate. As the sweep rate goes to zero, any capacitive current will drop to zero. Figure 4-2 indicates that (in the capacitive region of figure 4-1) a nonzero current results as the line is extrapolated to zero sweep rate. However, this non-zero current is small when compared to the capacitive currents at higher sweep rates. Steady-state polarization data showed no current flowing from 1.0 to -0.3 volts versus SCE. Double-layer capacitances as high as 100 $\mu F/cm^2$ were calculated at the lower sweep rates (i.e., 0.0083 V/sec), assuming faradaic reactions were negligible. At higher sweep rates, such as 0.166 V/sec, capacitances of roughly 65 $\mu F/cm^2$ were calculated, where the capacitive current had a relatively larger effect. The slope of the line in figure 4-2 gives a capacitance value which ignores any faradaic reactions. This slope is 61 $\mu F/cm^2$, which is still high. Evidently, something besides the faradaic reactions is responsible for the large capacitance values calculated. Perhaps the RDE surface was slightly porous so the actual area was larger than the one used in the calculations.

The double-layer capacitance can be expected to depend on ionic concentrations in solution. The effect of pH is shown in figure 4-3. The figure shows that as the pH decreases, the double-layer capacitance increases dramatically. If the diffuse-layer capacitance were

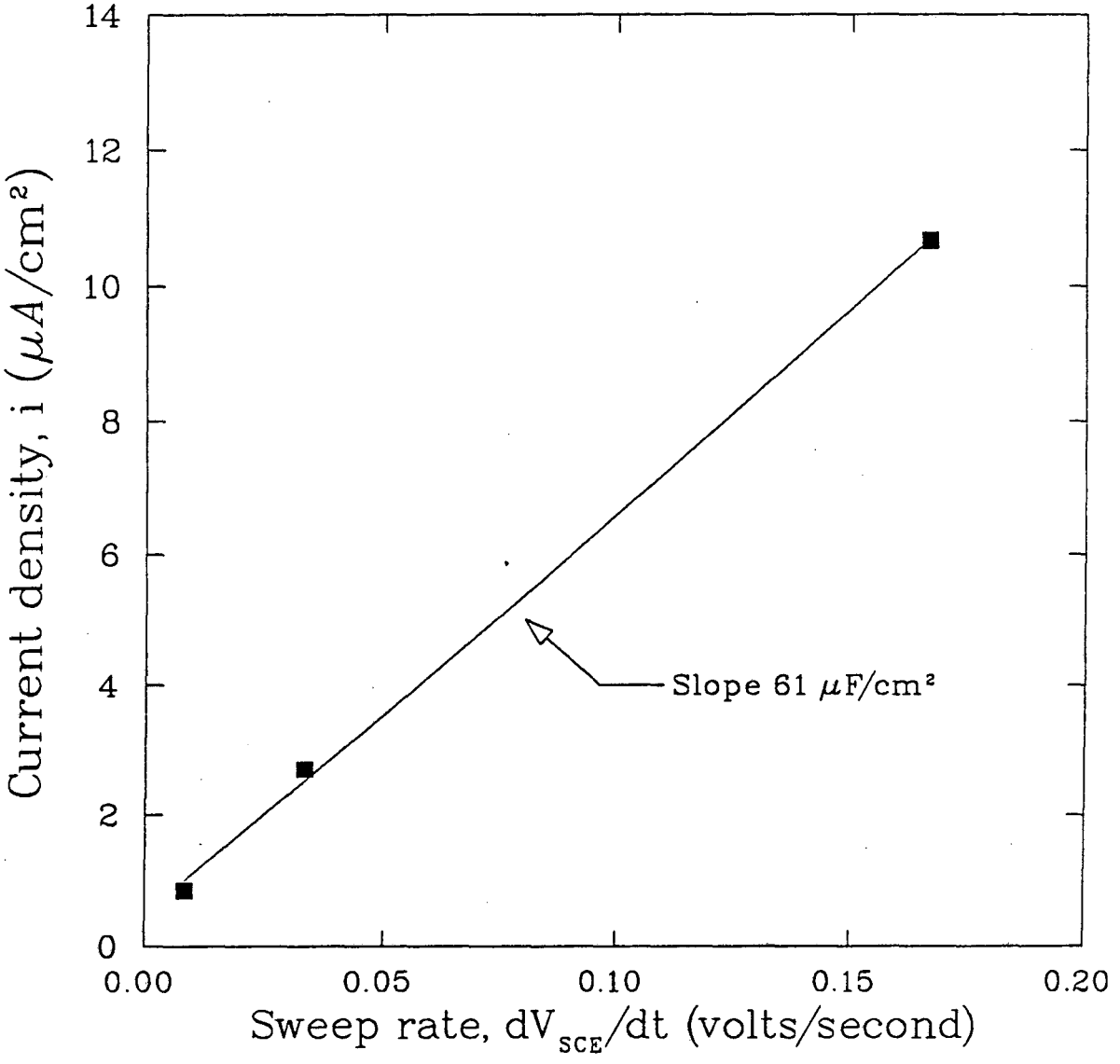

Figure 4-2. Current versus sweep rate for solution of 1 M NaCl and 149 ppm Zn^{++} at pH 6 in capacitive region (0.5 V versus SCE) on glassy carbon RDE.

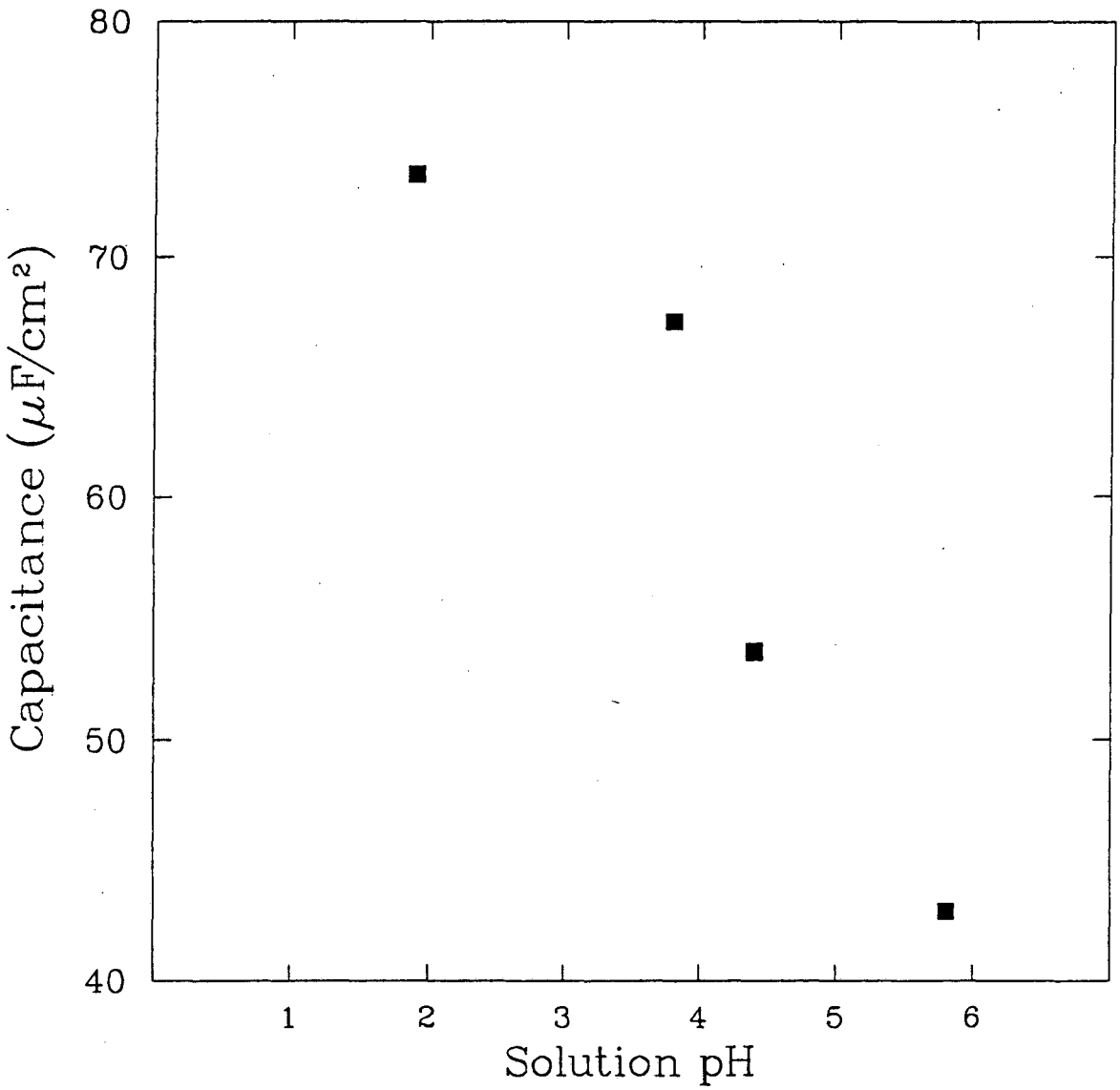

Figure 4-3. Double-layer capacity versus pH for glassy carbon at 0.5 V versus SCE in a solution of 0.1 M NaCl with 100 ppm Zn^{++}.

controlling, the definition of pH as the logarithm of the hydrogen ion concentration would predict a straight line for capacitance versus pH. In addition, the capacitance would be nearly constant because the overall ionic concentration in solution would not be changing by much. Evidently specific adsorption effects are important, leading to the strong dependence of the double-layer capacity on the pH.

Experiments were run to test the effect of cleaning the disk on the capacitance and on the faradaic currents and potentials. No reproducible results were found. Results here may have had relevance to the problem of electrode degradation with potential cycling, which was reported in the studies by Marquardt to limit electrode life.[29] The sweeps made with and without nitrogen sparging showed little difference.

Measurements of the disk open-circuit potential gave variable and drifting readings. This is expected for an ideally polarizable electrode. With no zinc plated on the disk, zinc cannot control the open-circuit potential. Most likely some mixed potential between hydrogen evolution, oxygen evolution, and the state of surface charge is found. The open-circuit potential was much more reproducible in the column experiments.

4.2. Column Results

Column experiments were performed to check the current-versus-time behavior against the theoretical prediction for charging an ideally-polarizable porous electrode. Zinc concentrations were monitored to determine whether the zinc concentration was responding to the applied potential.

4.2.1. Concentration Profiles

Figure 4-4 shows effluent zinc concentrations as a function of time during an experiment where the potential was cycled increasingly negatively. The concentration should respond to each change in potential. The steps with the potential at +0.2 volts were intended to regenerate the bed, while each successively more negative potential should have removed a larger fraction of the zinc. The plot shows an effluent profile which is smooth and unresponsive to the potential variations. Two possible explanations exist. First, the bed may have been in a removal regime at the potentials tried. The potentials used were all more negative than the open-circuit potential ($V_o \approx 0.3$ volts), which in the absence of knowledge about the point of zero charge is the best indicator concerning the relative charge of the bed. The bed may have been negatively charged throughout, thus attracting zinc. Testing this possibility requires using more positive potentials in attempts to regenerate the bed.

The second possibility is a nonelectrochemical adsorption mechanism, since activated carbon is an adsorbent by design. The

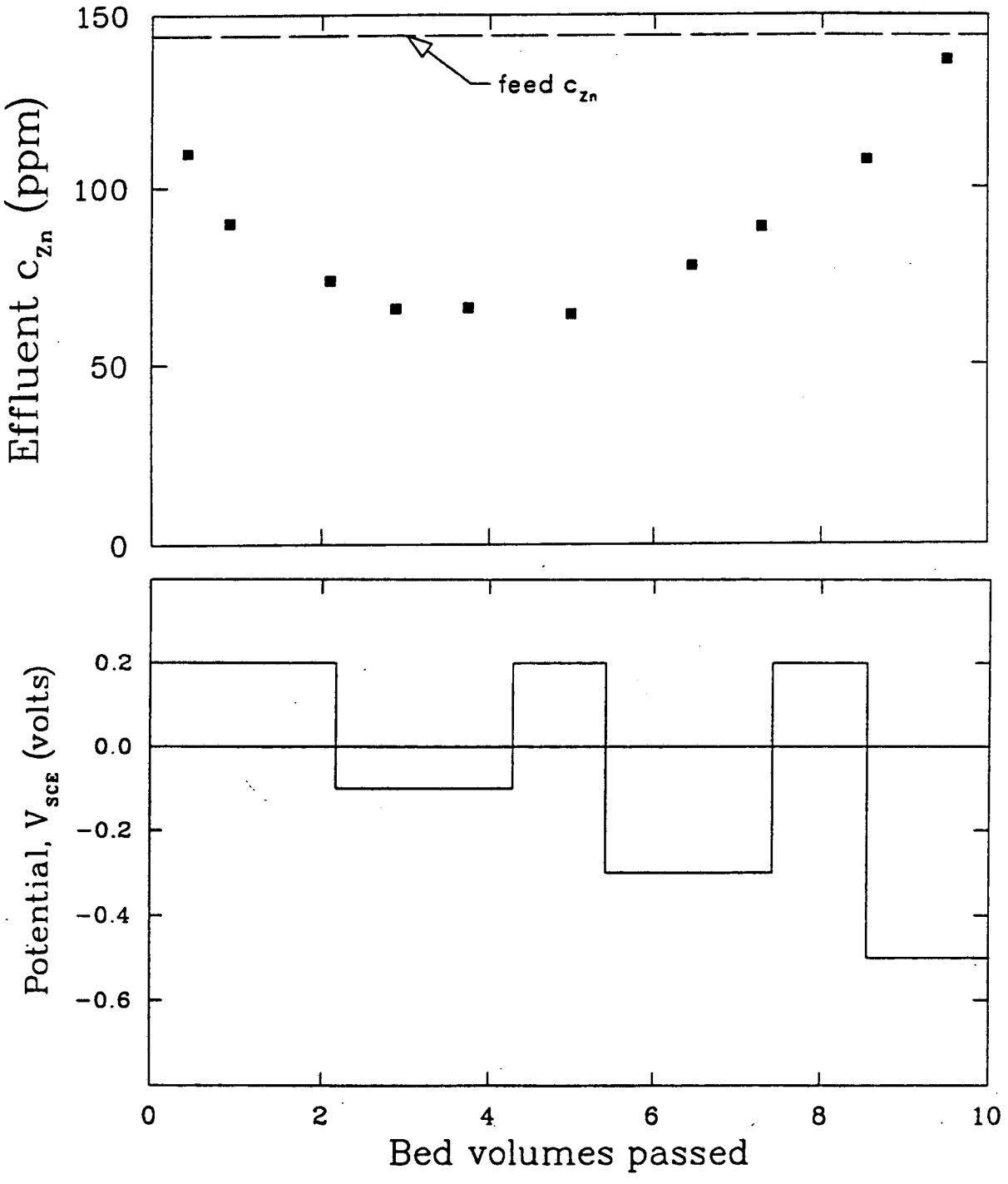

Figure 4-4. Effluent zinc concentration and applied potential versus bed volumes with a flow rate of 5.6 ml/min with a superficial residence time of 24 minutes, [NaCl] 1 M, and pH about 5. The potential is the working electrode versus the upstream saturated-calomel reference electrode.

smoothness of the curve with respect to potential also suggested a nonelectrochemical process. This was tested by running a fresh bed without potentiostatic control. Figure 4-5 shows the results. The bed had a strong affinity for zinc (in 1 M NaCl supporting electrolyte). For the time from the second to the sixth bed-volume mark, the bed effluent nearly met Federal regulations. This would be longer with a more realistic feed of 25 to 50 ppm metals. Figure 4-4 does not show such low concentrations because the bed was not fresh. Beyond the 13.5 bed-volume mark (on figure 4-5) and after a three-day wait, some very positive potentials were tried in an effort to regenerate the bed. The effluent zinc concentration actually decreased in response. This indicated that at least some of the zinc was anionically complexed and thus attracted to the positive bed. It also raised questions about the state of adsorbed zinc. If any adsorbed zinc was positively charged, it should have been repelled, perhaps negating the effect of adsorbing any anionically complexed zinc. The electrochemical adsorption occurred on a saturated bed. Could additional adsorption capacity result from applying positive potentials from the start?

Figure 4-6 shows a distribution diagram for zinc chloride solutions. At 1 molar chloride ion concentration, nearly 25% of the zinc in solution is anionically complexed. This could easily account for the additional zinc removal at the positive potentials tried. Perhaps no zinc with a positive charge was on the bed explaining why a net adsorption occurred when the potential was made positive. If

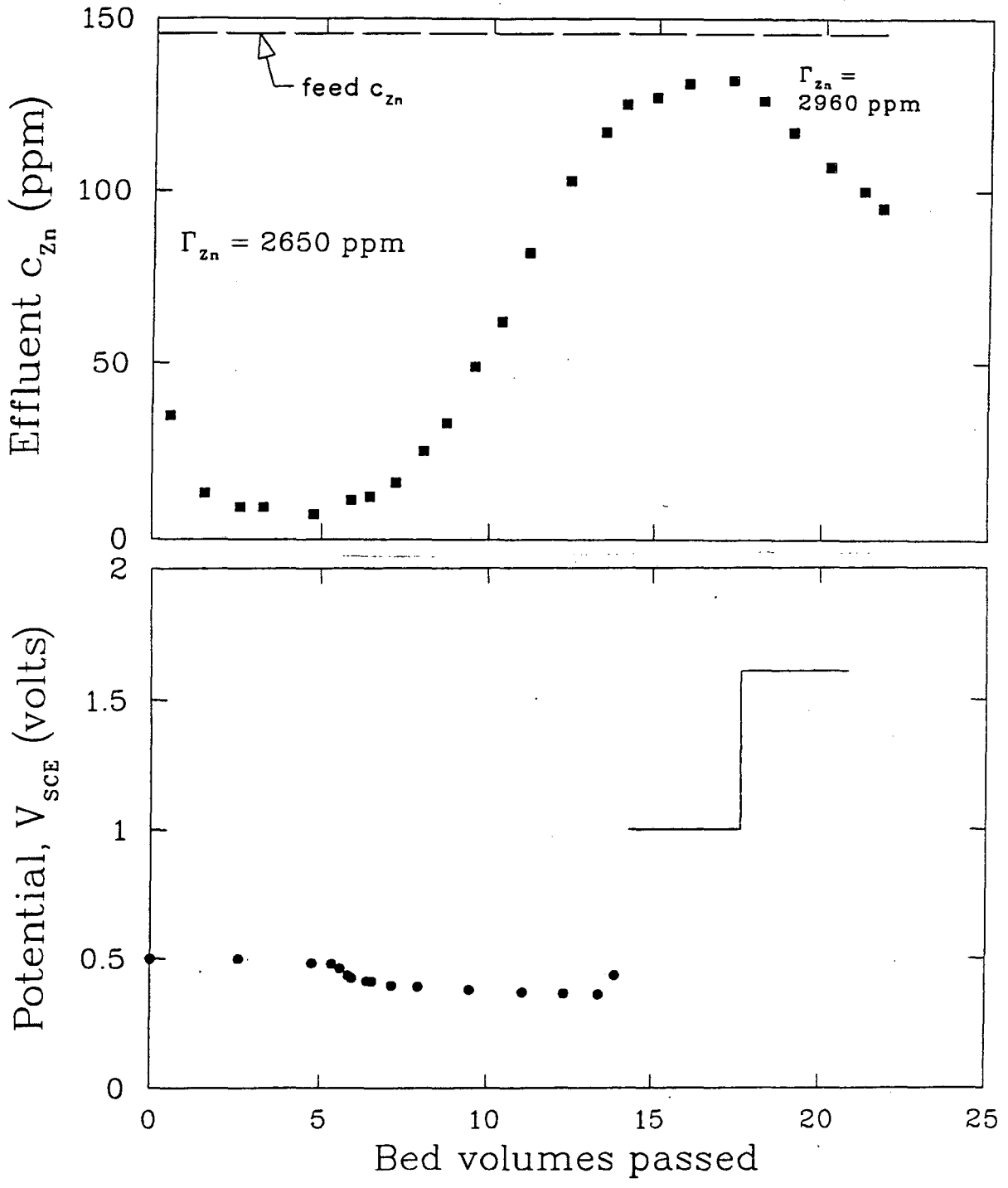

Figure 4-5. Nonelectrochemical adsorption with attempted potential-controlled regeneration (upstream SCE). The flow rate was 4.6 ml/min until 13.5 bed volumes and 5.6 ml/min after that, giving superficial residence times of 29 and 24 minutes, respectively. The [NaCl] was 1 M and the pH about 5. The symbols mean as follows: □ effluent zinc sample concentrations; • open-circuit potentials; (——) potentiostated.

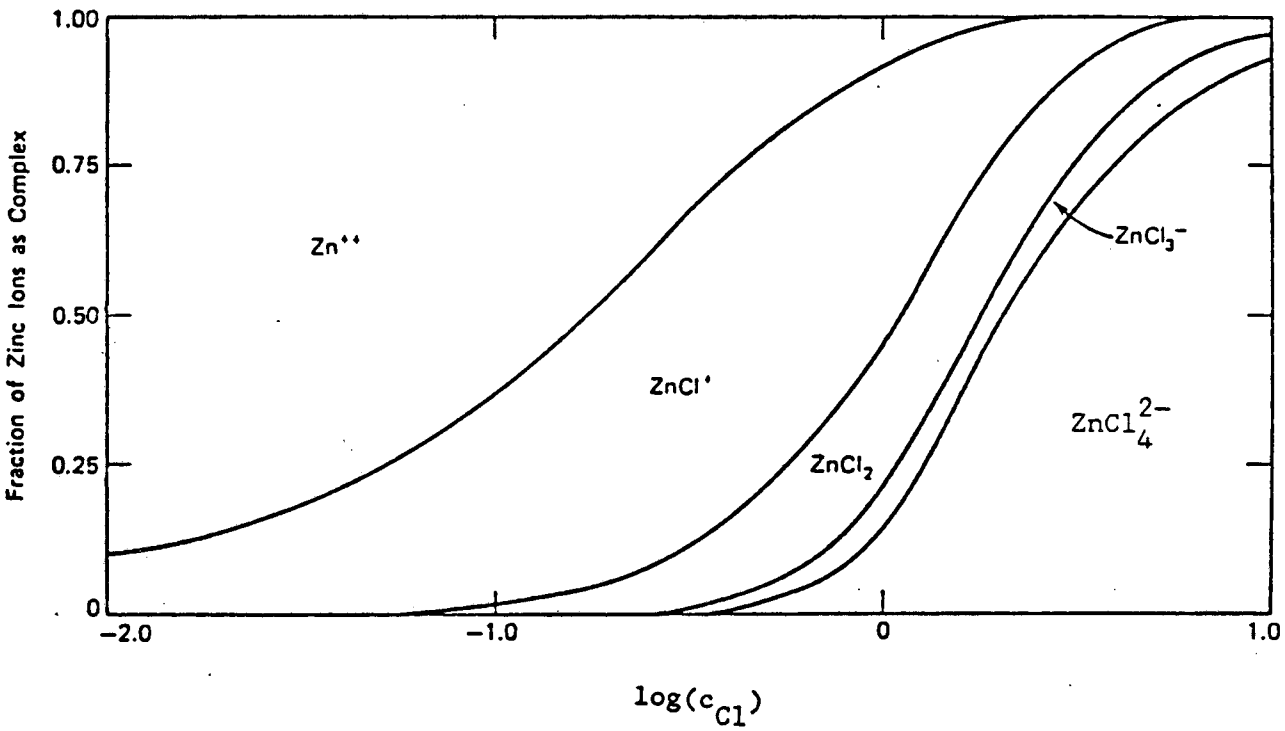

Figure 4-6. Distribution diagram for zinc chloride solutions at acidic pH.[46]

neutral $ZnCl_2$ was adsorbed during the first fourteen bed volumes on figure 4-5, it would not be expected to be attracted or repelled based on the potential of the bed.

In figure 4-5, the area under the feed level and above the effluent curve gives a measure of the amount of zinc removed. In terms of milligrams zinc per kilogram of activated carbon (ppm), the saturated bed contained 2650 ppm zinc. Applying the potentials increased the saturation coverage by 12% to 2960 ppm zinc. Based on a N_2-BET desorption area of 1581 m^2 per gram, the bed at 2650 ppm corresponds to 5800 $Å^2$/molecule. This is a large area per molecule. A lower area per molecule would result from doing calculations using an electrochemically active surface area, which Kelsey calculated to be perhaps an order of magnitude less than the BET area.[50] In a potential-step, double-layer charging experiment, Kelsey assumed a value for the double-layer capacitance C and, using equation 2-46, calculated a value for the specific surface area. Using either area, the zinc is quite widely spaced on the surface.

Under potentiostatic control in figure 4-5 (i.e., after the 13.5 bed-volume mark), the effluent curve had not bottomed out, and additional zinc would have been removed had the run continued. With potentials of 1.0 and 1.61 volts relative to the calomel reference electrode, no bubble nucleation was detected in the working electrode. The thermodynamic potential for oxygen evolution was about 0.8 volts versus SCE at the solution pH of near 4, so oxygen evolution was thermodynamically possible. At the 21 bed-volume mark, the

potential was shifted to 3.0 and then to 4.6 volts, passing half a bed volume of solution at each setting. The final data point in figure 4-5 would have been affected by these potentials but continued on the same trend as the samples from the 1.61 volt setting. At 3.0 and 4.6 volts versus SCE, bubbling was seen at the working electrode. These potentials are extremely positive and would allow side reactions to dominate.

During the open-circuit adsorption run (i.e., from zero to 13.5 bed volumes on figure 4-5), the open-circuit potential varied monotonically from 0.5 volts to 0.36 volts. Sampling caused a minor perturbation in the reading (±60 mV) due to the variation in flow rate caused by taking a sample. The reading recovered within 15 minutes. It would be interesting to investigate whether the state of saturation correlates reproducibly with the open-circuit potential. If so, perhaps a breakthrough monitor could be developed.

Having been unsuccessful in all attempts to regenerate the bed electrochemically, a chemical regeneration was tried. Figure 4-7 shows the favorable regeneration which resulted. The feed solution of 146 ppm zinc and 1 molar NaCl was replaced with a solution containing no zinc and 380 ppm NaCl at the two bed volume mark. Within two bed volumes, the majority of the zinc had been flushed out of the bed. Had this been expected, more samples would have been taken at early times. Integrating the area under the curve by cutting and weighing the paper on an analytical balance indicated that more zinc had come off than was initially removed. Perhaps the spike is nar-

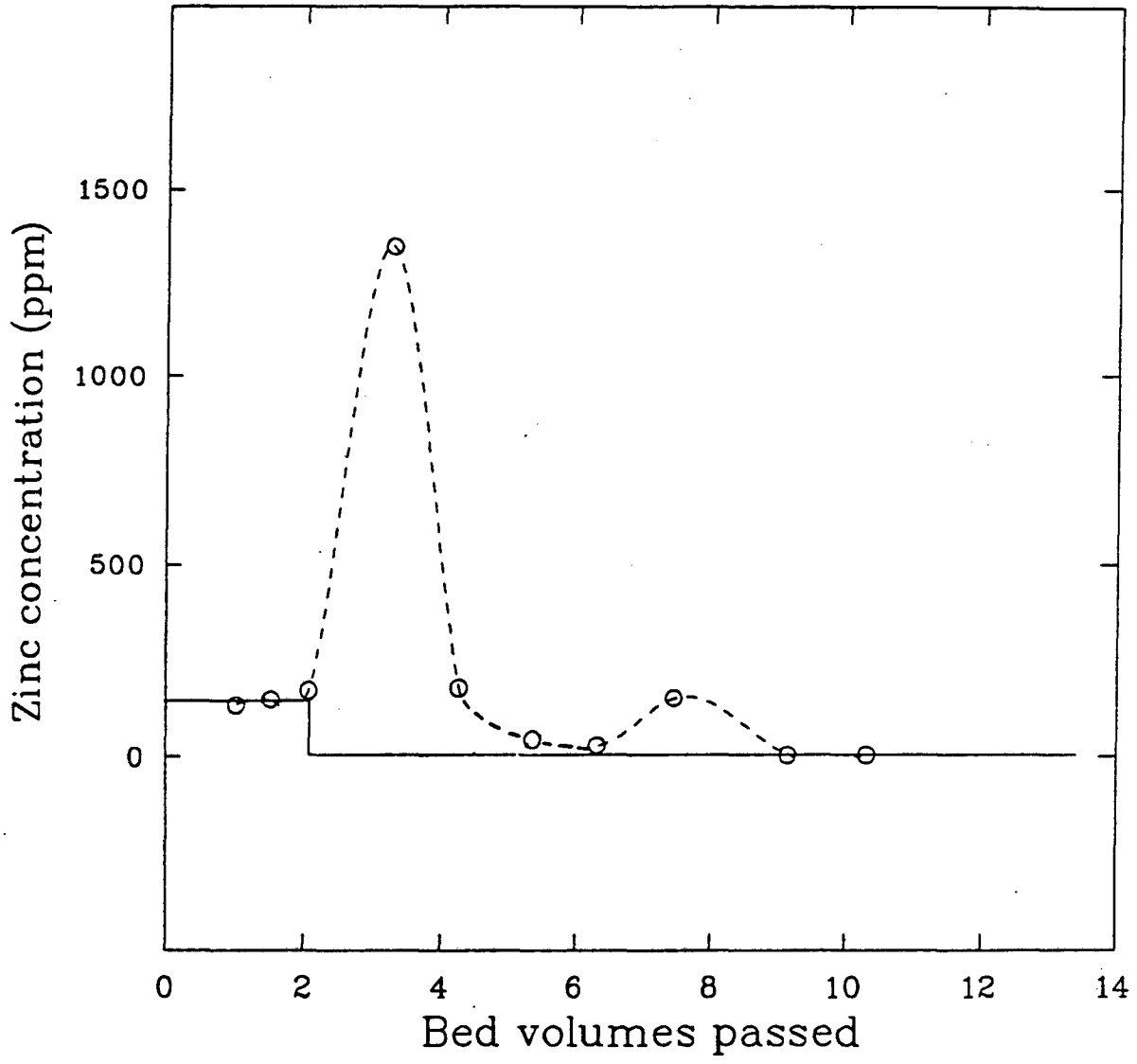

Figure 4-7. Profile of zinc concentration under chemical regeneration at pH about 5. The NaCl concentration was stepped from 1 molar to 380 ppm at two bed volumes. The solid line (———) represents the feed zinc concentration and the dashed line (-----) represents the effluent zinc concentration. Effluent sample concentrations are denoted O.

rower than that shown. The point at 1350 ppm on figure 4-7 is possibly not the absolute maximum, but is probably close. At the seven-bed-volume mark, the regeneration was stopped for 20 hours. The resulting jump in the effluent concentration indicates a mass-transfer process of a longer time constant was involved. Most likely this was internal particle diffusion. Lowering the flowrate on regeneration will provide time for internal diffusion to proceed and will contain a higher concentration of the heavy metal in a smaller volume.

The regeneration shown in figure 4-7 is very efficient. The clean regeneration of the carbon bed depends on the zinc-adsorption equilibria. The zinc adsorption appears to depend on the sodium chloride concentration in solution and perhaps on the zinc/chloride complexing. To examine the adsorption equilibria as a function of the background electrolyte concentration and on the type of electrolyte, some batch equilibrium experiments were performed. In the batch experiments, 2.5 grams of carbon were added to 50 ml of the solutions with various known initial concentrations of zinc ions. The vials were shaken overnight and tested for zinc remaining in solution. Figure 4-8 shows the amount of adsorption on acid-pretreated Darco® 20-40 activated carbon for various solution compositions. The top curve shows the zinc adsorbed from 1 molar NaCl solution. Zinc solutions with no NaCl, on the other hand, did not adsorb at all. The difference indicates that only complexed zinc is adsorbing. This explains the efficient regeneration achieved when

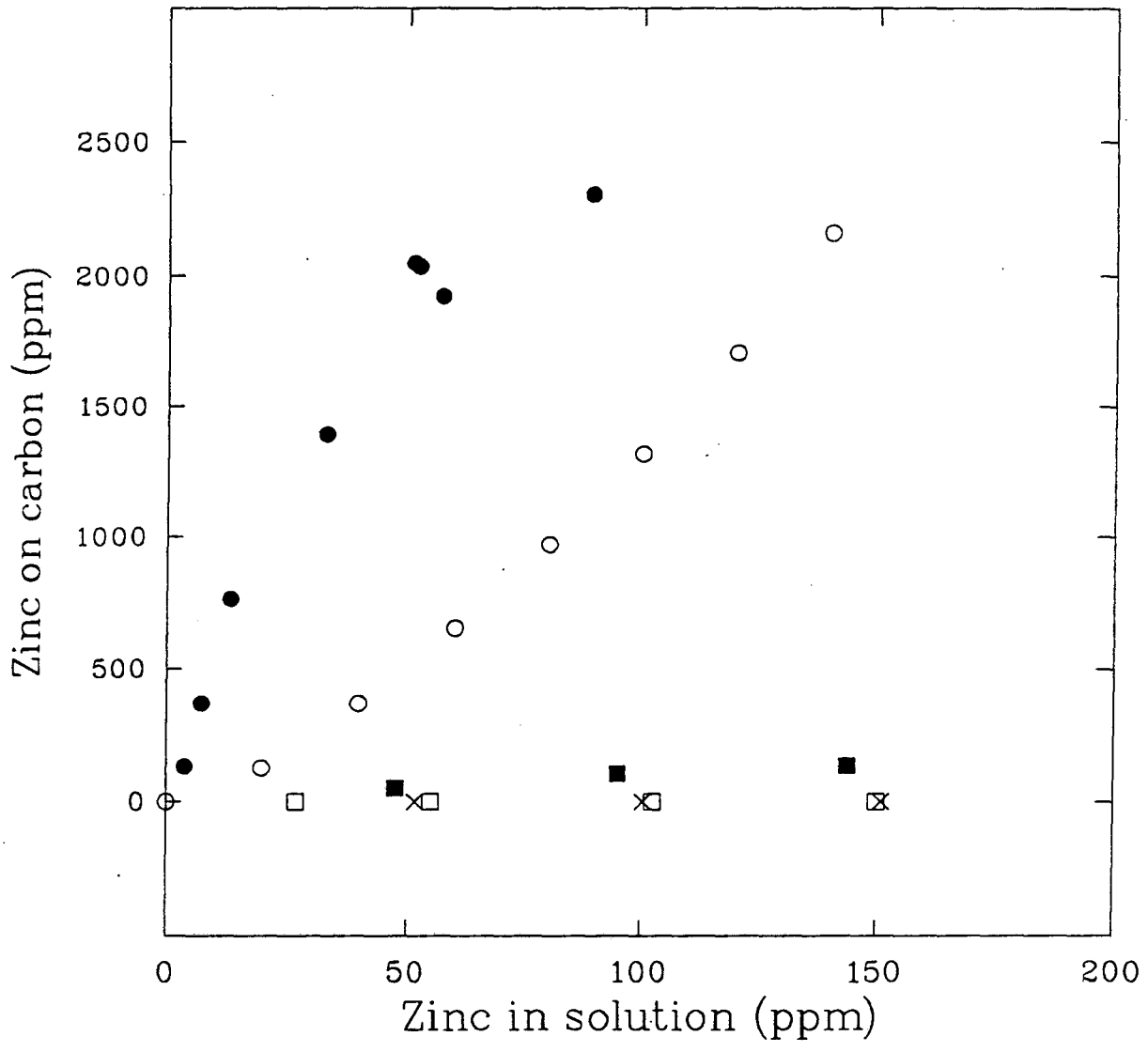

Figure 4-8. Equilibrium data for zinc on Darco® 20-40 activated carbon. The symbols mean as follows: ○ calculated from breakthrough data with 1 M NaCl and 146 ppm Zn^{++} feed at pH 5 in column; • batch equilibrium in 1 M NaCl at pH 2; □ batch equilibrium of $ZnCl_2$ at pH 2 with no supporting electrolyte; ▫ batch equilibrium in 1 condosity (1.15 M) $NaNO_3$ at pH 2; × batch equilibrium in 1 condosity (0.89 M) H_2SO_4.

the sodium chloride concentration dropped from 1 molar to nearly zero (figure 4-7).

Nitrate and sulfate solutions do not complex zinc in solution. Zinc in the nitrate and sulfate solutions did not adsorb to any appreciable degree. Thus it is the complexing of zinc and not the ionic strength of solution that contributes to the nonelectrochemical adsorption of zinc on this carbon. Use of a nitrate or sulfate type electrolyte would allow the isolation of the electrosorption by eliminating the competing chemical adsorption.

4.2.1.1. Mass-Transfer Effects

The column curve on figure 4-8 was constructed from the breakthrough curve of figure 4-5. The curve was calculated by assuming local equilibrium held throughout the column. This was accomplished by assuming the adsorption mass-transfer coefficient was infinite. The curve also neglects axial dispersion. Constructing an equilibrium curve from breakthrough data is a common procedure[47]. The calculated column equilibrium curve lies below the batch curve with which it should coincide. It also has a different shape. At 144 ppm in solution, the solid should contain 2650 ppm as integration of the area between the feed and effluent curves of figure 4-5 shows. The batch curve of figure 4-8 hits roughly 2650 ppm on the solid when the solution concentration is extrapolated to 144 ppm. This indicates the column was either not attaining the local and instantaneous equilibrium assumed (or that the equilibrium curve was not calculated correctly) or that channeling was occurring leading to premature

breakthrough. Channeling seems unlikely given the low liquid flow rates and tight packing of activated carbon in the column. More likely, some mass-transfer resistance between the bulk solution and the interior of an activated carbon granule is invalidating the local equilibrium approximation.

A time constant for diffusion into the granular activated carbon may be approximated by diffusion into a sphere. Taking the radius to be 1/60" for the 20 to 40 mesh carbon, the time constant becomes

$$\frac{r_p^2}{D_i} \approx 30 \text{ minutes}, \qquad (4\text{-}1)$$

where r_p is the particle radius and D_i is the effective diffusivity of adsorbing material in the particle. The effective diffusivity was taken to be 1×10^{-6} cm^2/sec. This value accounts for the microporosity and the tortuosity in the particle and thus is somewhat lower than a free-solution diffusivity. The time constant of 30 minutes is longer than an interstitial bed residence time, which is about 18 minutes at normal flow rates. Thus it is likely that solution flowing through the electrode will not have had time to equilibrate with the interior regions of a carbon particle. We have seen a manifestation of mass-transfer resistance in the chemical regeneration profile (figure 4-7) at the seven bed volume mark. The twenty hour wait prior to the seven-bed-volume mark allowed solution inside the carbon to equilibrate with the interstitial solution. The result was a spike in the effluent concentration upon restarting the flow. The disperse nature of the breakthrough curves of figures 4-4 and 4-5

also suggest the presence of mass-transfer resistances. Thus, analysis of data from a column containing the granular-activated carbon studied, whether electrochemical or not, should account for the mass-transfer resistance between the bulk and the interface.

Our double-layer adsorption model neglected mass-transfer resistance by averaging concentrations radially in the porous electrode. The model may have to be modified to account for mass-transfer resistance from the bulk to the adsorbing surface within the particle. Ruthven[48] lists many ways to account for mass-transfer resistances in adsorbing systems, with, for example, the simplest being to lump all the resistance into a single mass-transfer coefficient with a single driving force of bulk versus surface concentration. Other possible approaches will be studied more thoroughly before future modeling is undertaken.

4.2.2. Current-Time Behavior

Aside from analyzing the concentration histories of the column, the current-potential-time behavior must also be analyzed. As discussed in the theory section, a plot of $I\sqrt{t}$ versus time for charging an ideally-polarizable porous electrode due to a potential step, should be constant for times between the start-up time constant τ_1 and the saturation time constant τ_2. Figure 4-9 shows a typical plot of $I\sqrt{t}$ versus $\sqrt{t}$. The curve shows no horizontal plateau nor any tendency toward one. This indicates one of two things is occurring. The first possibility is that charge-transfer reactions are occurring and interfering with the adsorption reactions. The second is that

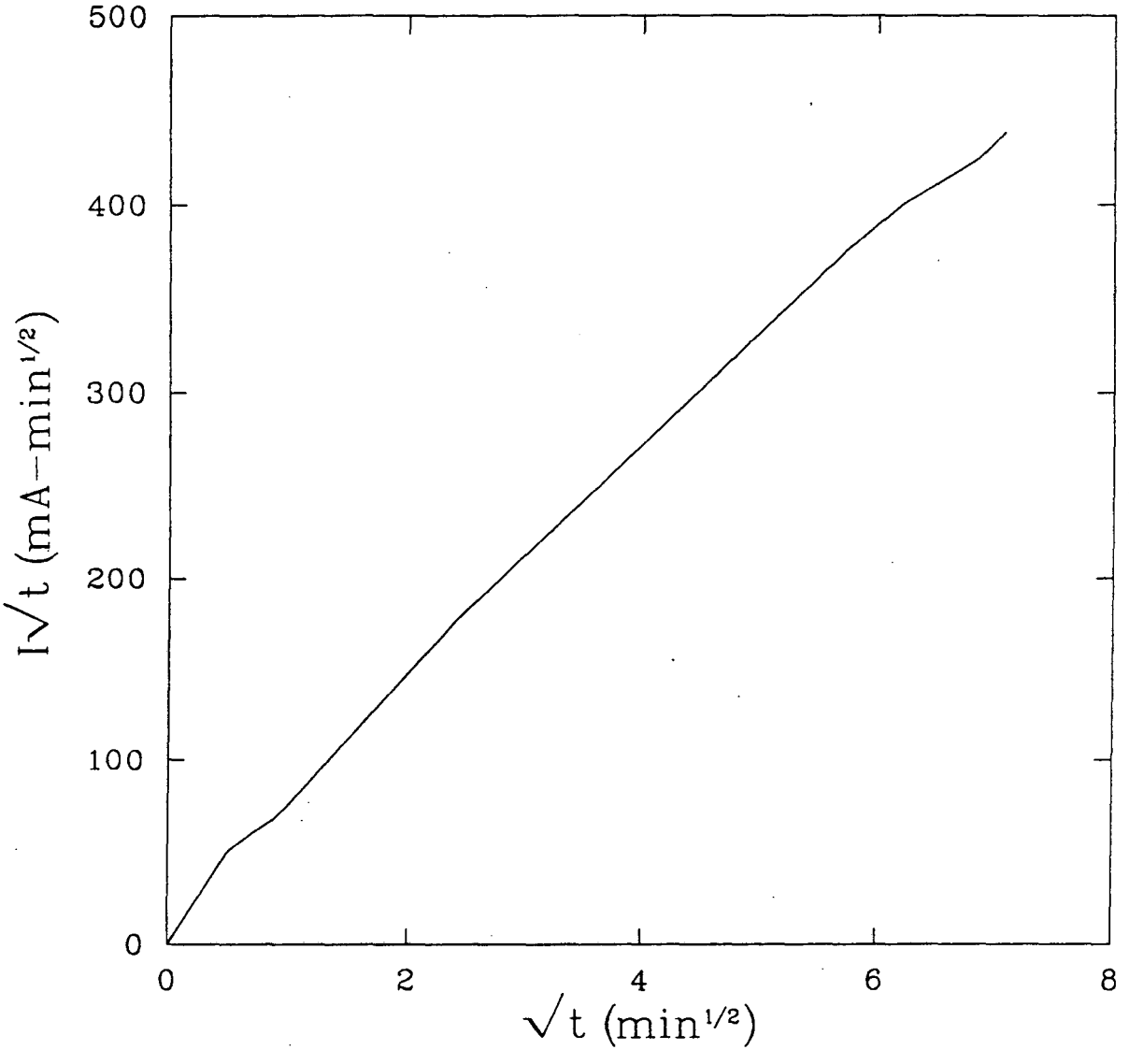

Figure 4-9. Plot of $I\sqrt{t}$ versus $\sqrt{t}$ for a potential step of 1 volt.

the start-up time constant τ_1 is so large that ohmic limitations are dominating even at times up to an hour. These possibilities will be examined in the next two sections.

4.2.2.1. Charge-Transfer Reactions

It appears a faradaic side reaction is operating in the column either in addition to, or in place of, the capacitive reaction. A faradaic reaction would not decay with the square root of time, as the capacitive reaction should. Thus the current "I" remains constant and $I\sqrt{t}$ continues to rise with time. The data were taken from a run in which the potential was stepped from +0.5 volts ($\phi_{WE} - \phi_{SCE}^{upstream}$) to -0.5 volts. The expected current at the instant of the step would be

$$I_{t=0} = \frac{\Delta VA}{R_T} = -230 \text{ mA}.$$

The actual current was -150 mA. Perhaps R_T is larger than we had thought. Additional resistance could result if the capacitors were not initially completely uncharged as the theory assumed. The current also decayed in one minute back to -75 mA and over the next 50 minutes only dropped to -62 mA. The background faradaic reaction appeared to have a magnitude of about -60 mA at this potential. Every potential step during experimentation caused a short time transient (i.e., $\approx$ 1 minute in length) in current which quickly decayed to what appeared to be a steady faradaic background current. The transients for charging the double layer should decay for nearly an hour. Figure 4-10 shows the residual faradaic currents at various

values of the working versus the upstream reference electrode potential. The plot brings out a few important points. First, the current passes through zero at roughly the value of the open-circuit potential, usually from 0.2 to 0.5 volts. This indicates that the faradaic reactions occurring are also determining the open-circuit potential. Perhaps eliminating the faradaic reactions would allow the open-circuit potential to reflect the state of charge on the bed more precisely. Refluxing the carbon for a longer time in HCl may lesson the faradaic reactions. The one-hour refluxing time used may not have been long enough to clean the carbon fully. A second point about the plot is that the faradaic currents are independent of the bed history. For example, the current at -0.2 volts is the same whether the previous voltage was positive or negative of -0.2 volts. A third observation relates to the magnitude of the current densities shown on this plot. The current densities shown are on the order of 10^{-11} amps/cm^2 based on a BET surface area. These current densities are much lower than faradaic current densities from a rotating disk polarization curve (see figure 4-11). Current densities from the rotating disk experiments are on the order of 10^{-5} amps/cm^2, at least in the hydrogen evolution regime. This indicates that the porous electrode is using an effective surface area for faradaic reaction which is much less than the BET area, or that reactions different from those on the RDE are occurring. The rotating-disk electrode was ideally polarizable between the potentials for the oxygen and hydrogen evolution reactions (see figure 2-2), but the porous electrode may or may not be. The porous electrode could not be polished, as

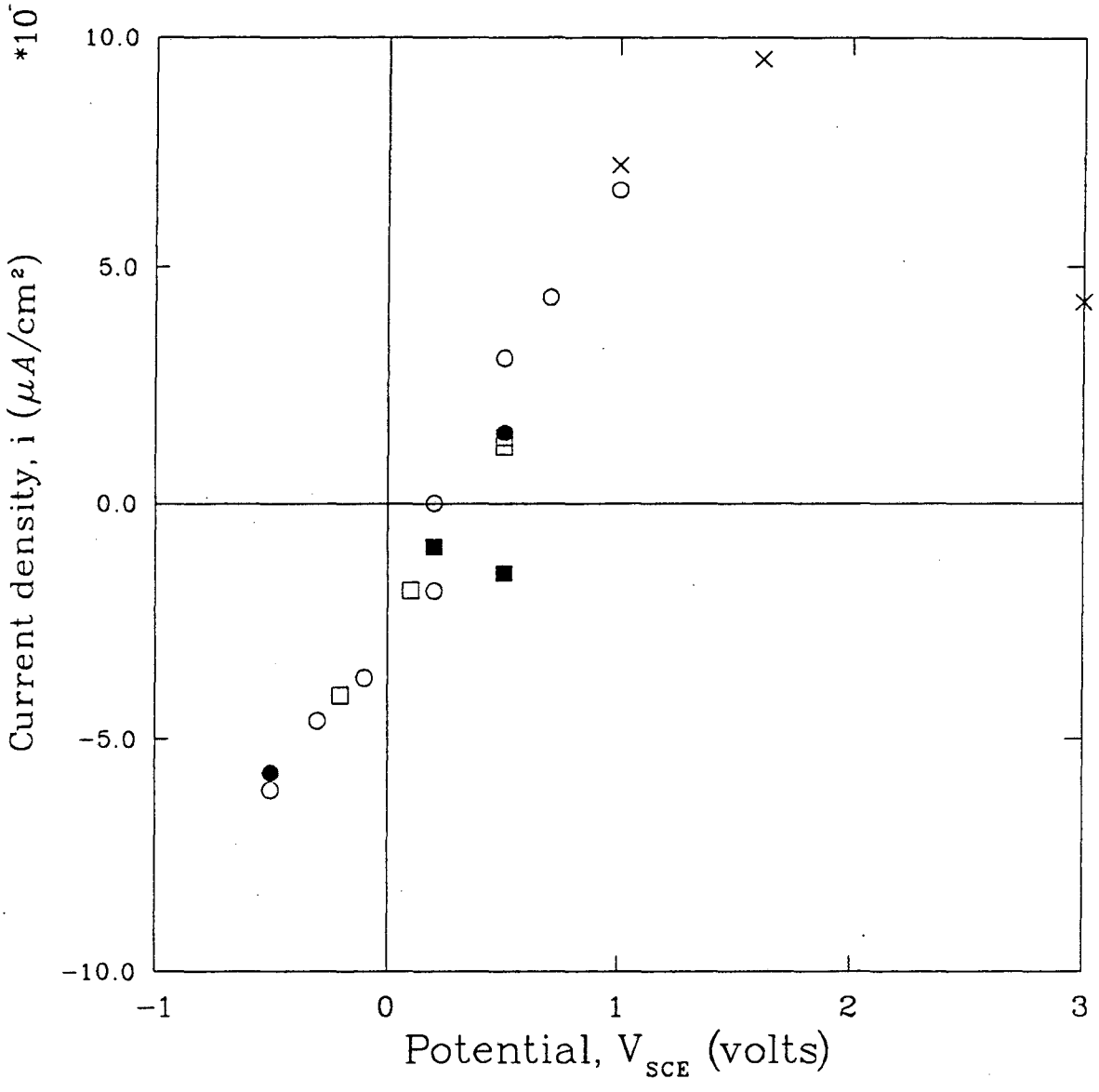

Figure 4-10. Background faradaic current densities (based on the BET area) in porous electrode experiments. The potential is relative to the upstream SCE, and the symbols represent various days of column operation with a feed of 149 ppm Zn^{++} in 1 M NaCl as follows: ○ 11/6/86; □ 11/14/86; □ 11/20/86; • 11/22/86; × 12/3/86 (new bed).

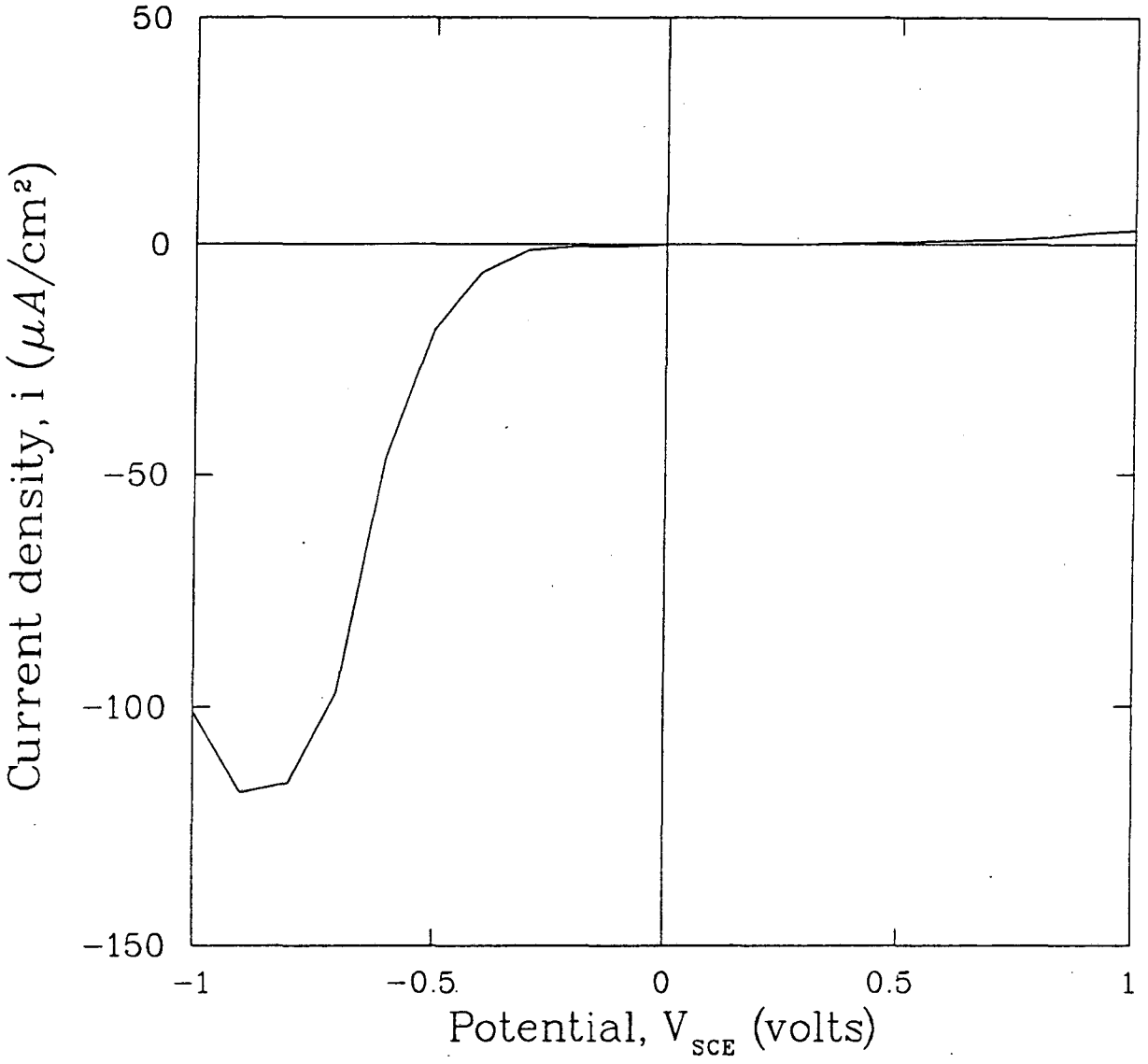

Figure 4-11. Polarization curve on glassy carbon RDE.

the RDE was, and it is an activated carbon, not a glassy carbon, as the RDE was. Thus it is quite possible that charge-transfer reactions other than hydrogen or oxygen evolution are occurring in the porous electrode.

Finally, a comparison of the magnitudes with the expected capacitive to the faradaic current densities is in order. Capacitive currents are expected to start at roughly 10^{-10} amps/cm^2 (i.e., $\approx$ 230 mA total) and decay with the square root of time to perhaps 10^{-12} amps/cm^2. Thus the capacitive currents may be larger at short times, but as a run proceeds the faradaic current (i.e., $\approx 10^{-11}$ amps/cm^2) becomes relatively larger and eventually dominates. Inside the electrode, the faradaic reaction is distorting the potential profile in addition to competing with the capacitive reaction. The faradaic reaction causes additional current to flow, resulting in larger ohmic potential drops and lower driving forces for adsorption.

4.2.2.2. Ohmic Limitations

In addition to faradaic reactions, ohmic limitations in the reactor can alter the current-versus time behavior from what is expected in the purely capacitive case with short start-up time. Calculation from equation 2-46, assuming the ideal case of a BET active surface area, shows the plateau should occur with

$$I\sqrt{t} = 4390 \text{ mA-min}^{1/2}.$$

Viewing the figure, we see values of $I\sqrt{t}$ of only 450 mA-min$^{1/2}$ at a time of 60 minutes, and a curve which is still rising. This could

indicate that the current is capacitive, but that the reactor is ohmically limited even at 60 minutes (i.e., τ_1 is very large). Recall that at times less than τ_1, the value of $I\sqrt{t}$ should rise toward the plateau value (i.e., see figure 2-7).

Further insight can be gained by analyzing the values of the time constants and cell parameters. These are shown in table 4-1 for two possible active surface areas. The table values were calculated for solutions of 1 M NaCl with 150 ppm zinc. The effective conductivity is corrected for bed porosity by

$$\kappa = \kappa_f \epsilon^{1.5}, \tag{4-2}$$

where κ_f is the free-solution conductivity outside the bed. We assume κ_f follows dilute-solution theory. Bruggeman[49] first showed that solution conductivity will vary with the porosity of the surrounding matrix phase to the 1.5 power. Equation 2-22 contains the porosity ϵ so that the conductivity is based on the entire bed cross section (i.e., $\kappa_f \epsilon$). Here the additional factor of $\epsilon^{0.5}$ empirically accounts for porosity and tortuosity effects in porous media on

Table 4-1. Cell Parameters Versus Active Area*

	a_{BET}	$0.05a_{BET}$
α (cm^2/s)	2.1×10^{-4}	3.8×10^{-3}
τ_1 (hours)	18.3	1
τ_2 (hours)	58	3.2
R_T (ohm-cm^2)	86.3	86.3

* (BET surface area for Darco® 20-40 mesh carbon is 6.8×10^6 cm^2/cm^3)

conductivity. With the bed porosity estimated at 0.75 and κ_f calculated to be 0.126 mho/cm, the effective conductivity κ was roughly 0.082 mho/cm. Also σ was 0.092 mho/cm, the cell length was 6.6 cm, and the double-layer capacitance was taken to be 30 $\mu F/cm^2$. The figure of $0.05a_{BET}$ comes from preliminary work on double-layer charging in porous carbon (Darco® 20-40) electrodes by Kelsey[50] in our laboratory. From his value of $I\sqrt{t}$ at the plateau versus the value predicted using a BET active area, he calculated that only 5% of the BET area was being utilized. This figure is taken as a probable value of active area in our bed. The amount of active surface area is possibly related to the distribution of macropores and micropores in the carbon. The micropores (i.e., diameter less than 20 Å) are perhaps not contributing during double-layer charging. Understanding how the active surface area relates to the pore structure and to the BET area is a fundamental task which deserves further study. From a practical viewpoint, the active area should be maximized. Note that both the short and long time constants, τ_1 and τ_2, are proportional to the active surface area "a." As the active area drops, τ_1 and τ_2 approach one another.

During initial experimental design calculations, the resistance between the bed and the reference electrode capillary tip was neglected, leading to a calculated τ_1 of 12 minutes (with $a = 0.05a_{BET}$). Accounting for this resistance will change the value of τ_1 significantly. The capillary tip separation was roughly 1 cm, $L_s = 1$ cm. Solution between the capillary tip and the bed has a

lower conductivity due to the presence of nonconducting solids in the path of current flow,[49] according to

$$\kappa_s = \kappa_f p^{1.5}, \tag{4-3}$$

where p is the void fraction in the space between the capillary tip and the front of the bed (assumed to be 0.3 for a bed of spheres), κ_f is the free-solution conductivity, and κ_s is the resulting effective conductivity in the separator region. This equation approximates the additional resistance (from the ramrod plate and the flow distributing glass beads) due to tortuosity between the capillary tip and the packed bed. When the additional resistances represented by equations 4-2 and 4-3 are accounted for, the calculated value of R_T more than doubles from 38.0 (e.i., assuming $\kappa = \kappa_s = \kappa_f$) to 86.3 ohm–$cm^2$. As a result τ_1 quadruples from 14 minutes to 1 hour. Thus the ohmically limited time of reaction was much longer than had been thought originally.

Two ways to decrease τ_1 are evident. Both involve lowering the resistance R_T. First, decreasing L_s to zero would bring τ_1 back down to 12 minutes. This could be accomplished by somehow working the capillary tip down to the top of the bed, lowering L_s. It could also be accomplished by using the downstream reference electrode. Since no current flows in solution beyond the current collector, no ohmic drop occurs, and the downstream reference electrode encounters no separator resistance. The theoretical analysis for a downstream reference electrode would likely, but not necessarily, result in the same time constants governing the system.

A second way to reduce τ_1 is to shorten the electrode length L. Reducing L from 6.6 cm to 1 cm would decrease τ_1 from 12 minutes (assuming $L_s/\kappa_s \rightarrow 0$) to 16 seconds. However, τ_2 would drop due to this change from 3.2 hours down to 4.4 minutes.

Maintaining the separation between τ_1 and τ_2 is essential if any useful desalting is going to occur. This necessitates a more careful design calculation.

4.3. Cell Redesign Calculations

This design deals only with the process of electrosorption of zinc from solution. It thus ignores the process reported on in the "Results and Discussion" section which was a chemical separation method based on the sodium chloride concentration in solution.

For the electrosorption process to work, the parameters governing cell performance and their interactions must be examined. The goal is to propose a cell design which will process a maximum number of bed volumes between regeneration steps while removing as much of the heavy metal as possible. The simplest way to improve the cell design was to put the design equations on the computer. The equations are algebraic. Most of them were discussed in the porous-electrode-theory section, but we will list them again for clarity.

4.3.1. Design Equations

Since τ_1 represents roughly the time for a potential step to result in a plateau on the $I\sqrt{t}$ versus time curve, this is a parameter we must minimize. At times shorter than τ_1, ohmic effects limit the charging rate. We want τ_1, given by

$$\tau_1 = \left(\frac{R_T (\kappa+\sigma)\kappa\sigma}{2\sqrt{\alpha}(\kappa^2+\sigma^2)} \right)^2, \qquad (2\text{-}41)$$

to be much less than a bed residence time to minimize solution lost during start-up. The key parameter in τ_1 is R_T, where

$$R_T = \frac{L}{\kappa+\sigma} + \frac{L_s}{\kappa_s}. \qquad (2\text{-}40)$$

Notice that τ_1 varies with the square of the electrode and the separator lengths. Also important is the path between the reference electrode capillary tip and the porous electrode. If this path is not straight, the conductivity κ_s in the region will be higher, according to

$$\kappa_s = \kappa_f p^{1.5}, \tag{4-3}$$

where p is the void fraction in this region. In our system, a porous insert plate and glass beads hindered the path between the capillary tip and the porous carbon. We let p be 0.3 to account for this situation.

Inside the porous electrode, the conductivity will be lower than the free-solution value by the same equation applied to the porous electrode region

$$\kappa = \kappa_f \epsilon^{1.5}. \tag{4-2}$$

Here ϵ is the bed porosity estimated to be 0.75 for the activated carbon used.

The saturation time constant

$$\tau_2 = \frac{L^2}{\alpha} \tag{2-42}$$

varies with the electrode length squared and inversely with the electrical diffusivity α, just as τ_1 did. Increasing the bed capacity per unit volume, aC, will increase both τ_1 and τ_2 linearly, as substitution of equation 2-30

$$\alpha = \frac{\kappa\sigma}{aC(\kappa+\sigma)} \tag{2-30}$$

into equations 2-41 and 2-42 above will show. Thus separating the magnitudes of τ_1 and τ_2 cannot be achieved by varying the bed length L or bed capacity per unit volume aC. Rather, it requires minimizing the separator resistance (L_s/κ_s) and finding an optimum conductivity. We will try various values of L_s while varying κ_f in the design calculations.

We still must lay out the expressions for the cell current. At times greater than τ_1 and less than τ_2, we expect the current to decay with the square root of time according to

$$I\sqrt{t} \longrightarrow \frac{\Delta VA}{R_T}\sqrt{\tau_1/\pi} = \frac{\Delta VA}{2\sqrt{\pi}}\frac{\kappa+\sigma}{\kappa^2+\sigma^2}\sqrt{aC(\kappa+\sigma)\kappa\sigma}. \tag{2-46}$$

At the instant of the potential step, the current cannot be infinite and is governed by the ohmic resistances in the cell

$$I_{t=0} = \frac{\Delta V\ A}{R_T}. \tag{2-45}$$

The average current for a half cycle of duration T is

$$I_{ave} = \frac{1}{T}\int_0^T I\ dt. \tag{4-4}$$

Assuming that the current decays with the square root of time from time zero allows us to evaluate the integral of equation 4-4. This assumption is strictly valid only for short start-up times (i.e., small τ_1) and for $T < \tau_2$. It should be approximately valid as long as $\tau_1 \ll T \ll \tau_2$, even if τ_1 is not extremely small. Solving for the half-cycle time gives

$$T = \frac{4\tau_1}{\pi}\left(\frac{\Delta V\ A}{R_T I_{ave}}\right)^2 . \qquad (4\text{-}5)$$

This equation shows that as the desired average current density is increased, the half-cycle time yielding that average current becomes shortened. This has important implications on the allowable half-cycle time because the zinc ions flowing into the cell require a minimum average current density if they are to be removed as equation 4-6 shows

$$I_{zinc} = c_{Zn}\ \dot{Q}\ z_{Zn}\ F, \qquad (4\text{-}6)$$

where $\dot{Q}$ is the volumetric flowrate through the electrode. In addition, not all of the current flowing through the cell goes toward removing zinc. Current will be "wasted" on adsorption reactions involving sodium and chloride and on charge-transfer reactions such as hydrogen evolution. In this design calculation we assume that current is divided between adsorption reactions for zinc and sodium only. We are ignoring chloride adsorption. Thus we can define a current efficiency for zinc adsorption, η_{zinc}, as the fraction of the total current which is contributing to zinc adsorption

$$\eta_{zinc} = \frac{I_{zinc}}{I_{ave}} = \frac{\Gamma_{Zn}}{\Gamma_{Na} + \Gamma_{Zn}}. \qquad (4\text{-}7)$$

A value can be assigned to η_{zinc} if we assume that the concentrations between the bulk and the surface follow a constant-separation-factor approximation

$$\frac{\Gamma_{Zn}}{c_{Zn}} \cdot \frac{c_{Na}}{\Gamma_{NA}} = 2.3 . \qquad (4\text{-}8)$$

This expression has the look of a relative volatility. The constant value 2.3 comes from the study at Marquardt [29] on desalting water by electrosorption. They reported a separation factor of 2.3 for divalent ions over monovalent ions in solution.

If we make a crude approximation that the ratio c_{Zn}/c_{Na} stays constant at the inlet value throughout the bed, then the ratio Γ_{Zn}/Γ_{Na} is fixed. From the ratio of adsorbed ion concentrations, a value for the current efficiency for zinc adsorption can be calculated by equation 4-8. In reality the ratio c_{Zn}/c_{Na} should decrease down the bed as the solution becomes depleted in zinc, the more "volatile" component. This will lead to a current efficiency slightly lower than the one calculated by assuming constant ratios.

Increasing the relative amount of sodium in the incoming stream also decreases the current efficiency η_{zinc}. The average cell current needed to remove all the zinc will increase in the presence of sodium competing for adsorption current. The magnitude of the necessary average cell current will depend upon the current needed for zinc adsorption and on the current efficiency according to

$$I_{ave} = \frac{I_{zinc}}{\eta_{zinc}}. \qquad (4\text{-}9)$$

The average current calculated here can be substituted into equation (4-5) to calculate a maximum half-cycle time for the process.

In the design calculation, we have assumed κ to be constant (inside the porous electrode). Recall that equations 2-42, 2-46, and 2-49 above are only valid for constant κ, σ, and α. In practice,

assuming constant conductivity is a good assumption when the overall solution concentration is high. If the concentration is 0.1 molar (i.e., $\kappa_f \approx 0.01$ mho/cm), the cation concentration is roughly 3000 ppm. The electrosorption process will not affect this conductivity significantly. At lower conductivities, however, the conductivity may be expected to vary significantly.

In this design calculation we are requiring an average current which will remove all the zinc ions in solution regardless of the level of competition from sodium (equation 4-9). The average currents required could tend to alter the solution conductivity which would violate the assumption of constant conductivity. Yet as a first approximation this approach should yield a satisfactory design.

4.3.2. Design Procedure

The free-solution conductivity will be calculated from dilute-solution theory by using

$$\kappa_f = \sum_i c_i |z_i| \lambda_i . \qquad (4\text{-}10)$$

Here i represents sodium, zinc, and chloride, and λ_i is the equivalent ionic conductance of an ion in an infinitely dilute solution. The conductivity κ_f is then used in equations 4-2 and 4-3 to calculate κ and κ_s. In the design calculation, we set κ_f, c_{Zn}, and the flow rate Q. Other parameters, such as τ_1, τ_2, R_T, α, are determined by the cell geometry and carbon conductivity. The cell geometry is set by L, L_s, and A. A voltage step ΔV of 1 volt is assumed. The starting point for solution composition and

conductivity is zinc chloride at from 25 to 150 ppm Zn^{++}. From this point an increase in solution conductivity is due to addition of sodium chloride. Thus a high conductivity will lower the resistance through the bed but cause more competition from sodium for adsorption current.

With κ and c_{Zn} set, and the chloride concentration written in terms of zinc and sodium concentrations by stoichiometry, the sodium concentration can be calculated from equation 4-8. This leads to calculation of the current efficiency η_{zinc} (equations 4-6 and 4-7), the necessary average cell current (equation 4-9), and the required half-cycle time T (equation 4-5). As the sodium concentration increases, the average half-cycle time will decrease because high currents will be required for the removal. If this time becomes as short as the residence time for fluid in the bed, the process becomes inefficient. In that case, treated fluid will not have left the bed before regeneration is required. The residence time in the bed is

$$t_{res} = \frac{L\,\epsilon}{v}. \qquad (4\text{-}11)$$

Note that L/v is the superficial residence time where v is the superficial velocity (equal to Q/A). Multiplying by the bed void fraction gives an actual residence time. In the design scheme, the bed volumes per half cycle must be maximized. This parameter is given in equation 4-12,

$$\text{bed volumes at 100\% zinc removal} = \frac{T}{t_{res}}. \qquad (4\text{-}12)$$

If T/t_{res} can be maximized such that $\tau_1 \ll T < \tau_2$, an adequate design

will have been found. As we shall see, the treatable bed volumes (T/t_{res}) decreases monotonically with the fraction of sodium in the feed. It therefore is a maximum at the lowest conductivities, where the feed is pure zinc chloride. However, as the conductivity drops, the resistance R_T increases and therefore τ_1 increases. We cannot allow τ_1 to become comparable to T, or to become large in absolute value. We must optimize between maximizing T/t_{res}, minimizing τ_1/T, and minimizing τ_1.

4.3.3. Design Results

The design results will begin with an analysis of the system as used in the experiments. We will examine the variation of τ_1 and τ_2 with conductivity, the dependence of τ_1 on L_s, and lastly the variations of the bed volumes per half cycle (T/t_{res}) and the half cycle versus start-up times (T/τ_1) on conductivity and flow rate. Later, essentially the same analysis will be applied to a system with somewhat improved operating parameters.

4.3.3.1. Results from Experimental Cell Analysis

Figure 4-12 shows the variation of τ_1 and τ_2 with conductivity for the present system. The parameters from the experimental cell are shown in table 4-1. The value of aC assumed is roughly 5% of the BET capacity. It appears that the separation between τ_1 and τ_2 is a minimum when κ_f is just less than 0.1 mho/cm. Perhaps the actual minimum occurs when $\kappa \approx \sigma$. Moving to lower conductivities increases τ_2 by decreasing the electrical diffusivity α, but also increases τ_1

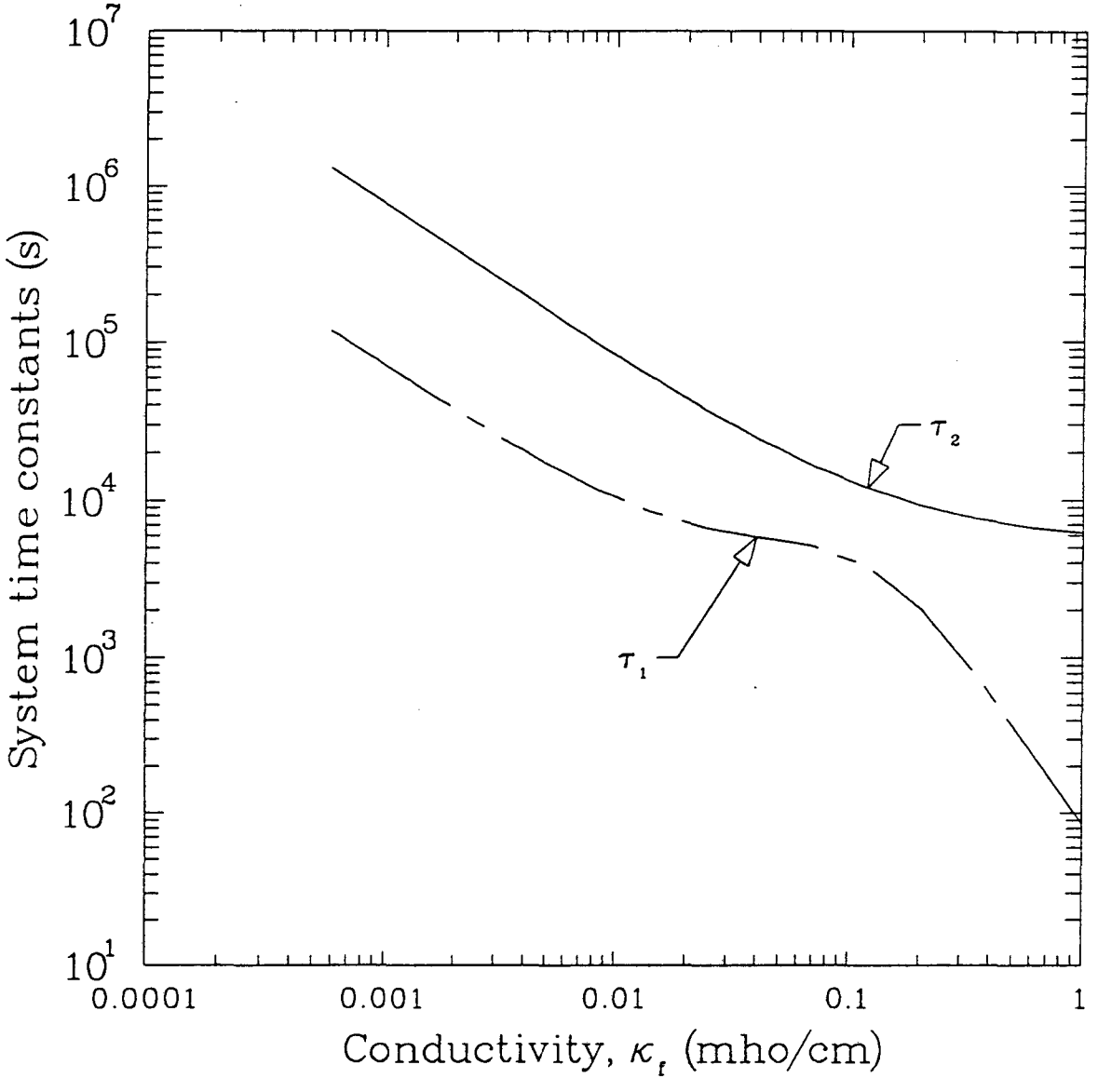

Figure 4-12. Variation of the system time constants τ_1 and τ_2 with free-solution conductivity κ_f (experimental cell).

Table 4-1. System Parameters from Experimental Cell

parameter	value	units
κ	0.126	mho/cm
σ	0.092	mho/cm
A	20.27	cm^2
aC	11.5	F/cm^3
L	6.6	cm
L_s	1.0	cm
t_{res}	1074	s
T	5	s
τ_1	3900	s
τ_2	11900	s
η_{zinc}	0.56	%
$\dot{Q}$	5.6	ml/min
c_{Zn}	150	ppm
ϵ (bed)	0.75	void frac
p (sep)	0.3	void frac

due to the increasing separator resistance. The curves separate at higher conductivities; however, even a saturated sodium chloride solution has a conductivity of less than 0.3 mho/cm. Cell operation at high conductivities may result in ideal current-versus-time behavior, but any useful deionizing would be negligible due to the low current efficiencies for zinc in such an excess of sodium.

At low conductivities, the current efficiency is high, but any separator resistance dominates the total resistance. Figure 4-13 illustrates the effect of the capillary tip separation L_s on the start-up time constant τ_1. The top curve represents the experimental cell with a separation of 1.0 cm. At $\kappa_f \approx 0.001$, τ_1 is about 10^5

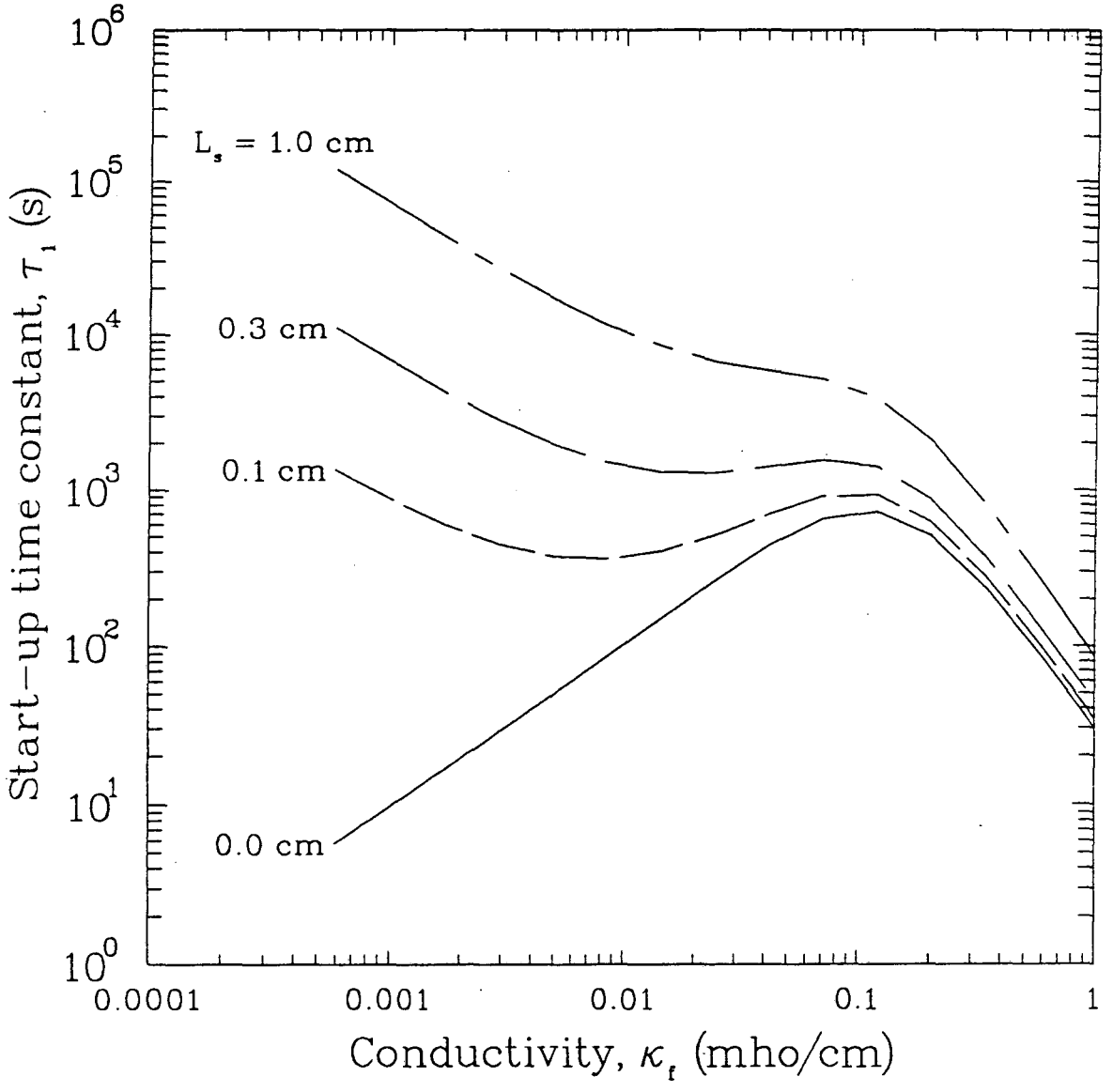

Figure 4-13. Dependence of the start-up time constant τ_1 on free-solution conductivity κ_f at various reference electrode separations L_s (experimental cell).

seconds (or 28 hours). This is so large that it makes the entire process unfeasible. Eliminating the separator resistance would decrease τ_1 by four orders of magnitude and make the process very feasible. Recall also that τ_2 and T are independent of L_s. Reducing L_s is thus the single most efficient change possible toward improving the process. Realistically, the separator distance can be lowered to about 0.1 cm. This figure will be used for the improved-cell calculations later.

As mentioned earlier, the keys to designing the cell are in maximizing the half-cycle time T relative to both the residence time t_{res} and the start-up time τ_1. Figure 4-14 shows how poorly the experimental cell should be expected to perform. At all conductivities, the start-up time τ_1 is much larger than the half-cycle time, implying that $I\sqrt{t}$ never becomes constant and we have violated a major design assumption. Also, the half cycle time is never larger than the bed residence time, meaning treated fluid cannot exit the bed before regeneration must occur. The half-cycle time increases quickly at low conductivities because the current efficiency increases (i.e., higher fraction of zinc ions) causing the required average current to decrease (see equation 4-5). Raising T/τ_1 and T/t_{res} to values greater than unity requires varying the operational parameters.

Lowering the flow rate through the bed will lower the current required for zinc removal (see equation 4-6). This will lower the necessary average cell current without changing τ_1. The flow rate

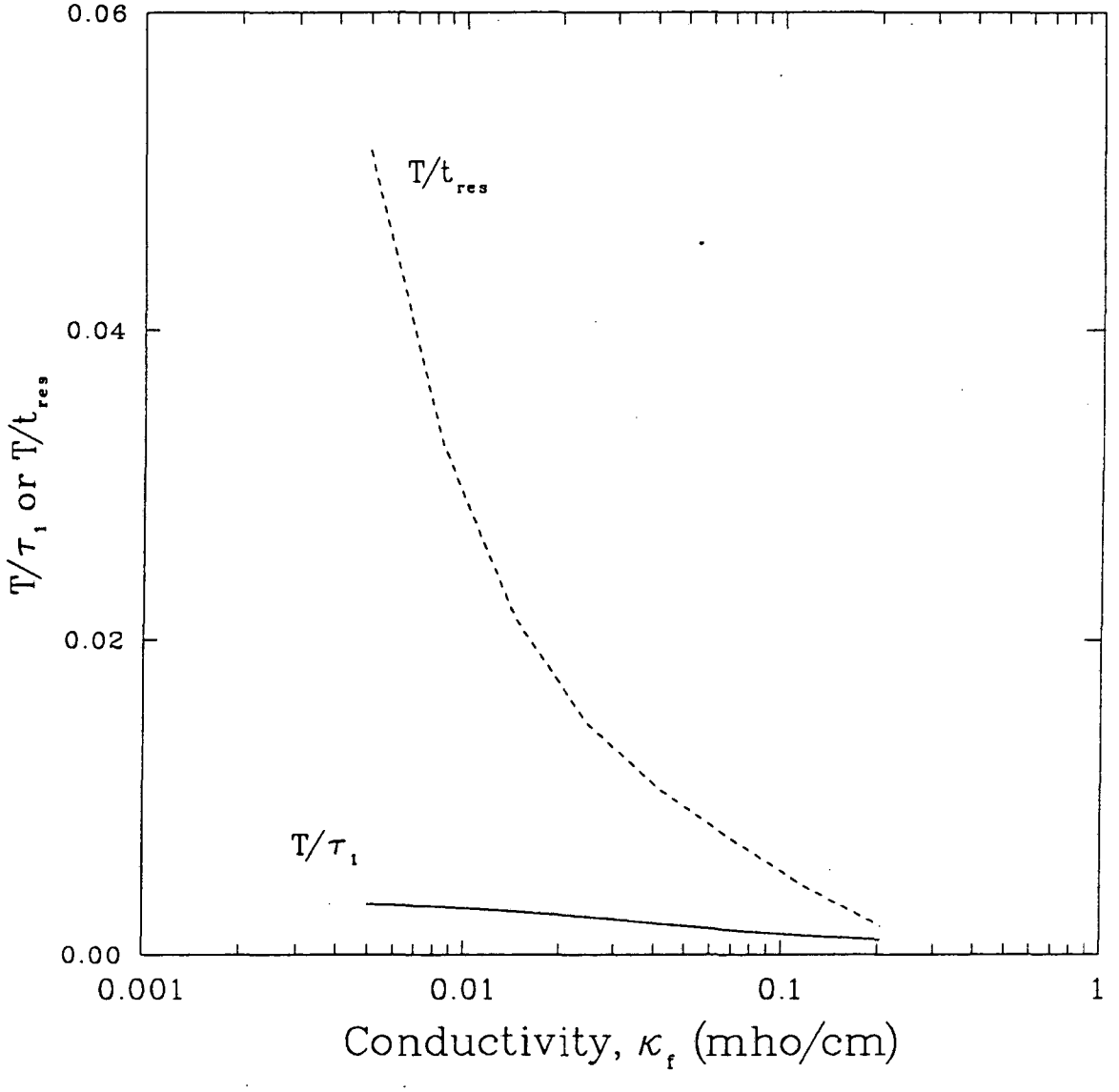

Figure 4-14. The number of bed residence times or start-up time constants in a bed half cycle versus conductivity (experimental cell).

was reduced 75%, but this did not raise T by enough to make it larger than τ_1. Lowering the flow rate also increased the ratio T/t_{res}. This occurs because t_{res} varies inversely with flow rate but T varies to the inverse second power. Figure 4-15 shows the influence of flow rate on T/t_{res} for the experimental cell. Only at extremely low flow rates and low conductivities could the cell process more than one bed volume to saturation. Yet because τ_1 is greater than t_{res}, the cell does not achieve steady charging in the time of a bed volume.

4.3.3.2. Improved Cell Design Analysis

In order to improve the cell according to our design criteria, τ_1 must be lowered, T must be raised, and t_{res} must be lowered. Looking to our equations (see sect. 4.3.1), we see that the cross-sectional area A, the voltage step ΔV, the zinc concentration c_{Zn}, and the solution flow rate $\dot{Q}$ will all affect T without altering τ_1 (or τ_2). The flow rate and cross-sectional area will affect t_{res} as well. The bed length L and separator distance L_s, on the other hand, affect τ_1 and τ_2 without altering T. The approach taken involved choosing a practical minimum for L_s, lowering L, doubling the cross-sectional area A, lowering the zinc concentration in the feed, leaving σ and aC unchanged, and varying κ_f and $\dot{Q}$ to maximize T/τ_1 and T/t_{res}. Table 4-2 gives values of operating parameters for the improved cell. Many of the parameters simply have been changed in the desired direction. This includes the bed length L, the separator length L_s, the zinc concentration c_{Zn}, and the flow rate $\dot{Q}$. The conductivity was considered an optimum, as we shall see in figure 4-18.

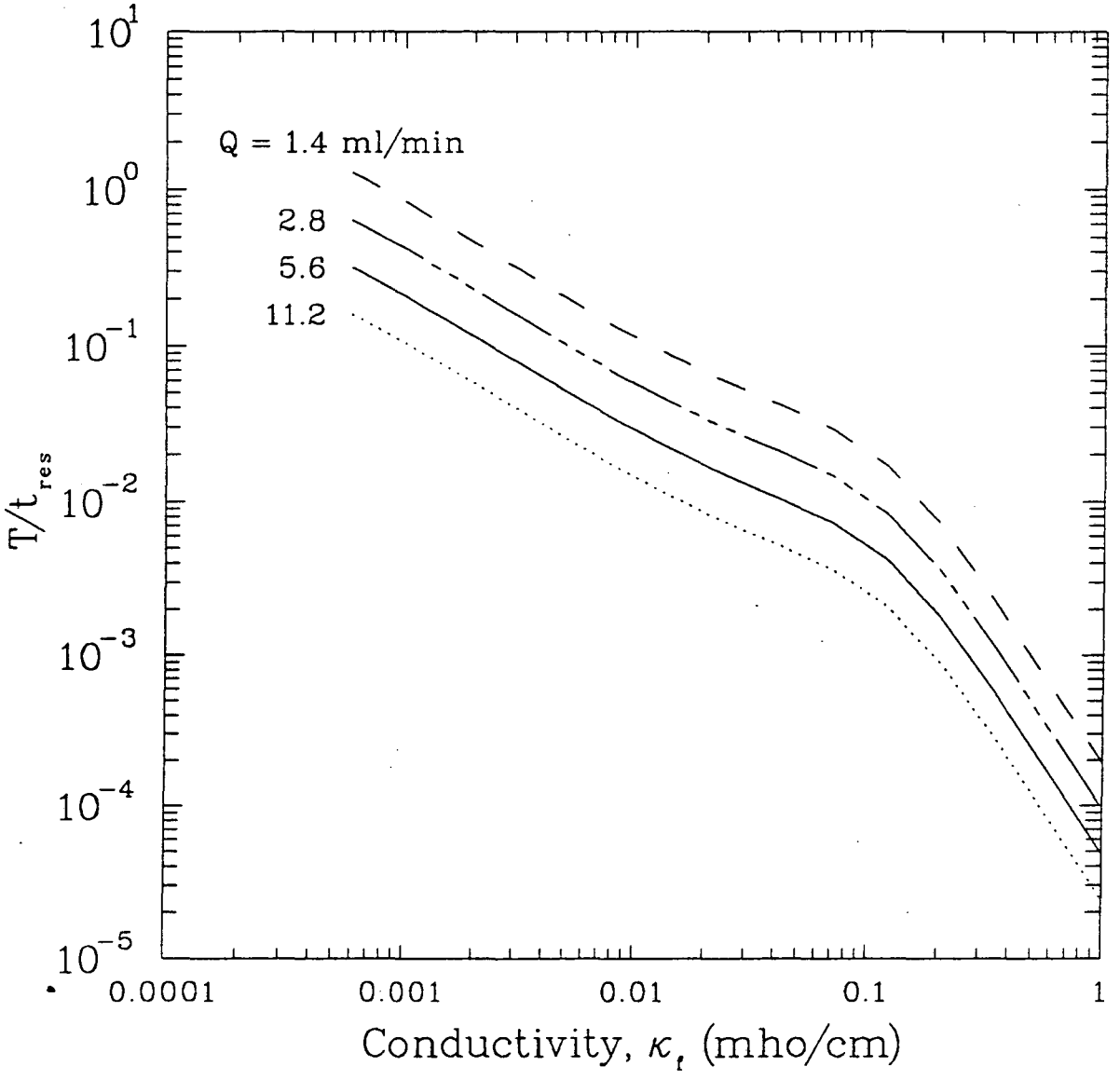

Figure 4-15. The number of bed volumes treatable to 100% zinc removal at various flow rates (experimental cell).

Table 4-2. Improved Parameters for New Design

parameter	value	units
κ	0.005	mho/cm
σ	0.092	mho/cm
A	40.54	cm^2
aC	11.5	F/cm^3
L	1.0	cm
L_s	0.1	cm
t_{res}	650	s
T	900	s
τ_1	180	s
τ_2	3600	s
η_{zinc}	8.0	%
$\dot{Q}$	2.8	ml/min
c_{Zn}	25	ppm
ϵ (bed)	0.75	void frac
p (sep)	0.3	void frac

Shortening the bed length much below 1 cm would result in half-cycle times surpassing the saturation time τ_2. The zinc concentration and separator length were lowered to practical minimums. A waste stream of 25 ppm heavy metals is quite normal. The flow rate is probably way too low; 2.8 ml/min is only one gallon per day.

The next three figures result from a design analysis using the geometric parameters, the concentration of zinc, and the flowrate given in table 4-2. Arguments leading to the choice of conductivity and half-cycle time will now be given.

Figure 4-16 shows the improvement these changes make on the time constants of the cell. Comparison with figure 4-12 indicates that τ_1 decreased by nearly two orders of magnitude at all conductivities. Figure 4-16 also shows the half-cycle time T having values between τ_1 and τ_2. When the conductivity is greater than roughly 0.1 mho/cm, T decreases beyond τ_1. This means that during a half cycle, $I\sqrt{t}$ is not constant (steady charging is never obtained) and we cannot supply current for enough time to remove the zinc in the presence of competing sodium. The residence time (not shown) is 650 seconds at the conditions plotted. At conductivities above about 0.008 mho/cm, the half-cycle time T approaches the residence time t_{res}. When the half-cycle time equals the residence time, the process efficiency drops to zero. Only conductivities less than 0.008 mho/cm can thus be considered in order to increase the half-cycle time relative to the residence time. If the separator length L_s can somehow be made less than 0.1 cm, the value of τ_1 will drop dramatically at the lower conductivities and a potentially ideal process would result. This process would have $\tau_1 \ll T < \tau_2$, $\tau_1 \ll t_{res}$, and $T \gg t_{res}$. With a finite L_s at the lower conductivities, τ_1 remains much higher than ideality would prescribe. The result is $\tau_1 \approx t_{res}$, and bed volumes are lost during every change in potential due to slow start up.

Varying the flow rate could be expected to affect T and t_{res} while leaving τ_1 unaffected. Decreasing the flow rate would thus decrease the ratio τ_1/t_{res}. As figure 4-17 shows, decreasing the flow rate also increases the ratio T/t_{res}. Comparing ordinate values

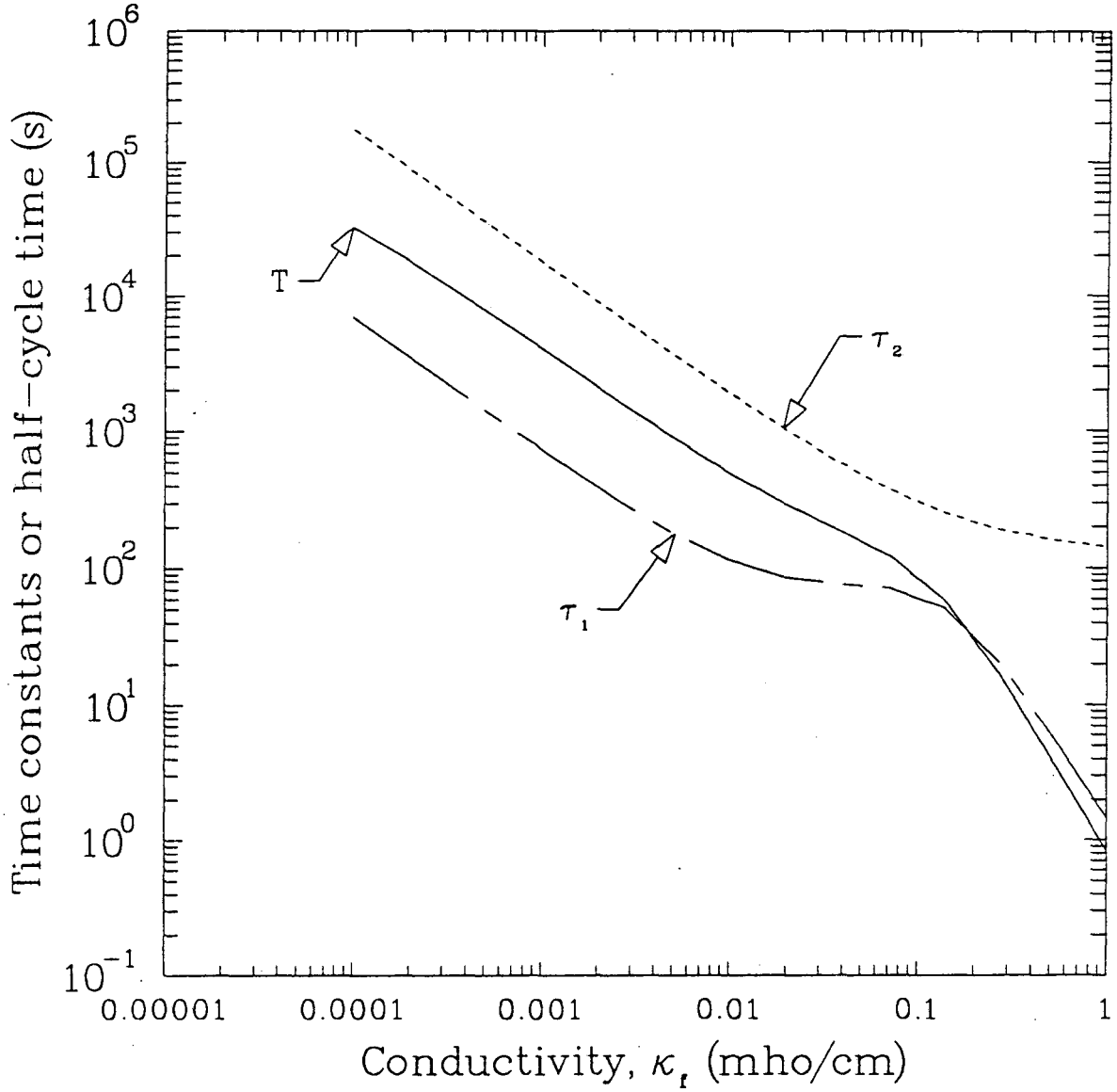

Figure 4-16. Variation of τ_1, τ_2, and T with conductivity (improved cell).

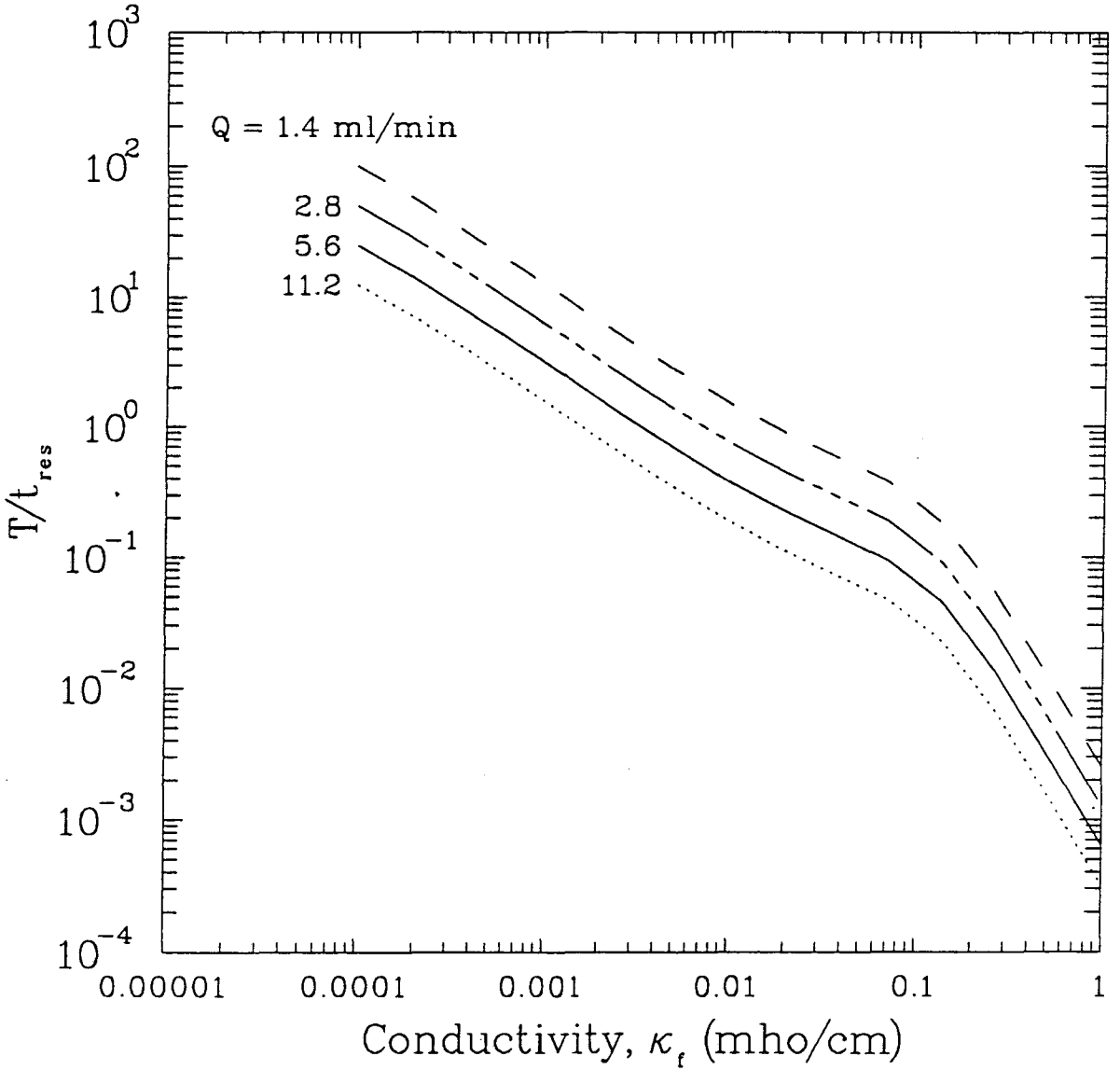

Figure 4-17. The number of bed volumes treatable to 100% zinc removal at various flow rates (improved cell).

with those of figure 4-15 shows a 100-fold increase in treatable bed volumes from the initial design to the improved one at any conductivity. This occurred because the shorter bed has a shorter residence time while the wider cross-sectional area provides higher total currents at all times and thus a longer half-cycle time for a specified average current. If the flow rate halves, the ratio T/t_{res} doubles. The flow rate should not be made so low that axial diffusion becomes important or that only impracticably small solution volumes can be processed. It is unfortunate that the design ratio (T/t_{res}) and the system flow rate $\dot{Q}$ work against one another. We actually should want to maximize $\dot{Q}$ as well.

At a flow rate of 2.8 ml/min, the value of T/t_{res} is greater than 1.0 for conductivities below 0.008 mho/cm. Figure 4-18 replots the curve at 2.8 ml/min from figure 4-17 on a linear scale and also shows the ratio T/τ_1 versus conductivity. The ordinate values are about 20 times greater than they were for the conditions of figure 4-14. The improvement is largely the result of decreasing L from 6.6 to 1.0 cm and lowering L_s from 1.0 to 0.1 cm as a means of reducing the cell resistance R_T. Lowering R_T allows higher currents to pass and more desalting to occur. It also opens the option of processing dilute solutions (i.e., $\kappa_f \leq 0.01$mho/cm), which increases the cell resistance (perhaps slightly beyond the level with high conductivity and large L and L_s) but also increases the current efficiency for zinc. The double-layer charging process is expected to be the most competitive with other deionization methods as the ionic concentra-

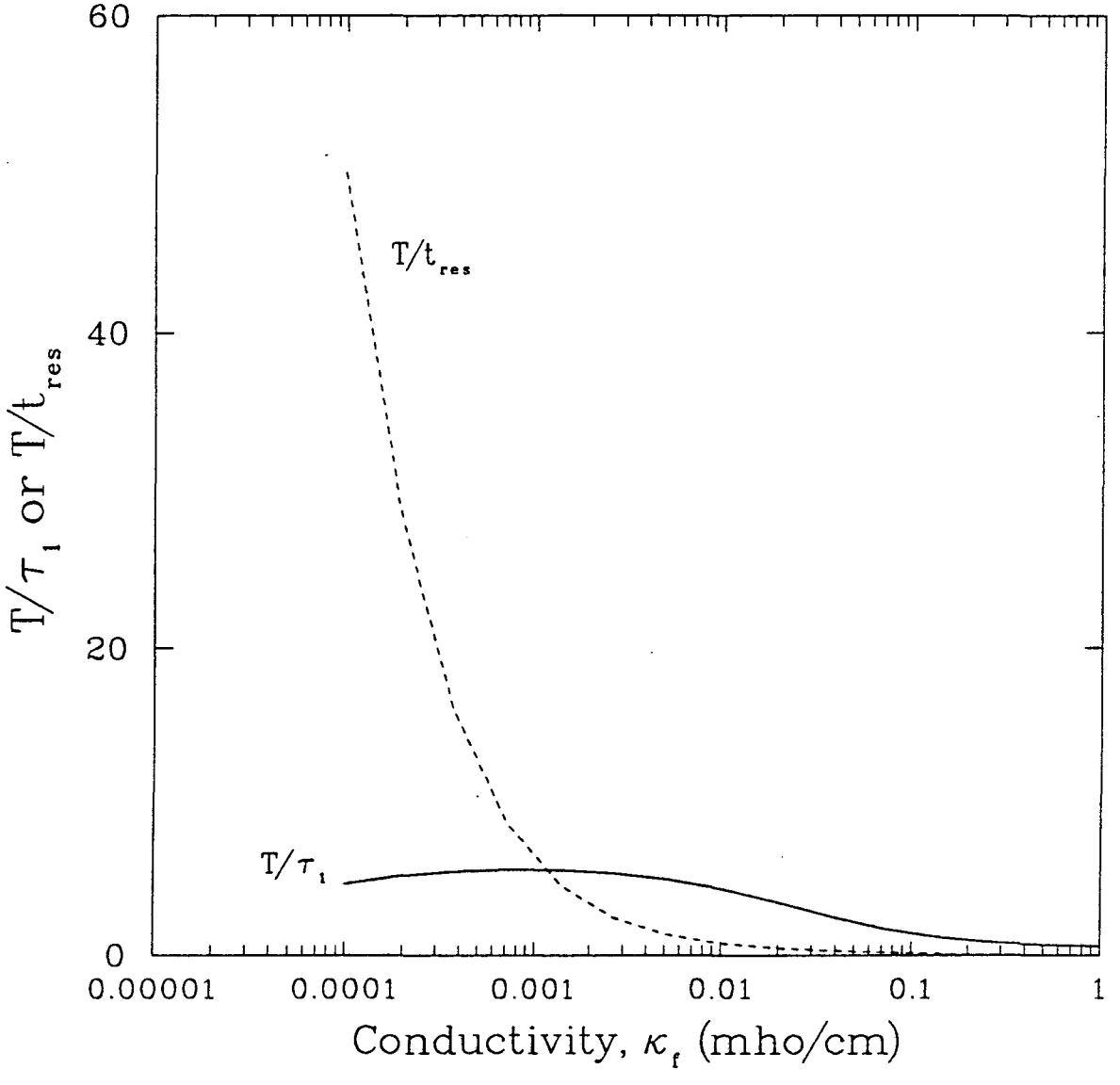

Figure 4-18. The number of bed residence times or start-up time constants in a bed half cycle versus conductivity (improved cell).

tion decreases, much like ion exchange and electrodialysis. Thus it is appropriate to target the design towards treating dilute solutions.

On figure 4-18, the curve displaying T/τ_1 does not vary much but shows a maximum at $\kappa_f \approx 0.0014$ mho/cm. At this conductivity, the maximum number of start-up times can be passed in a half cycle, according to our design assumptions. However, τ_1 is about 850 seconds at this conductivity. Thus steady charging would not be achieved for over 14 minutes after a potential step. Given the likely degree of error in the assumptions leading to the calculation of T, minimizing τ_1 deserves a higher priority than maximizing T/τ_1 or (T/t_{res}). Raising the conductivity to 0.005 mho/cm drops τ_1 to 3 minutes. A drawback of using a higher conductivity is that the half-cycle time T decreases (see figure 4-16). When $\kappa_f = 0.005$ mho/cm, only 1.3 bed volumes can be processed per half cycle (i.e., $T/t_{res} \approx 1.3$); yet it is essential that τ_1 be minimized because the entire design calculation has been based on the assumption of steady charging from time zero. At $\kappa_f = 0.005$ mho/cm, roughly 5.0 start-up times pass in a half cycle (i.e., $T/\tau_1 \approx 5.0$). Since steady charging occurs after a time τ_1 has passed, about 4.0/5.0 of the run can be thought to occur with $I\sqrt{t}$ equal to a constant. Lowering L_s below the assumed value of 0.1 cm would raise both T/t_{res} and T/τ_1 both by raising T (see equation 4-5) and by lowering τ_1. This would allow even more dilute solutions of heavy metals to be processed and still higher current efficiencies for metals removal. With close placement

of a reference-electrode capillary tip and with the use of ohmic compensation on the potentiostat, an effective L_s of less than 0.1 cm is perhaps achievable.

As conductivity decreases, the start-up time τ_1 continues to grow for $L_s > 0$ (see figure 4-13). When τ_1 grows beyond t_{res} (i.e., below κ_f = 0.0012 mho/cm in figure 4-18) bed volumes are lost with each change in potential. The ohmic drop between the working and counter electrodes also becomes huge at very low conductivities. For example, to push 100 mA when κ_f is 0.001 mho/cm and A = 40 cm^2 requires 2.5 volts for each centimeter the counterelectrode is separated. In the experimental cell, the counterelectrode was about 25 cm away, meaning that over 60 volts would be required to push 100 mA. It will be necessary to minimize the distance from the porous electrode to the counterelectrode if cells of low conductivities are to be operated.

At higher conductivities, the half-cycle time during which all zinc ions entering the cell can be removed decreases due to competition between zinc and sodium for current. A higher average current is required to remove the zinc because the current efficiency is lower. Above $\kappa_f \approx 0.01$ mho/cm, the half-cycle time has dropped below the bed residence time, and the process efficiency drops dramatically. A solution conductivity of 0.005 mho/cm appears to be a good starting point for future experimental work. It represents a balance between minimizing cell resistance (i.e., high κ_f) and maximizing the current efficiency for zinc (i.e., low κ_f). Table 4-2 (once again)

shows the parameters.

CHAPTER 5

Conclusions

While the study was not comprehensive, much was learned which can be valuable to future researchers in the area. The conclusions are as follows:

1. Cell geometry and operating conditions are important considerations in the design of a double-layer adsorption process. The reference electrode capillary tip separation must be minimized to reduce the ohmic resistance through the cell and thus lower r_1. If porous cation and anion responders are pressed together to form a cell, as in practice, then the separator thickness must be minimized, whatever charging mode is chosen (i.e., galvanostatic). Ohmic limitations in the experimental cell inhibited the onset of the capacitive charging current.

2. The effluent concentration of zinc did not follow the predicted form. The new design for the experimental cell should improve the process dramatically. If a nonchemisorbing electrolyte is used (i.e., sulphate solution), and if the current-versus-time behavior obeys the theory, the concentration profiles can be expected to follow.

3. At very positive bed potentials, anionic complexes were electrosorbed. This showed that the process could select a zinc complex in a huge excess of uncomplexed monovalent competing ions.

4. Potential-dependent faradaic reactions occurred in the porous electrode, and these appeared to determine the cell open-circuit potential. The reactions may also have interfered with the charging current by perturbing the potential profiles in the bed, although the current densities were small. At potentials in a hydrogen-evolution regime, current densities were five orders of magnitude less on the porous electrode than on the rotating-disk electrode. Faradaic reactions also occurred in the porous electrode between the potentials for hydrogen and oxygen evolution. Thus, reactions other than hydrogen or oxygen evolution appeared to occur on the porous electrode.

5. The double-layer capacities calculated from rotating-disk experiments were high. The capacity was also quite sensitive to the pH in solution. Apparently additional charge storage ability resulted from specific adsorption (i.e., adsorption at the inner Helmholtz plane) at pH-sensitive surface groups.

6. Within a range of potentials from -0.5 V to 1.0 volts versus SCE, glassy carbon behaved as ideally polarizable. This range was relatively independent of solution concentrations of NaCl or Zn^{++} and of pH. The porous electrode appeared to have even a wider range of potentials between the hydrogen and oxygen evolution reactions, neglecting the faradaic reactions discussed in "conclusion 4" above.

7. Mass transfer within carbon particles appears to be a slow step, leading to disperse breakthrough curves in column experiments.

Fluid-phase axial (molecular) diffusion was not important.

8. Specific adsorption in sodium-chloride solutions is due to formation and adsorption of zinc complexes on activated carbon. The adsorbed complexes could not be removed by varying the electrode potential. Zinc ions did not adsorb from the sodium-salt solutions of nitrate or sulfate, apparently due to the lack of zinc complexing in these solutions.

9. Zinc ions could be effectively removed from a saturated bed in sodium-chloride solutions by lowering the sodium-chloride concentration in solution.

CHAPTER 6

Future Work

Continuation of the project should include both experimental and theoretical work.

6.1. Experimental

Future experimental work should involve building and operating the cell proposed in the design section. In building the cell, certain features of the existing cell should be improved upon. The present cell housed a counterelectrode some 25 cm from the working electrode. Thus large voltages are required to drive current in solutions of low conductivity. The cell did have the advantage that current lines ran approximately parallel to the flow lines, simulating the one-dimensional model used. A new cell should house the counterelectrode close to the porous electrode, while keeping the current and flow lines parallel. Use of a platinum screen in the shape of a disk and placed normally to the flow as a counterelectrode would accomplish this. Platinum provides a noncorrosive surface with low overpotentials for the hydrogen and oxygen evolution reactions occurring at the counterelectrode. The disk geometry would maintain parallel current and flow lines even at close distances. A membrane could be inserted as before to prevent mixing of the porous electrode and counterelectrode solutions.

The faradaic reactions which occurred during experimentation should be minimized. Standard Oil of Ohio markets a capacitor which contains several porous electrodes in series.[54] They claim to have virtually eliminated faradaic reactions in the carbon electrodes. The pretreatment method they use involves baking the commercial activated carbon at high temperatures and low pressures to remove adsorbed impurities and then soaking the carbon for several days in sulfuric acid. Various methods of carbon pretreatment should be compared as part of future experimental work. The time of acid reflux during pretreatment should be increased to 6-8 hours to determine whether this reduces the faradaic current.

Other considerations for a new cell should be discussed as well. The present cell had large holdup times for solution waiting to enter the bed and for solution exiting the bed prior to sampling. For example, the feed concentration could not be changed without mixing with the original feed for nearly an hour. This made it impossible to change the feed precisely during operation. Also bed effluent traveled for about seven minutes prior to sampling. A new design should minimize the upstream and downstream holdup and perhaps have two feed ports to minimize holdup in the tubes for a change in feed concentration. This would minimize the time for effluent to mix and will thus maintain any separation achieved.

A new cell should be designed so that the bed length can be varied. The cell can be built so that layers can be inserted to lengthen the bed. The situation is similar to inserting leaves in a

dinner table.

Another consideration is the reference electrodes. The upstream capillary tip should be placed down onto the bed. The downstream reference electrode needs no capillary tube because no current flows beyond the bed. In a galvanostatic mode, minimizing the reference electrode separation will allow solution potentials approximating those at the ends of the bed to be measured, and is thus desirable. An improvement could be made if each electrode was equipped with capillary tips which could somehow traverse the bed. With the porous-electrode potential controlled relative to one reference electrode, the other reference electrode could traverse the bed, determining the solution-phase potential profile and ohmic drop in solution. A notch in the tube wall would allow a capillary tube to traverse without disrupting the electrode geometry.

As for experiments to run, at least one could be run on the existing cell. For extremely high conductivities, r_1 and r_2 separate and r_1 becomes small (see figure 4-12). In this case, ohmic losses are negligible, and the existing cell could be used to check the current-versus-time behavior. A run with near-saturated, sodium-chloride solution should suffice.

A new cell could be used to examine the competitive adsorption of zinc and sodium. The selectivity for zinc over sodium can be checked. Solution conductivities should be monitored alongside the concentrations to see how much it actually changes. Cosorption of chloride ions with the cations is also worth studying. Current

opposite that for zinc is required for chloride to adsorb and desorb, and thus cosorption represents a process efficiency which should perhaps be maximized. In contrast is the situation of a water-desalting application where cosorption of sodium and chloride represent a process inefficiency. Adsorption of $ZnCl_2$ requires no current at all. The problem is that the $ZnCl_2$ may not desorb by varying the potential, which would lessen the process usefulness.

It is likely that the increasing solution resistance during a deionizing run will prevent a complete desalting. A conductivity cell at the bed exit could monitor solution conductivity. This would give a measure of the degree of overall deionization occurring and of the magnitude of conductivity changes that the cell induces.

Many other phenomena could be studied as well. The type of carbon (i.e., basic or acidic, activated or graphitic) and the pretreatment technique might have an effect on performance. The amount of active surface area for a given carbon will directly determine process capabilities. Various carbons should be tested to determine which ones show the highest capacities per unit volume. The pretreatment procedure may also affect this capacity. The question of the useable surface area in a porous electrode is of fundamental interest as it is often desirable to maximize the area for electochemical reaction in systems such as batteries and fuel cells.

Different heavy metals of the same valence, such as zinc and lead, could be treated to determine whether ions of the same valence might perform differently. This would also show whether the

adsorption of zinc is perturbed by the presence of another heavy metal. Metals or metal complexes of higher valence could also studied. Metal-cyanide complexes of tri- or tetra- valent states might be expected to adsorb strongly, based on charge number alone. If concentrated solutions are to be studied, a nitrate or sulfate anion can be used to eliminate the problem of complexing of metals with chloride or cyanide ion. Chloride complexing should not occur in dilute solutions, but stronger cyanide complexes would still exist.

Double-layer capacity studies should continue. A closer comparison with the double-layer capacity of the granular-activated carbon is necessary than the glassy-carbon disk provided. An approach might be to construct a very thin granular-activated-carbon electrode which would equilibrate quickly with the applied potential. This would more directly address the issue of determining the double-layer capacity of the activated carbon material. It would also allow a more careful comparison with the behavior of the glassy-carbon, rotating-disk electrode. The comparison would provide insight into the question of whether a rotating-disk electrode, made of similar material as a porous electrode, can be used to characterize the porous electrode.

Use of AC impedance, where a small voltage or current perturbation is oscillated around the steady value, should yield accurate capacities. These could be compared with the capacities calculated from the potential-sweep experiments. An AC-impedence technique would also yield the capacity as a function of potential, allowing

the Johnson, et al., model assumption of constant double-layer capacity to be evaluated.

A major experimental concern has been the lack of knowledge about the point of zero charge for the porous electrode. The point of zero charge marks the approximate potential for the electrode to change from anion to cation responsiveness. Measurements of the point of zero charge have generally been difficult on solid surfaces due to the inability to measure surface tensions. Golub, *et al.*,[51] however, have reported measuring the point of zero charge on porous carbon electrodes by measuring the variation of electrode length with potential. They argue that with the high surface-to-volume ratio of porous carbons, the repulsive forces due to surface charges can be expected to be detectable by an increase in electrode length. At the point of zero charge, repulsive forces are minimized and the electrode length is a minimum. In our study, knowing the point of zero charge would help direct the choice of potentials between which to cycle and thus is necessary. The new cell, or a separate cell, could be equipped to make the electrode-length measurement for determination of the point of zero charge. Perhaps simpler would be to use the AC-impedence method of capacity determination and look for the minimum in a capacitance-versus-potential curve. The point of zero charge is typified by this minimum in capacitance.[52]

6.2. Theoretical

Modeling should accompany the additional experimental work. Certain assumptions of the porous electrode model presented should be

relaxed. A practical cell must treat very dilute solutions. Conductivity will decrease on desalting and increase on regeneration. Thus the model should treat variable conductivity in the bed. Concentration variations in the axial direction must be included if conductivity is allowed to vary. The composition of adsorbed ions must be known to calculate factors including the conductivity change, the concentration gradients, and the double-layer capacity (i.e., the sum of all adsorbed charges per unit potential difference). A surface model accounting for the adsorption of each species depending on the potential difference from solution to the surface, the concentrations of each species, and the valence of each ion would yield the adsorbed-ion concentrations.

Solving the model could involve slicing the bed into many "stages." Starting at the entrance, the ions adsorbing at each stage could be subtracted from the local bulk concentration, much like a stage-to-stage distillation calculation. The model should include mass-transfer resistance from the bulk to the surface, but retain the original assumption that the double-layer equilibrates locally very quickly. The potentials in the matrix and solution phases could be updated based on the fraction of the current flowing in each phase and the conductivity at the particular stage. The matrix-phase conductivity will remain constant.

The procedure of working down the column and calculating concentrations and potentials could be repeated for each instant of time. The calculation for a regeneration cycle may require some assumptions

about how the ions leave the surface at various positions and times.

An opportunity to refine the model of the double-layer-adsorption process awaits further experimental justification. The process can still find usefulness as a waste-water cleanup technique, though not without further study. It is also possible that a properly designed porous-electrode, double-layer-charging process could be a useful analytical technique. Applying a potential step to a given porous electrode could yield an electrochemically active surface area or the double-layer capacity. This has been done on lead acid battery electrodes by Tiedemann and Newman.[53] The technique of charging a porous electrode can also be used to make high-energy-density capacitors. Standard Oil[54] makes a capacitor made of two compressed porous-carbon electrodes separated by a microporous membrane. The capacitors possess a nearly unlimited cycle life. The entire energy transfer is due to electrostatic effects in the double layer, so the electrodes do not corrode. The high surface area of the carbon creates the high energy densities.

In summary, the process for heavy-metal-ion removal by double-layer adsorption deserves further study. Fundamental questions about the interfacial phenomena and the point of zero charge on the porous electrode need answering. The surface area used in double-layer charging on a given carbon must be known and (ideally) predicted. If carbons show differing active surface areas, then the reasons why should be explained. If certain properties are found to affect the active surface area, carbons displaying these properties can be

selected for further experimental work. Individual ion-adsorption isotherms should be elucidated experimentally and predicted theoretically. Process design questions should also be addressed. Half-cycle times and potentials for the removal and regeneration steps should be varied and optimized. Coupling an interfacial-adsorption model with the macroscopic porous-electrode equations may allow a theoretical optimization of the half-cycle times. The predictions could be checked experimentally.

List of Symbols

symbol	definition and units
A	cross sectional area of porous or planar electrode, cm^2
a	specific surface area in porous electrode, cm^2/cm^3
C	overall double-layer capacitance, $farad/cm^2$
C_T	overall double-layer capacity, farad
c_i	solution concentration of species i, molar or ppm
d_o	distance from surface to IHP, Å
d_1	distance from IHP to OHP, Å
D_i	effective diffusivity of species i in a porous media (porosity and tortuosity factors are assumed to be included), cm^2/sec
E	electric field strength, volts/cm
F	Faraday's constant, 96487 coul/equivalent
I	total current, amps
$\bar{I}$	Laplace transform of the total current, coulombs
I_{ave}	average current in the porous electrode after a potential step, amps
$I_{t=0}$	initial current in porous electrode following a potential step, amps
I_{zinc}	minimum current needed to remove all the zinc entering the porous electrode, amps
i	current density: current per unit electrode area, $amps/cm^2$
i_1	superficial current density in matrix phase of porous electrode (current per unit cross-sectional area), $amps/cm^2$

i_2	superficial current density in pore solution of porous electrode, amps/cm^2
L	porous electrode length, cm
L_s	separator length (length from porous electrode to reference electrode capillary tip), cm
N_i	superficial flux of species i, moles/(cm^2-sec)
p	void fraction between the porous bed and the reference electrode capillary tip, cm^3/cm^3
ppm	milligrams zinc per kilogram solution or carbon, mg/kg
Q	charge passed from time zero, coulombs
$\dot{Q}$	volumetric flow rate through the porous electrode, cm^3/sec
q	adsorbed charge density in porous electrode, coulombs/cm^2
$Q_{enclosed}$	total charge in a Gaussian enclosure, coulombs
q_i	adsorbed charge density for species i in porous electrode, coulombs/cm^2
q_{IHP}	charge density at the inner Helmholtz plane, coulombs/cm^2
q_M	charge density on the metal electrode, coulombs/cm^2
q_{OHP}	charge density in the diffuse double layer (if charge projected to a plane), coulombs/cm^2
r_o	radius of the rotating disk electrode, cm
r_p	radius of a carbon granule (assumed spherical), cm
R_1	superficial resistance in the matrix of the porous electrode, ohm-cm^2
R_2	superficial resistance of the solution in the porous electrode, ohm-cm^2

R_s	superficial resistance of the solution in the separator region, ohm-cm^2
R_T	superficial resistance from the working to the reference electrode in the porous electrode, ohm-cm^2
R	resistance from the rotating disk electrode to a reference electrode infinitely far away, ohm
S	surface area of a Gaussian enclosure, cm^2
s	Laplace transform variable, sec^{-1}
T	absolute temperature, K
T	half-cycle time, seconds
t	time, seconds
t_{res}	actual residence time in bed, seconds
U	thermodynamic electrode potential versus a reference electrode at open circuit, volts
u_i	mobility of species i, mole-cm^2/joule-sec
V	volume of a Gaussian enclosure, cm^3
V	potential of a planar working electrode (or of the current collector of the porous electrode) versus a reference electrode, volts
$\bar{V}$	Laplace transform of the working versus the reference electrode potential, volt-sec
V_o	potential of the working versus the reference electrode at open circuit, volts
V_o'	potential of the working versus the reference electrode relative to the value at open circuit, volts
ΔV	the magnitude of a potential step of the working versus the reference electrode potential, volts
V_{SCE}	potential of the current collector of the porous or rotating-disk electrode versus a saturated-calomel reference electrode, volts
v	superficial velocity in porous electrode, cm/sec

x	axial distance in the porous electrode, cm
y	distance from the planar electrode interface, cm
Y	matrix versus solution phase current density in porous electrode, volts/cm
$\bar{Y}(x,s)$	Laplace transform of Y, volts/cm-sec
z_i	valence of species i, unitless

Greek letters

α	electrical diffusivity in porous electrode, cm^2/sec
Γ_i	adsorbed ion concentration, $moles/cm^2$
γ	surface tension, $joule/cm^2$
ϵ	overall porosity (macro plus micro) of porous electrode, cm^3/cm^3
ϵ	permittivity of solution, farads/cm
ϵ_i	permittivity of solution between the surface and the inner Helmholtz plane, farads/cm
ϵ_1	permittivity of solution between the inner and outer Helmholtz planes, farads/cm
η_{zinc}	current efficiency for zinc adsorption in presence of competing sodium, unitless
θ	matrix versus solution potential in the porous electrode, volts
κ	conductivity of rotating-disk solution or effective solution conductivity within porous electrode, mho/cm
κ_f	free-solution conductivity as calculated from dilute-solution theory, mho/cm
κ_s	effective solution conductivity in separator region between porous electrode and reference electrode capillary tip (i.e., conductivity in the presence of a porous matrix of non-conducting spheres), mho/cm

λ_i	ionic equivalent conductance, mho-cm^2/equivalent
μ	chemical potential, joules/mole
ν	potential sweep rate, volts/sec
ρ	density of porous matrix, grams/cm^3
ρ_e	electric charge density, coulombs/cm^3
σ	matrix conductivity, mho/cm
τ_1	start-up time constant, seconds
τ_2	saturation time constant, seconds
ϕ	electric potential, volts
ϕ_1	potential of porous matrix, volts
ϕ_2	potential of solution in pores, volts
ϕ_{IHP}	potential at the inner Helmholtz plane, volts
ϕ_M	potential of a metal electrode, volts
ϕ_{NHE}	potential of a normal hydrogen reference electrode, volts
ϕ_{OHP}	potential at the outer Helmholtz plane, volts
ϕ_{RE}	potential of the reference electrode, volts
ϕ_{SCE}	potential of a saturated-calomel reference electrode, volts
ϕ_{WE}	potential of the working electrode (or of the current collector of a porous electrode), volts
Ω	rotation rate of rotating disc electrode, sec^{-1}

superscripts

upstream	region in porous electrode prior to where solution enters the bed
downstream	region in porous electrode after solution exits the bed

Literature Cited

[1]. Lacy G. Thomas, Founder *Ecology Protection Systems*, 27 Bonaventura Drive, San Jose, CA 95134. personal communication (June 1986).

[2]. John Griffin, Public Information Section "East Bay Municipal Utility District (MUD) Sewage Treatment Plant," Oakland, CA phone:(415)465-3700 ext.127 personal communication (June 1986).

[3]. M.H. Gerardi, "Effects of Heavy Metals Upon the Biological Wastewater Treatment Process," *Public Works*, 117 (no. 6, 1986) 77-80.

[4]. "Electroplating Point Source Category," *Code of Federal Regulations*, *title 40*, *part 413*, Revised as of July 1, 1986.

[5]. "Water Act Prosecution Obtains Guilty Plea by USM," *Chemical Marketing Reporter* (January 5, 1987) 7.

[6]. "Control and Treatment Technology for the Metal Finishing Industry. In Plant Changes; Ion Exchange," *EPA Report 625/8-82-008*, Summary Report (January 1982) 30pp.

[7]. R.H. Perry and Don Green, *Perry's Chemical Engineers' Handbook*, Sixth Edition, McGraw-Hill (1984), Chapter 26.

[8]. G. McIntyre, *et al.*, "Inexpensive Heavy Metal Removal by Foam Flotation," *Journal of the Water Pollution Control Federation*, 55 (no. 9, 1983) 1144-1149.

[9]. F.J. DeLuise, "Water Reuse by Metal Removal from Industrial Plating Effluents," *Rhode Island Water Resources Center Report* project no. A-073-RI.

[10].Friedrich Helfferich, *Ion Exchange*, McGraw-Hill (1962).

[11].A. Netzer and D.E. Hughes, "Adsorption of Copper, Lead and Cobalt By Activated Carbon," *Water Resources*, 18 (no. 8, 1984) 927-933.

[12].C.P. Huang and D.W. Blankenship, "The Removal of Mercury(II) From Dilute Aqueous Solution by Activated Carbon," *Water Resources*, 18 (no. 1, 1984) 37-46.

[13].A.G. Rowley, *et al.*, "Mechanisms of Metal Adsorption from Aqueous Solutions by Waste Tyre Rubber," *Water Resources*, 18 (no. 8, 1984) 981-984.

[14].M.J. Semmens and W. Martin, "Studies on Heavy Metal Removal from Saline Waters by Clinoptilolite," *AIChE Symposium Series*, 76 (1980) 367-376.

[15]. Nord L. Gale and Bobby G. Wixson, "Removal of Heavy Metals from Industrial Effluents by Algae," *Developments in Industrial Microbiology*, 20 (1978) (Pub. 1979) 259-273.

[16]. N. Friis and P. Myers-Keith, "Biosorption of Uranium and Lead by Streptomyces longwoodensis," *Biotechnology and Bioengineering*, 28 (1986) 21-28.

[17].George W. Heise, "Porous Carbon Electrodes," *Transactions of the American Electrochemical Society*, 75 (1939) 147-166.

[18].Joseph Wang, "Reticulated Vitreous Carbon- A New Versatile Electrode Material," *Electrochemica Acta*, 26 (no. 12, 1981) 1721-1726.

[19].James A. Trainham and John Newman, "The Effect of Electrode Placement and Finite Matrix Conductivity on the Performance of Flow-Through Porous Electrodes," *Journal of the Electrochemical Society*, 125 (1978) 58-68.

[20].Douglas N. Bennion and John Newman, "Electrochemical removal of copper ions from very dilute solutions," *Journal of Applied Electrochemistry*, 2 (1972) 113-122.

[21].Richard Alkire and Brian Gracon, "Flow-Through Porous Electrodes," *Journal of the Electrochemical Society*, 122 (1975) 1594-1601.

[22].John Van Zee and John Newman, "Electrochemical Removal of Silver Ions from Photographic Fixing Solutions Using a Porous Flow-Through Electrode," *Journal of the Electrochemical Society*, 124 (1977) 706-708.

[23].M. Enriquez-Granados, G. Valentine, and A. Storck, "Electrochemical Removal of Silver Using a Three-Dimensional Electrode," *Electrochimica Acta*, 28 (1983) 1407-1414.

[24].Gary G. Trost, "Applications of Porous Electrodes to Metal-Ion Removal and the Design of Battery Systems," *Ph.D. dissertation, University of California, Berkeley* (1983), LBL-16852.

[25].James Trainham and John Newman, "The Removal of Lead Ions from Very Dilute Solutions Using a Porous Flow-Through Electrode," *Inorganic Materials Research Division Annual Report 1973*, 51-53, Lawrence Berkeley Laboratory, University of California (April 1974) LBL-2299.

[26].Michael Matlosz and John Newman, "Experimental Investigation of a Porous Carbon Electrode for the Removal of Mercury from Contaminated Brine," *Journal of the Electrochemical Society*, 133 (1986) 1850-1859.

[27].A.T. Kuhn, "Antimony Removal from dilute solutions using a restrained bed electrochemical reactor," *Journal of Applied Electrochemistry*, 4 (1974) 69-73.

[28].I.C. Agarwal,*et al.*, "Electrodeposition of Six Heavy Metals on Reticulated Vitreous Carbon Electrode," *Water Resources*, 18 (no. 2, 1984) 227-232.

[29].Allan M. Johnson, *et al.*, "The Electrosorb Process for Desalting Water. Final Report," *U.S. Department of the Interior, Office of Saline Water*, contract no. 14-01-0001-1444 (December 1969).

[30].Allan M. Johnson and John Newman, "Desalting by Means of Porous Carbon Electrodes," *Journal of the Electrochemical Society*, 118

(no. 3, 1971) 510-517.

[31].John Newman, *Electrochemical Systems*, Prentice-Hall, Inc., 1973.

[32].David C. Grahame, "Measurement of the Capacity of the Electrical Double Layer at a Mercury Electrode," *Journal of the American Chemical Society*, 71 (1949) 2975-2978.

[33].Allen J. Bard and Larry R. Faulkner, *Electrochemical Methods*, John Wiley and Sons, Inc. (1980) 13-14.

[34].S. Evans, "Differential Capacity Measurements at Carbon Electrodes," *Journal of the Electrochemical Society*, 113 (*no. 2*, 1966), 165-168.

[35].John Newman, "Resistance for Flow of Current to a Disc" *Journal of the Electrochemical Society*, 113 (1966) 501-502.

[36].David C. Graham, "The Electrical Double Layer and the Theory of Electrocapillarity," *Chemical Reviews*, 41 (1947) 441-501.

[37].Andreas Acrivos, "Method of Characteristics Technique: Application to Heat and Mass Transfer Problems," *Chemical Reviews*, 48 (no. 4, 1956) 703-710.

[38].Kemal Nisancioglu and John Newman, "The Transient Response of a Disk Electrode," *Journal of the Electrochemical Society*, 120 (no. 10, 1973) 1339-1346.

[39]."Thorium to Zinc," *Encyclopedia of Industrial Chemical Analysis*, volume 19, Interscience Publishers.

[40]."Identification of Test Procedures," Title 40, Code of Federal Regulations(CFR), part 136.3 .

[41].American Society for Testing and Materials(ASTM), D1669-84, volume 11.01 (1985) 709-719.

[42].M. Bouzanne, "Redissolution Anodique sur E.F.M.," *Analusis*, 9 (no. 10, 1981) 461-467 (in French).

[43].W.J. Blaedel and Joseph Wang, "Anodic Stripping Voltammetry at a Reticulated Mercury Vitreous Carbon Electrode," *Analytical Chemistry*,51 (1979) 1724-1728.

[44].Orion Research Incorporated, The Schraff Center, 529 Main St., Boston, MA 02129. informational inquiry (1986).

[45].V.G. Levich, *Physicochemical Hydrodynamics*, Prentice-Hall, Englewood Cliffs, N.J. (1962) 60-72.

[46].R.J. Brodd and V.E. Leger, *Encyclopedia of Electrochemistry of the Elements, volume 5*, A.J. Bard, editor, Dekker, New York (1976).

[47].Thomas K. Sherwood, Robert L. Pigford, Charles R. Wilke, *Mass Transfer*, McGraw-Hill, Inc. (1975) 554-561.

[48].D.M. Ruthven, *Principles of Adsorption and Adsorption Processes*, New York: Wiley (1984) chapters 7-8.

[49].D.A.G. Bruggeman, *Ann. Physik*, 24 (1935) 636.

[50].John Kelsey, "Zinc Adsorption Using Porous Carbon Electrodes," Unpublished undergraduate research for John Newman, Chemical Engineering Department, UC Berkeley (April 12, 1984) 12 pp.

[51].Dan Golub, Yoren Oren, and Abraham Soffer, "Electrosorption, The Electrical Double Layer and their Relation to Dimensional Changes of Carbon Electrodes," *Carbon*, 25 (no. 1, 1987) 109-117.

[52].Paul Delahay, *Double Layer and Electrode Kinetics*, Interscience Publishers, New York (1965).

[53].William Tiedemann and John Newman, "Double-Layer Capacity Determination of Porous Electrodes," *Journal of the Electrochemical Society*, 122 (no. 1, 1975) 70-74.

[54].J.C. Currie, *et al.*, "Energy Storage at High Surface Area Carbon Electrodes," *Proceedings - Electrochemical Society* 85-8 Proceedings of the Symposium on the Chemistry and Physics of Composite Media (1985) 169-183.

LAWRENCE BERKELEY LABORATORY
TECHNICAL INFORMATION DEPARTMENT
UNIVERSITY OF CALIFORNIA
BERKELEY, CALIFORNIA 94720